

Supporting Information

Changes in Ligand Coordination Mode Induce Bimetallic C-C Coupling Pathways

Kyle M.K. Jackman^{††}, Guangchao Liang^{†§}, Paul D. Boyle[†], Paul M. Zimmerman^{§} and Johanna M. Blacquiere^{*†}*

[†] Department of Chemistry, University of Western Ontario, London, Canada, N6A 5B7

[§] Department of Chemistry, University of Michigan, Ann Arbor, Michigan 48109, United States

Table of Contents

I Synthetic Procedures.....	S1
I.I General Considerations.....	S1
I.II Ligand Synthesis.....	S3
I.III Complex Synthesis.....	S4
II Experimental Procedures.....	S9
II.I Kinetic Data.....	S9
II.II Radical Tests	S14
II.III Crossover Experiments	S15
II.IV General Thermolysis Procedure	S16
II.V Relationship Between 2 and 3	S21
III Compound NMR Spectra.....	S22
IV IR Spectra.....	S35
V Mass Spectra.....	S37
VI Reaction NMR Spectra.....	S41
VII Computational Details	S41
VIII Crystallographic Details	S58
IX References.....	S66

I Synthetic Procedures

I.I General Considerations

Reactions were conducted in a nitrogen atmosphere glove box or using standard Schlenk line techniques under an argon atmosphere, unless otherwise indicated. All glassware was oven dried and cooled under nitrogen atmosphere prior to use unless otherwise stated. Ground-glass syringes were stored in a desiccator containing Drierite. All reagents used were obtained from commercially available sources and used without further purification, unless otherwise indicated. Potassium Hydride was purchased from Alfa Aesar as a 30% w/w suspension in mineral oil, and

was purified by filtration through a fritted funnel, the solid KH was washed with dry hexanes and diethyl ether (20 mL/g KH), the solid was dried under vacuum and stored under inert atmosphere for use. The following materials were prepared following literature procedures: PdCl(CH₃)(COD),¹ PtCl(CH₃)(COD),² 2-diphenylphosphinoaniline,³ **H[L1]**,³ **1**,⁴ **K[L1]**,⁴ and Pd(CH₃)₂(COD).⁵ All reaction solvents were obtained from an Innovative Technology 400-5 Solvent Purification system, dry and degassed, and stored over activated 4 Å molecular sieves under N₂ prior to use, unless stated otherwise. Pyridine was dried over CaH₂, distilled under vacuum, and stored over activated 4 Å sieves prior to use in an inert atmosphere. Deuterated NMR solvents were obtained from commercial sources and stored over activated 4 Å sieves in an inert atmosphere. Molecular sieves were activated by heating the sieves at 160 °C under vacuum overnight.

All NMR spectra were obtained on a 400 MHz Bruker or 600 MHz Varian spectrometer at 25 °C unless otherwise stated. ¹H and ¹³C{¹H} spectra were referenced internally, using residual solvent values, to TMS at 0 ppm as follows: benzene-*d*₆ (¹H, 7.16 ppm; ¹³C{¹H}, 128.1 ppm), CDCl₃ (¹H, 7.26 ppm; ¹³C{¹H} 77.2 ppm), toluene-*d*₈ (¹H, 2.08 ppm), and acetone-*d*₆ (¹H, 2.05 ppm; ¹³C{¹H}, 29.8 ppm). ³¹P{¹H} spectra obtained in deuterated solvents were referenced internally to H₃PO₄ at 0.00 ppm. ³¹P{¹H} spectra obtained in non-deuterated solvents were externally referenced to a sample of 85% H₃PO₄. Multiplicities are described as s (singlet), d (doublet), t (triplet), sept (septet), m (multiplet), and br (broad). Chemical shift assignments were obtained using 1D NMR spectroscopy, and hetero- and homonuclear 2D NMR spectroscopy (ie. COSY, HSQC, and HMBC). X-ray diffraction measurements were made on a Bruker Kappa Axis Apex2 diffractometer at a temperature of 110 K. Infrared spectra were collected on solid samples using a Bruker ALPHA II FTIR spectrometer. Charge-transfer Matrix Assisted Laser Desorption/Ionization (MALDI) mass spectrometry data were collected on an AB Sciex 5800 TOF/TOF mass spectrometer using pyrene as the matrix in a 20:1 molar ratio to complex. Solutions were prepared in C₆H₆ and spotted on a sample plate under an inert atmosphere and transferred to the instrument in a sealed Ziplock[®] bag. The instrument is equipped with a 349 nm OptiBeam On-Axis laser. The laser pulse rate was 400 Hz and data were collected in reflectron positive mode unless otherwise indicated. Reflectron mode was externally calibrated at 50 ppm mass tolerance. Each mass spectrum was collected as a sum of 500 shots. The acquired data sets were plotted in Microsoft Excel, and simulations for peaks of interest were acquired from chemcalc.org⁶ and plotted in Microsoft Excel. Quantification of ethane and methane was performed using an Agilent 7890a gas chromatogram with a flame ionization detector (GC-FID), fitted with HP-Plot/U column. GC-FID injections were performed manually using a 10 μL Hamilton 1700 Series gas tight syringe, unless otherwise indicated. Manual injections were performed by washing the gas-tight syringe with gaseous analyte headspace (5 × 10 μL), followed by a 5 μL gaseous headspace injection into the GC-FID instrument. Headspace gas chromatography mass spectrometry (GC-

MS) measurements to confirm ethane and methane formation were obtained on a Shimadzu GCMS-QP2010 instrument, fitted with a HP-Plot/U column.

I.II Ligand Synthesis

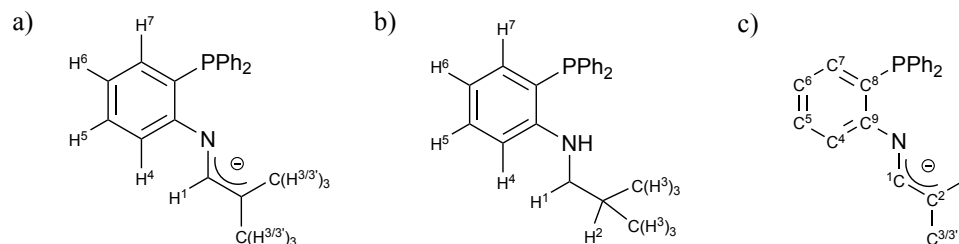


Figure S1. General labelling scheme for a) phosphine 1-azaallyl (P[^]AzA) ligand **L1**; b) phosphine amine ligand **H[L2]**; c) P[^]AzA ligand **L1**. This scheme will be used consistently for all compounds throughout the experimental. The denotations H³, H^{3'}, C³, and C^{3'} are used to distinguish between cases where atoms H³ and C³ are not equivalent.

Synthesis of Ph₂P(*o*-C₆H₄)NH(*i*-Bu), **H[L2]**:

A 100 mL Schlenk flask was charged with LiAlH₄ (92 mg, 2.41 mmol) and suspended in THF (8 mL). The Schlenk flask was then cooled to 0 °C and a solution of **L1** (200 mg, 0.60 mmol) in THF (2 mL) was added dropwise via ground-glass syringe, resulting in a colour change from clear and colourless to yellow-green. The flask was warmed to rt and stirred for 24 h. The reaction was then cooled to 0 °C, and the solution was diluted with Et₂O (10 mL). Water (0.09 mL) was added dropwise changing the solution colour from yellow-green to grey. A NaOH solution (15%, in 0.09 mL H₂O) and additional water (0.27 mL) were added sequentially and the reaction was warmed to rt and stirred for 15 min. Anhydrous Na₂SO₄ was then added and the reaction was stirred for another 15 min. The suspension was filtered, and the solvent was removed under vacuum to afford **H[L2]** as a clear oil, which slowly solidified at room temperature to form a waxy white solid. Yield = 156 mg (78%) ¹H NMR (599 MHz, CDCl₃): δ 7.25 – 7.20 (m, 10H, P-Ph(*H*)), 7.20 – 7.11 (m, 1H, *H*⁵), 6.71 (ddd, *J* = 7.7 Hz, 6.0 Hz, 1.7 Hz, 1H, *H*⁶), 6.59 – 6.47 (m, 2H, *H*⁴, *H*⁷), 4.59 (br, 1H, NH), 2.83 (t, *J* = 6.1 Hz 2H, *H*¹), 1.71 (septd, *J* = 6.7 Hz, 6.1 Hz, 1H, *H*²), 0.74 (d *J* = 6.7 Hz, 6H, *H*³). ¹³C {¹H} NMR (101 MHz, CDCl₃): δ 151.3 (d, ²*J*_{CP} = 19.2 Hz, C⁹), 135.6 (d, ²*J*_{CP} = 8.1 Hz, C⁷), 134.6 (d, *J*_{CP} = 5.1 Hz, P(Ph-C)), 133.9 (d, *J*_{CP} = 19.2 Hz, P(Ph-C)), 130.7 (C⁵), 128.8 (P(Ph-C)), 128.6 (d, *J*_{CP} = 6.1 Hz, P(Ph-C)), 118.6 (d, ¹*J*_{CP} = 10.1 Hz, C⁸) 116.8 (d, ³*J*_{CP} = 4.0 Hz, C⁶), 110.1 (d, ³*J*_{CP} = 2.0 Hz, C⁴), 51.8 (C¹), 27.8 (C²), 20.4 (C³). ³¹P {¹H} NMR (243

MHz, CDCl₃): δ -21.1. ATR-FTIR (cm⁻¹): ν 3502 (N-H) 2944 (Csp³-H) ESI-MS: m/z found 334.16; calc'd [H[L2]]⁺ 334.16.

Synthesis of K[Ph₂P(*o*-C₆H₄)N(*i*-Bu)], **K[L2]**:

In a 20 mL vial, **H[L2]** (198 mg, 0.59 mmol) was dissolved in THF (2 mL) and added dropwise to a stirring suspension of potassium hydride (48 mg, 1.19 mmol) in THF (2 mL). The vial containing **H[L2]** was washed with THF (3 \times 1 mL) and the mixture was stirred for 24 h. A gradual colour change was observed over the course of the first 20 min from clear and colourless, to bright yellow. Bubbles were also observed indicating the release of H₂. After 24 h the reaction mixture was filtered through Celite to remove excess KH, and the reaction vial was rinsed with 0.5 mL portions of THF until the washes were no longer yellow. The washes were filtered through Celite, combined with the bulk filtrate, and the solvent was removed under vacuum to afford a yellow oil. This oil was triturated with pentane (3 \times 5 mL) and dried under vacuum to give **K[L2]** as a yellow powder. Yield = 211 mg (95%). ¹H NMR (599 MHz, (CD₃)₂CO): δ 7.42 – 7.35 (m, 6H, P(Ph-*H*)), 7.34 – 7.27 (m, 4H, P(Ph-*H*)), 7.25 – 7.19 (m, 1H, *H*⁵), 6.77 – 6.73 (m, 1H, *H*⁶), 6.70 – 6.65 (m, 1H, *H*⁴), 6.59 – 6.53 (m, 1H, *H*⁷), 2.92 (d, J = 6.8 Hz, 2H, *H*¹), 1.78 – 1.72 (m, 1H, *H*²), 0.81 (d, J = 6.8 Hz, 6H, *H*³). ¹³C {¹H} NMR (101 MHz, CDCl₃): δ 151.9 (d, ² J_{CP} = 17.2 Hz, *C*⁹), 136.5 (d, ² J_{CP} = 8.1 Hz, *C*⁷), 135.1 (d, J_{CP} = 5.1 Hz, P-Ph(*C*)), 134.2 (d, J_{CP} = 19.2 Hz, P-Ph(*C*)), 131.5 (*C*⁵), 129.6 (P-Ph(*C*)), 129.4 (d, J_{CP} = 14.1 Hz, *C*¹) 117.3 (d, J_{CP} = 3.0 Hz, *C*⁶), 51.9 (*C*¹), 28.3 (*C*²), 20.5 (*C*³). ³¹P {¹H} NMR (243 MHz, CDCl₃): δ -21.3. MALDI MS (pyrene) collected in negative ion mode m/z found: 255.1, calc'd [L2-C₆H₅]⁻: 255.1. m/z found: 332.2, calc'd [L2]⁻: 332.2.

I.III Complex Synthesis

Synthesis of Sn(CD₃)₄:

In a glovebox, magnesium turnings (500 mg, 21.1 mmol) and diethyl ether (7 mL) were added to a two-neck 100 mL Schlenk flask. The flask was sealed with two rubber septa, removed from the glovebox and fitted with a reflux condenser on one neck. Deuterated iodomethane (2.78 g, 19.2 mmol) was slowly added in small dropwise portions through the side arm of the flask with a ground glass syringe, while the flask was periodically warmed with a heat gun to initiate reflux. Once reflux had begun the heat was removed and the remaining iodomethane was added dropwise at a rate maintaining gentle reflux. The reaction was stirred at rt for 2 h. The reaction was then cooled down to -30 °C and a solution of SnCl₄ (1.00 g, 3.84 mmol) in toluene (3 mL) was added dropwise through the side arm of the flask. The reaction was stirred for 16 h. The next day the grey mixture was quenched by slow addition of water (10 mL) at 0 °C. The suspension was filtered

through a gravity funnel with a filter paper, and the filtrate was extracted with diethyl ether (3×5 mL), the organic layers were washed with water (3×10 mL) and dried over Na_2SO_4 . The clear suspension was filtered through a gravity funnel with a filter paper and the filtrate was used immediately without further purification, a 50% yield was assumed for the subsequent reaction (*vide infra*). A 500 μL aliquot was removed and used directly for ^2H NMR spectroscopy. ^2H NMR (92.1 MHz, CH_2Cl_2): δ 0.62 (s, 12D, Sn- CD_3). A 100 μL aliquot was diluted with 400 μL of CD_2Cl_2 , this solution was used for $^{119}\text{Sn}\{^1\text{H}\}$ NMR spectroscopy. $^{119}\text{Sn}\{^1\text{H}\}$ NMR (223.8 MHz, CD_2Cl_2): δ -0.67 to -1.93 (m).

Synthesis of $\text{Pd}(\text{CD}_3)\text{Cl}(\text{COD})$:

The freshly made $\text{Sn}(\text{CD}_3)_4$ solution (30 mL), and dichloromethane (60 mL) were added to a 200 mL Schlenk flask. Against a flow of argon, $\text{PdCl}_2(\text{COD})$ (240 mg, 0.841 mmol) was added to the flask. The reaction was then allowed to stir until the colour changed from yellow to grey (ca. 16 h). The suspension was filtered through Celite, into a collection flask cooled and held at 0 °C. The reaction flask was washed with DCM (3×10 mL), and the washes were also filtered through Celite into the cooled collection flask. The volatiles were removed under reduced pressure at 0 °C to afford a beige powder. This powder was washed with cold diethyl ether (3×10 mL) to yield pure $\text{Pd}(\text{CD}_3)\text{Cl}(\text{COD})$. The previously removed volatiles were then collected and re-reacted with $\text{PdCl}_2(\text{COD})$ (100 mg, 0.37 mmol) as above. This was repeated until 95% of the theoretical yield based on starting $(\text{SnCD}_3)_4$ was achieved. Total yield = 293 mg (61%). Note: $\text{Pd}(\text{CD}_3)\text{Cl}(\text{COD})$ is thermally unstable and must be stored in a freezer. ^1H NMR (599 MHz, CDCl_3): δ 5.97 – 5.85(m, 2H, $\text{HC}=\text{CHCH}_2$) 5.20 – 5.08 (m, 2H, $\text{HC}=\text{CHCH}_2$), 2.75 – 2.40 (m, 8H, $\text{CHCH}_2\text{CH}_2\text{CH}$). ^2H NMR (92.1 MHz, CHCl_3): δ 1.15 (s, Pd- CD_3). $^{13}\text{C}\{^1\text{H}\}$ NMR (151 MHz, CDCl_3): δ) 124.0 ($\text{HC}=\text{CHCH}_2$), 100.7 ($\text{HC}=\text{CHCH}_2$), 31.0 ($\text{CHCH}_2\text{CH}_2\text{CH}$), 27.7 ($\text{CHCH}_2\text{CH}_2\text{CH}$), 11.7 (1:3:6:7:6:3:1 sept, $^1J_{\text{CD}} = 31.0$ Hz, Pd- CD_3). ATR-FTIR (cm^{-1}): ν 3010 ($\text{C}_{\text{sp}^2}\text{-H}$), 2925 ($\text{C}_{\text{sp}^3}\text{-H}$). All NMR data obtained from $\text{Pd}(\text{CD}_3)\text{Cl}(\text{COD})$ is consistent with the NMR data previously reported for its protio analogue $\text{Pd}(\text{CH}_3)\text{Cl}(\text{COD})$.¹

Synthesis of $[\text{Pd}(\text{CD}_3)(\text{L1})]_2$, **1-d₆**:

Prior to the beginning of the reaction, all glassware (except pipettes) and the reagents were stored in a freezer at -20 °C for at least 30 minutes. In a glovebox, **K[L1]** (65 mg, 0.18 mmol) was dissolved in cold THF (2 mL) and added dropwise to a suspension of $\text{PdCl}(\text{CD}_3)(\text{COD})$ dissolved in cold THF (2 mL). The reaction was stirred for 10 min and then placed in the freezer at -20 °C for 10 min. The reaction was filtered through Celite into a Büchner flask. The reaction volume was reduced in the Büchner flask to ca. 2 mL and the solution was transferred to a new 20 mL vial. The reaction vial was capped and stored in the freezer at -20 °C for 10 minutes. The volume was reduced to ca. 1 mL under vacuum and the solution was returned to the freezer at -20 °C for 5

minutes. Cold pentane (6 mL) was added with vigorous stirring to precipitate **1-d₆** as a yellow solid. The excess pentane was removed via pipette, and **1-d₆** was washed with cold pentane (3 × 1 mL) and dried under vacuum. Yield = 52 mg (76%). Note: **1-d₆** is thermally unstable and must be stored in a freezer, decomposition in solution occurs within 24 h at 25 °C while solid state decomposition occurs over several days at 25 °C. ¹H NMR (599 MHz, C₆D₆): δ 7.91 – 7.83 (m, 4H, P(Ph-*H*)), 7.51 (dd, *J* = 11.6 Hz, 7.5 Hz, 4H, (P(Ph-*H*))), 7.41 (dd, *J* = 8.4 Hz, 4.9 Hz, 2H, *H⁵*), 7.17 – 7.15 (m, 4H, P(Ph-*H*)), 7.12 – 7.07 (m, 2H, *H⁶*), 7.05 – 7.00 (m, 8H, P(Ph-*H*)), 6.99 – 6.95 (m, 4H, *H⁴*, *H⁷*), 6.64 – 6.58 (m, 2H, *H¹*), 1.72 (s, 6H, *H³*), 1.42 (br s, 6H, *H³*). ²H NMR (92 MHz, C₆H₆): δ = 0.44 (m, Pd-CD₃). ³¹P{¹H} NMR (243 MHz, C₆D₆): δ 43.7 (s). MALDI MS (pyrene) *m/z* found 435.1, calc'd [Pd(**L1**)]⁺ 435.0. All NMR data obtained from **1-d₆** is consistent with the NMR data previously reported for its protio analogue **1**.⁴

Synthesis of [Pd(CH₃)(**L2**)]₂, **4**:

Prior to beginning the reaction, all glassware (except pipettes) and the reagents were stored in a freezer at –20 °C for at least 30 minutes. In a 20 mL vial, PdCl(CH₃)(COD) (39 mg, 0.15 mmol) was dissolved in THF (1 mL). To this vial was added 375 μL (0.19 mmol) of a 500 μM stock solution of pyridine in THF. Ligand **K[L2]** (65 mg, 0.17 mmol) was dissolved in THF (1 mL) and added dropwise to the Pd solution. The solution changed colour from yellow dark orange almost immediately. The reaction was stirred for 10 min and filtered through Celite. The vial was washed with THF (3 × 1 mL) and the washes were filtered through Celite. The filtrates were combined, and the solvent was removed under vacuum to produce a dark orange residue. Cold pentane (5 mL) was added to dissolve the residue, and the vial was stored in the freezer at –20 °C to produce yellow crystals of **4**. Yield = 35 mg (45%). **Note**: it was not possible to fully remove pyridine from the sample, ca. 20 mol% py was present as judged by ¹H NMR spectroscopy. Compound **4** is thermally unstable and must be stored in a freezer, decomposition in solution occurs within 24 h at 25 °C, while solid state decomposition occurs over several days at 25 °C. ¹H NMR (599 MHz, C₆D₆): δ 7.96 – 7.87 (m, 8H, P-Ph(*H*)), 7.29 – 7.25 (m, 2H, *H⁵*), 7.12 – 7.03 (m, 14H, P-Ph(*H*), *H⁶*), 6.82 – 6.78 (m, 2H, *H⁴*), 6.37 – 6.33 (m, 2H, *H⁷*), 3.03 (d, *J* = 6.6 Hz, 4H, *H¹*), 1.96 (sept, *J* = 6.6 Hz, 2H, *H²*), 0.81 (d, *J* = 6.6 Hz, 12H, *H³*), 0.43 (d, *J*_{HP} = 1.8 Hz, 6H, Pd-CH₃). ¹³C{¹H} NMR (101 MHz, CDCl₃): δ 167.4 (d, *J*_{CP} = 23.23 Hz, C⁹), 134.5 (P-(Ph-C)), 134.0 (d, *J*_{CP} = 53.5 Hz, P-(Ph-C)), 133.9 (d, *J*_{CP} = 11.1 Hz, P-(Ph-C)), 133.5 (d, *J*_{CP} = 2.0 Hz, C⁷), 130.1 (d, *J*_{CP} = 3.0 Hz, P-(Ph-C)), 128.6 (d, *J*_{CP} = 11.2 Hz, P-(Ph-C)), 112.7 (d, *J*_{CP} = 57.6 Hz, C⁸), 111.6 (d, *J*_{CP} = 13.1 Hz, C⁶), 110.1 (d, *J*_{CP} = 9.09 Hz, C⁴), 57.5 (C¹), 28.2 (C²), 21.2 (C³), –4.6 (d, *J*_{CP} = 6.06 Hz, Pd-CH₃). ³¹P{¹H} NMR (243 MHz, C₆D₆): δ 46.8. MALDI MS (pyrene) found 876.1, calc. [(**4**-(Me)₂)]⁺: 876.1. ATR-FTIR (cm⁻¹): ν 1451 (C_{sp²}-P), 1095 (C-N). Crystals suitable for X-ray diffraction were obtained by slow evaporation of pentane from a solution of **4** at –20 °C, details are provided in Section VIII.

Synthesis of [Pt(CH₃)(L1)]₂, **5**:

In two separate 20 mL vials, **K[L1]** (56 mg, 0.15 mmol) and [Pt(CH₃)Cl(COD)] (44 mg, 0.13 mmol) were dissolved in THF (1.5 mL) and stored in a freezer at -20 °C for ca. 10 min prior to the reaction. **K[L1]** was then added dropwise to a stirred solution of [PtCl(CH₃)(COD)] resulting in an immediate colour change from clear to orange. The reaction was stirred for 10 minutes. The reaction was then filtered through a pipette plugged with a microfiber filter and Celite into a vial. The solvent of the filtrate was reduced under vacuum to ca. 1 mL and the vial was stored in the freezer at -20 °C for ca. 10 min. Cold pentane (10 mL) was added with vigorous stirring to precipitate **5** as an orange solid. The pentane was then decanted and the orange solid was washed with cold pentane (3 × 1 mL) and dried under vacuum. Yield = 47 mg (69%). **5** is thermally unstable and must be stored in a freezer, decomposition in solution occurs within 24 h at 25 °C, while solid state decomposition occurs over several days at 25 °C. Mass purity 98% as judged by ¹H NMR spectroscopy. ¹H NMR (599 MHz, C₆D₆): δ 8.10 – 7.92 (m, 4H, P-Ph(*H*)), 7.65 – 7.55 (m, 4H, P-Ph(*H*)), 7.51 (dd, *J* = 8.3, 4.8 Hz, 2H, *H*⁶), 7.22 – 7.16 (m, 4H, P-Ph(*H*)), 7.09 – 7.00 (m, 8H, P-Ph(*H*)), 7.00 – 6.94 (m, 4H, *H*^{5/7}), 6.67 – 6.58 (m, 2H, *H*⁴), 1.66 (s, 12H, *H*^{3/3'}), 0.77 (d, ³*J*_{HP} = 1.9 Hz, 6H, Pd-CH₃). ¹³C{¹H} NMR (151 MHz, CDCl₃): δ 165.4 (*C*⁹), 142.8 (*C*¹), 134.4 (d, *J*_{CP} = 18.9 Hz, P-Ph(*C*)), 133.4 (d, *J*_{CP} = 16.6 Hz, Ph(*C*), 132.1 (P-Ph(*C*)), 130.9 (P-Ph(*C*)), 130.6 (P-Ph(*C*)), 129.9 (P-Ph(*C*)), 128.6 (*C*), 122.2 (*C*⁷), 120.3 (*C*²), 23.8 (*C*³), 18.35 (br, *C*³) – 15.1 (Pd-CH₃). ³¹P{¹H} NMR (243 MHz, C₆D₆): δ 20.4 (s, with ¹⁹⁵Pt satellites, ¹*J*_{P-Pt} = 4399 Hz). MALDI MS (pyrene) *m/z* found 524.1, calc. [**5**-(Pt(L1)(Me)₂)]⁺: 524.1. *m/z* found 1049.2, calc. [**5**-(Me)₂]⁺: 1049.2. ATR-FTIR (cm⁻¹): ν 1434 (*Csp*²-P), 1100 (C-N).

Synthesis of Pt(L1)₂, **6**:

In a glovebox, **5** (45 mg, 0.04 mmol) was dissolved in C₆H₆ (5 mL) and added to a 25 mL Schlenk tube. The tube was sealed and removed from the box, and heated at 70 °C for 2.5 h under a flow of argon. The reaction was cooled to room temperature and the solvent was removed via vacuum to produce a dark brown residue. The residue was washed with pentane (3 × 3 mL), the washes were combined and the solvent was removed to produce a yellow solid. The solid was washed with diethyl ether (3 × 3 mL), the washes were combined and the solvent was removed to afford **6** as an orange solid which was dried under vacuum. Mass purity 97% as judged by ¹H NMR spectroscopy. Yield = 19 mg (54%). ¹H NMR (599 MHz, C₆D₆): δ 7.34 – 7.25 (m, 4H, P-Ph(*H*)), 7.12 – 7.07 (m, 2H, *H*⁵), 6.96 (m, 2H, *H*¹), 6.95 – 6.90 (m, 4H, P-Ph(*H*)), 6.86 – 6.80 (m, 8H, P-Ph(*H*)), 6.75 – 6.69 (m, 8H, P-Ph(*H*), *H*^{6/7}), 6.35 – 6.28 (m, 2H, *H*⁴), 1.96 (s, 6H, *H*^{3/3'}), 1.92 (s, 6H, *H*^{3/3'}). ¹³C{¹H} NMR (151 MHz, CDCl₃): δ 166.9 – 166.1 (m, *C*⁹), 135.9 (*C*¹), 133.9 – 133.2 (m, P-Ph(*C*), *C*⁸), 132.3 (P-Ph(*C*)), 130.4 (*C*⁵), 130.2 (P-Ph(*C*)), 128.1 (P-Ph(*C*)), 120.3 (*C*⁴), 117.3 (m, *C*²), 114.0 (*C*⁶), 113.8 – 113.5 (m, *C*⁷), 23.4 (*C*³), 18.5 (s, *C*³). ³¹P{¹H} NMR (243 MHz, C₆D₆): δ 28.0 (s, with ¹⁹⁵Pt satellites, ¹*J*_{P-Pt} = 5208 Hz). MALDI MS (pyrene) *m/z* found 524.1, calc. [**6**-

[L1]⁺: 524.1. *m/z* found 855.2, calc. **[6]**⁺: 855.2. Crystals suitable for X-ray diffraction were obtained by solvent diffusion from a THF solution of **6** while using pentane as the anti-solvent at -20 °C, details are provided in Section VIII.

Synthesis of K[Pd(CH₃)₂(L1)], **K[7]**:

Prior to the beginning of the reaction, all glassware (except pipettes) and reagents were stored in a freezer at -30 °C for at least 30 minutes. In a glovebox, ligand **K[L1]** (78 mg, 0.21 mmol) and Pd(CH₃)₂(COD) (43 mg, 0.17 mmol) were weighed out in two separate 20 mL vials. Ligand **K[L1]** was dissolved in THF (1 mL) and the two vials were placed in a freezer at -30 °C for ca. 15 min Cold THF (0.5 mL) was then added to dissolve Pd(CH₃)₂(COD), and the cold solution of **K[L1]** was immediately added dropwise to the solution of Pd(CH₃)₂(COD). The reaction vial was swirled and placed in the freezer at -30 °C for 10 min The solution was then filtered through Celite and the solvent was removed under vacuum to generate an orange residue. The residue was triturated with pentane (3 × 3 mL) to produce **K[7]** as a yellow crystalline solid and dried under vacuum. Yield = 87 mg (99%). **K[7]** is thermally unstable and must be stored in a freezer, storage longer than 2 weeks leads to decomposition even at -30 °C. Mass purity 90% as judged by ¹H NMR spectroscopy. ¹H NMR (599 MHz, (CD₃)₂CO): δ 7.61 (m, 4H, P-Ph(*H*)), 7.31 – 7.23 (m, 6H, P-Ph(*H*)), 6.82 – 6.76 (m, 1H, *H*⁵), 6.72 – 6.66 (m, 1H, *H*⁶), 6.20 – 6.14 (m, 1H, *H*⁷), 6.04 (s, 1H, *H*¹) 5.79 (m, 1H, *H*⁴), 1.73 (s, 3H, *H*^{3/3'}), 1.48 (s, 3H, *H*^{3/3'}), 0.00 (d, *J* = 7.2 Hz, 3H, P-Pd-*cis*-CH₃), -0.05 (d, 7.8 Hz, 3H, P-Pd-*trans*-CH₃). ¹³C{¹H} NMR (151 MHz, 0 °C, (CD₃)₂CO): δ 165.8 (d, *J*_{CP} = 30.2 Hz, C⁹), 138.8 (d, *J*_{CP} = 25.7 Hz, P(Ph-C), 135.7 (C¹), 133.9 (d, *J*_{CP} = 13.6 Hz, C⁸), 133.3 (C⁵), 128.6 (P(Ph-C)), 128.8 (d, *J*_{CP} = 10.6 Hz, C⁴) 127.9 (d, *J*_{CP} = 9.1 Hz, P(Ph-C), 115.5 (d, *J*_{CP} = 39.3 Hz P(Ph-C), 113.6 (C²), 112.4 (d, *J*_{CP} = 12.1 Hz, C⁷), 107.4 (d, *J*_{CP} = 6.0 Hz, C⁶), 21.9 (C^{3/3'}), 17.7 (C^{3/3'}), 7.9 (d, ²*J*_{CP} = 117.8 Hz, P-Pd-*trans*-CH₃), -11.6 (d, ²*J*_{CP} = 6.04 Hz, *cis*-Pd-CH₃). ³¹P{¹H} NMR (243 MHz, (CD₃)₂CO): δ = 22.5. ATR-FTIR (cm⁻¹): ν 1433 (Csp²-P), 1098 (C-N). MALDI MS (pyrene) collected in negative ion mode *m/z* found 330.2, calc. **[L1]**⁻: 330.1. *m/z* found 436.1, calc. **[7-(Me)₂]**⁻: 436.1. *m/z* found 766.2, calc [(C₂₂H₂₁NP)₂Pd]⁻: 766.2.

Attempted Synthesis of [Pd(L1)₂Pd(CH₃)₂], **8**:

Room Temperature: In a glovebox, **3** (6 mg, 0.008 mmol) and Pd(CH₃)₂(COD) (Run a: 28 mg, 0.12 mmol; or Run b: 4 mg, 0.015 mmol) were weighed into two separate 4 mL vials and dissolved in C₆D₆ (250 μL each). Complex **3** was then added dropwise to each of the solutions of Pd(CH₃)₂(COD) and the mixtures were each added to an NMR tube. The NMR tubes stood at rt for ca. 16 h total inside a glovebox and ¹H and ³¹P{¹H} NMR spectra were acquired on each tube after 30 minutes, 1 h, 4.5 h, and 16 h. Complete conversion from **3** to **1** was observed in Run a

after 4.5 h. Complete conversion was not observed in Run b and several new minor products were observed by $^{31}\text{P}\{^1\text{H}\}$ NMR spectroscopy. Complex **8** was not observed during either reaction.

0 °C: A similar procedure to the room temperature experiments was used with the following changes: $\text{Pd}(\text{CH}_3)_2(\text{COD})$ (5 mg, 0.020 mmol), and $\text{tol-}d_8$ was the solvent. The NMR tube stood in an ice bath held at 0 °C for 6 h total. ^1H and $^{31}\text{P}\{^1\text{H}\}$ NMR spectra were acquired after 30 minutes, 1 h, 4.5 h, and 6 h. Complete conversion was not observed, and conversion did not increase from 4.5 h to 6 h. Complex **8** was not observed during this reaction.

Table S1. Summary of Selected ^1H , and $^{13}\text{C}\{^1\text{H}\}$ NMR Spectroscopy Data for Known 1-Aza complexes.^{3,4}

	H^1	C^1	C^2
$\kappa^1\text{-N}$	7.28	149.8-187.5	66.3-114.8
$\eta^3\text{-NCC}$	N/A	151.9-184.9	42.0-64.5
$\mu(\kappa^1\text{-N};\eta^2\text{-CC})$	5.97	109.0	74.5

II Experimental Procedures

II.I Kinetic Data:

Rate Data:

Two solutions of **1** in C_6H_6 were prepared (22 mM, 62 mM) and added to two separate NMR tubes (A and B), along with a sealed capillary of triphenylphosphine oxide (TPPO) in C_6H_6 (47 mM). Each NMR tube was placed into the spectrometer and an initial spectrum (time = 0, T_0) was acquired at room temperature with the T_1 relaxation delay set to 5 s. The tube was removed from the spectrometer and placed in a fridge (4 °C) while the instrument heated to 70 °C. Each tubes was placed into the spectrometer and a $^{31}\text{P}\{^1\text{H}\}$ NMR spectrum was acquired every 5 minutes for 2 h (T_1 relaxation delay of 5 s.) The consumption of **1** was monitored vs. TPPO, and plots of $[\mathbf{1}]$, $\text{Ln}[\mathbf{1}]$, and $1/[\mathbf{1}]$ vs. Time (min) were constructed using this data. The resulting rate plot from $\text{Ln}[\mathbf{1}]$ vs. Time gave an excellent linear fit, consistent with a first order reaction. These reactions were performed in duplicate.

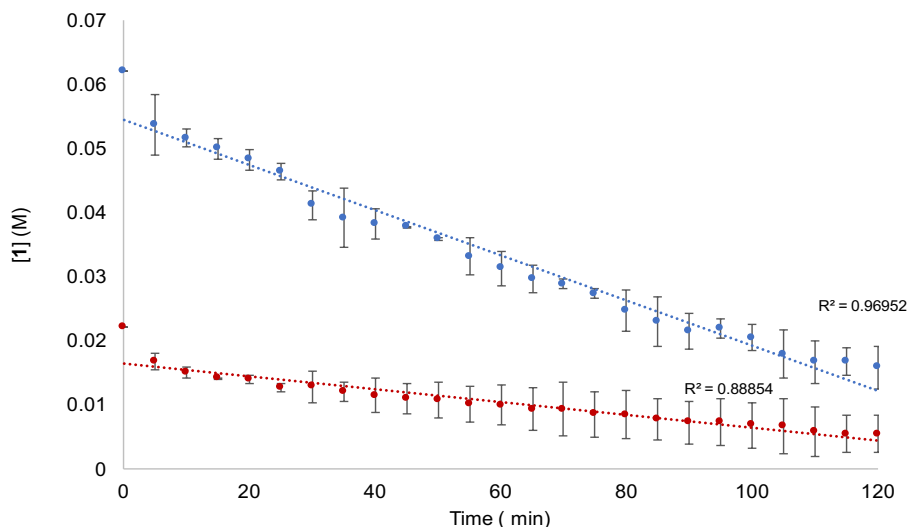


Figure S2. Zero order in **1** manipulation. Plot of concentration of **1** (M) vs. time (min) generated from $^{31}\text{P}\{^1\text{H}\}$ NMR spectroscopy integrations from spectra of a solution of **1** in C_6H_6 heated at 70°C for 2.5 h. A $^{31}\text{P}\{^1\text{H}\}$ NMR spectrum was acquired every 5 min with a T_1 delay = 5 s. Concentration of **1** determined by integration relative to TPPO (47 mM). Initial concentrations of **1** = 62 mM (blue), and 22 mM (red). Error bars are an average of two runs.

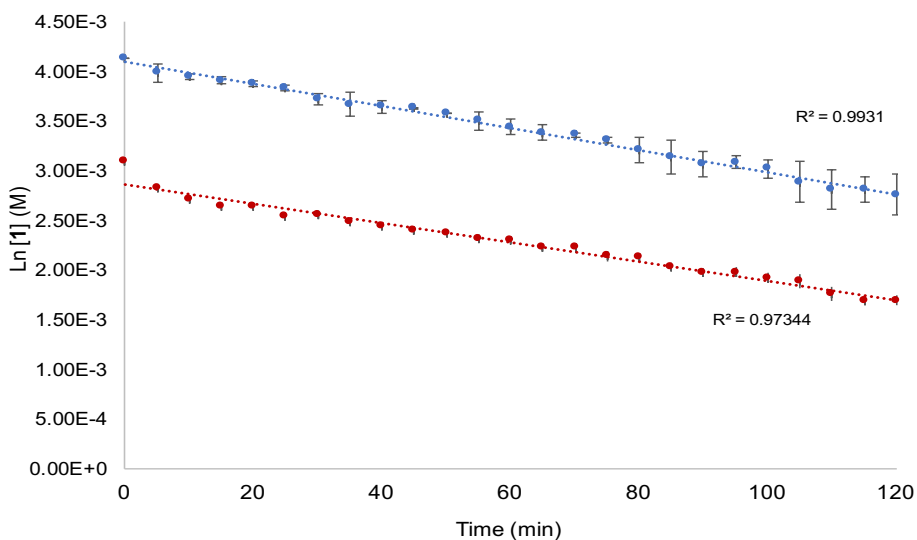


Figure S3. First order in **1** manipulation. Plot of $\text{Ln}[1]$ (M) vs. time (min) generated by $^{31}\text{P}\{^1\text{H}\}$ NMR spectroscopy integrations from spectra of a solution of **1** in C_6H_6 heated at 70°C for 2.5 h. A $^{31}\text{P}\{^1\text{H}\}$ NMR spectrum was acquired every 5 min with a T_1 delay = 5 s. Concentration of **1** determined by integration relative to TPPO (47 mM). Initial concentrations of **1** = 62 mM (blue), and 22 mM (red). Error bars are an average of two runs.

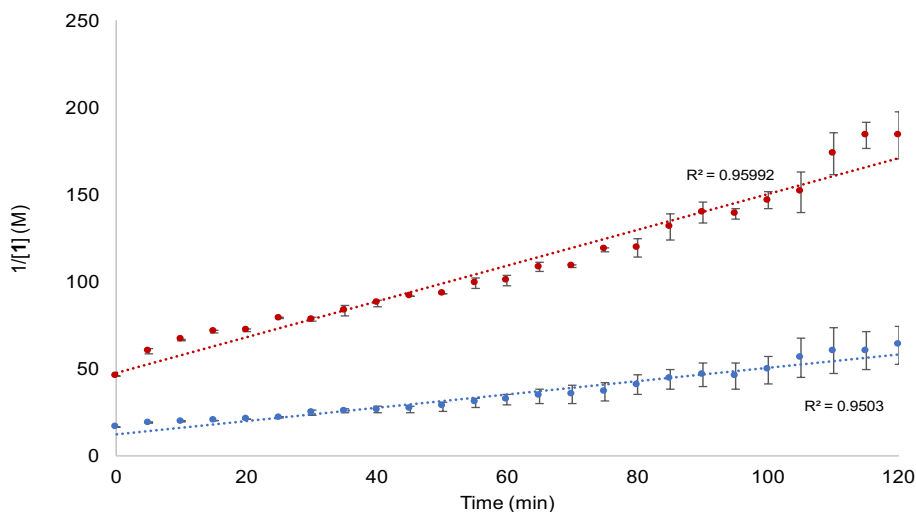


Figure S4. Second order in **1** manipulation. Plot of concentration of $1/[1]$ (M) vs. time (min) generated by $^{31}\text{P}\{^1\text{H}\}$ NMR spectroscopy integrations from spectra of a solution of **1** in C_6H_6 heated at 70°C for 2.5 h. A $^{31}\text{P}\{^1\text{H}\}$ NMR spectrum was acquired every 5 min with a T_1 delay = 5 s. Concentration of **1** determined by integration relative to TPPO (47 mM). Initial concentrations of **1** = 62 mM (blue), and 22 mM (red).

Eyring Analysis

An 8 mL stock solution of **1** in C_6D_6 (80 mM) was prepared and stored in a freezer at -20°C prior to NMR analysis. The sample was thawed and a $500\ \mu\text{L}$ aliquot was removed and added to an NMR tube, along with a sealed capillary of dimethyl terephthalate (DMTP) in C_6D_6 (31 mM). The NMR tube was then placed into an NMR spectrometer and an initial (T_0) ^1H NMR spectrum was acquired at room temperature. The tube was removed from the spectrometer and placed in a fridge (4°C) while the instrument was heated to 70, 60, 55, 50, or 40°C . A ^1H NMR spectrum was then acquired every 45 s for 1.15 h at the given temperature. The consumption of **1** was monitored vs. DMTP, and plots of $\text{Ln}[\mathbf{1}]$ vs. Time (s) were constructed for each set of data at the five different temperatures. The resulting rate plots gave excellent linear fit, and the rate constants (k) were extracted from the slope of each generated plot. An Eyring plot of $\text{ln}(k/T)$ vs. $1/T$ ($\times 10^3\ \text{K}^{-1}$) was generated using the acquired rate constants. The ΔS^\ddagger for the reaction was extracted from the y-intercept. The ΔH^\ddagger for the reaction was extracted from the slope. The ΔG^\ddagger for the reaction at $T = 273.15$ and $343.15\ \text{K}$ was acquired using the Gibbs Free Energy formula, and the calculated values of ΔH^\ddagger and ΔS^\ddagger .

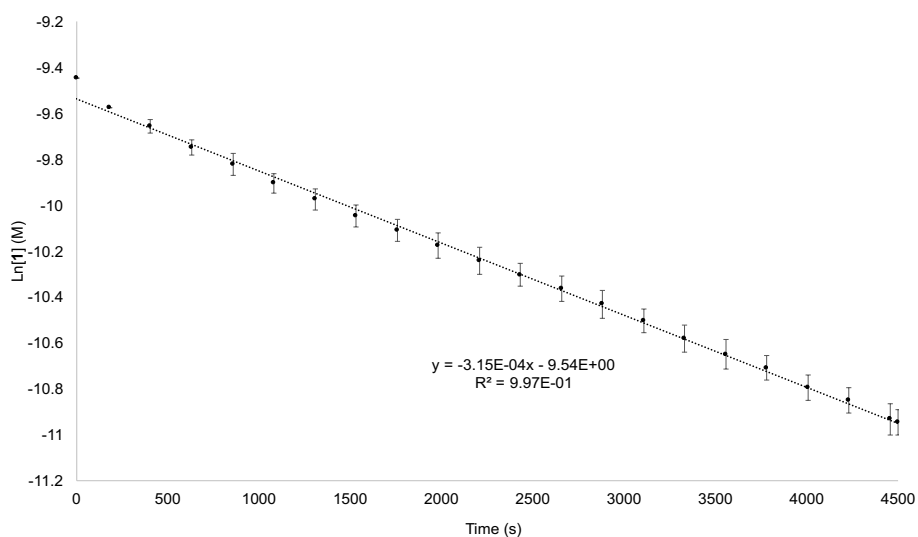


Figure S5. Plot of Ln[1] (M) vs. time (s) generated by ^1H NMR spectroscopy integrations from spectra of a solution of **1** in C_6D_6 heated at $70\text{ }^\circ\text{C}$ for 1.15 h heating a solution. A ^1H NMR spectrum was acquired every 45 s. Concentration of **1** determined by integration relative to DMTP (31 mM). Error bars are an average of two runs.

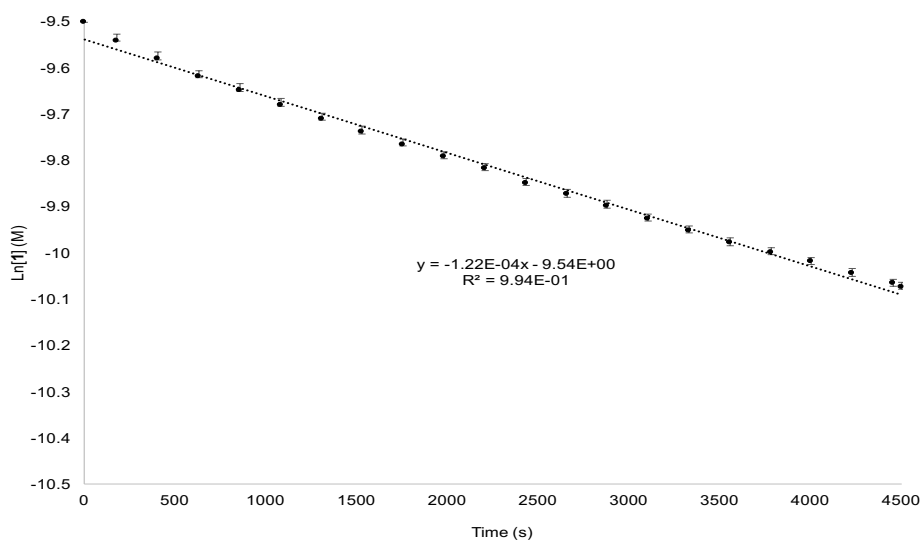


Figure S6. Plot of Ln[1] (M) vs. time (s) generated by ^1H NMR spectroscopy integrations from spectra of a solution of **1** in C_6D_6 heated at $60\text{ }^\circ\text{C}$ for 1.15 h heating a solution. A ^1H NMR spectrum was acquired every 45 s. Concentration of **1** determined by integration relative to DMTP (31 mM). Error bars are an average of two runs.

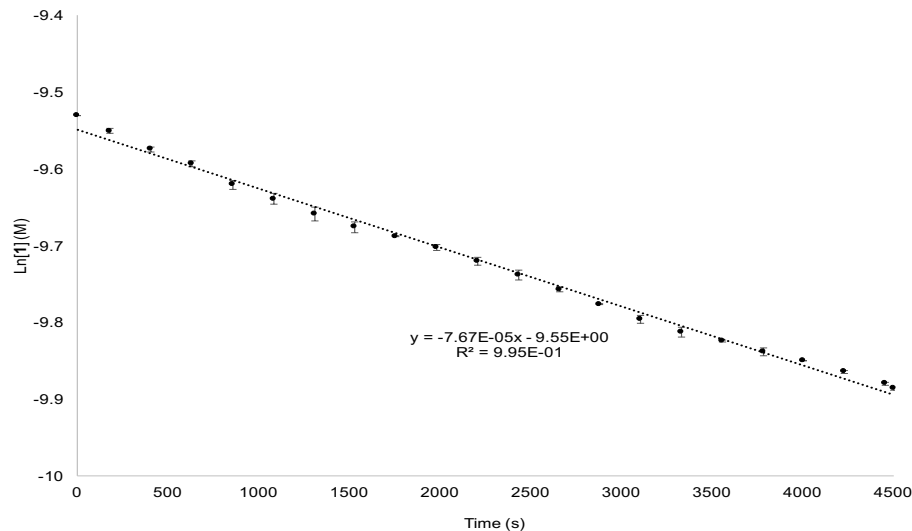


Figure S7. Plot of $\text{Ln}[1]$ (M) vs. time (s) generated by ^1H NMR spectroscopy integrations from spectra of a solution of **1** in C_6D_6 heated at $55\text{ }^\circ\text{C}$ for 1.15 h heating a solution. A ^1H NMR spectrum was acquired every 45 s. Concentration of **1** determined by integration relative to DMTP (31 mM). Error bars are an average of two runs.

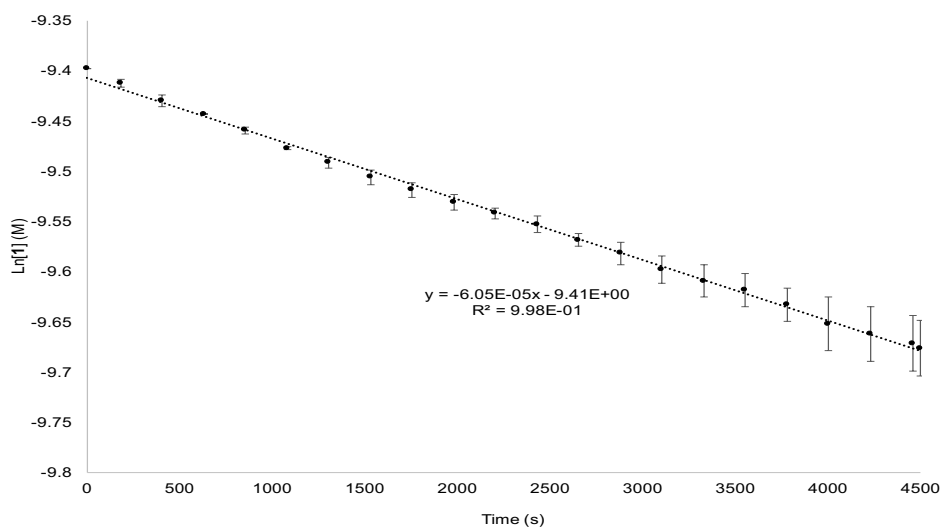


Figure S8. Plot of $\text{Ln}[1]$ (M) vs. time (s) generated by ^1H NMR spectroscopy integrations from spectra of a solution of **1** in C_6D_6 heated at $50\text{ }^\circ\text{C}$ for 1.15 h heating a solution. A ^1H NMR spectrum acquired was every 45 s. Concentration of **1** determined by integration relative to DMTP (31 mM). Error bars are an average of two runs.

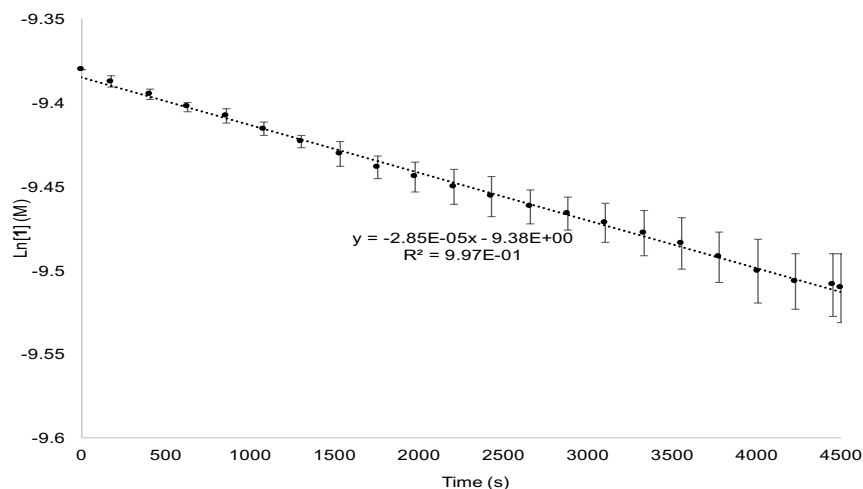


Figure S9. Plot of $\text{Ln}[1]$ (M) vs. time (s) generated by ^1H NMR spectroscopy integrations from spectra of a solution of **1** in C_6D_6 heated at 40°C for 1.15 h heating a solution. A ^1H NMR spectrum was acquired every 45 s. Concentration of **1** determined by integration relative to DMTP (31 mM). Error bars are an average of two runs.

II.II Radical Tests

Complex **1** (11 mg, 0.012 mmol) was dissolved in C_6D_6 (500 μL) and the solution was added to an NMR tube along with a sealed capillary containing DMTP dissolved in C_6D_6 (31 mM). The NMR tube was sealed with a rubber septum, and a T_0 ^1H NMR spectrum was acquired at room temperature. The tube was removed from the spectrometer and 35 equiv of the selected H-atom donor (1,4-cyclohexadiene or 9,10-dihydroanthracene) was added to the tube via a 100 mM solution in C_6D_6 via syringe. The NMR tube was hand swirled for 20 s and heated at 70°C for 2.5 h in an oil bath. The NMR tube was cooled to room temperature and ^1H and $^{31}\text{P}\{^1\text{H}\}$ NMR spectra were acquired.

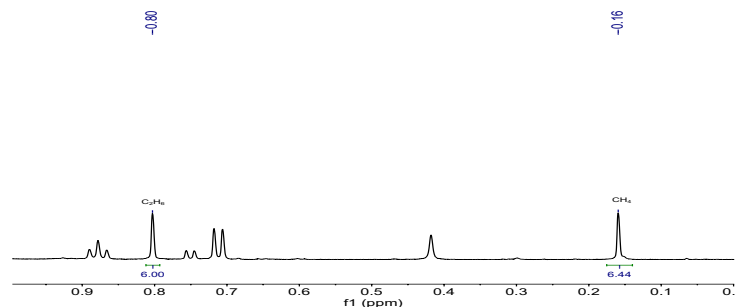


Figure S10. ^1H NMR spectrum of a solution of **1** and 35 equiv of 1,4-CHD in C_6D_6 that was heated at 70°C for 2.5 h. The NMR tube was cooled to rt prior to obtaining the spectrum. The chemical shift range of 0-1 ppm is shown, which is the range for product signals of C_2H_6 , and CH_4 (599 MHz, C_6D_6).

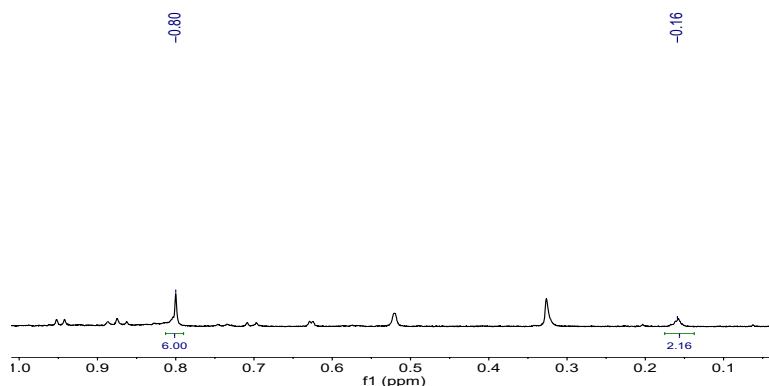


Figure S11. ^1H NMR spectrum of a solution of **1** and 35 equiv of 9,10-DHA in C_6D_6 that was heated at 70°C for 2.5 h. The NMR tube was cooled to rt prior to obtaining the spectrum. The chemical shift range of 0-1 ppm is shown, which is the range for product signals of C_2H_6 , and CH_4 (599 MHz, C_6D_6).

II.III Crossover Experiments

Filled Tube Experiment

Complex **1** (11 mg, 0.125 mmol) and **1- d_6** (11 mg, 0.125 mmol) were each dissolved in C_6D_6 (500 μL) and added to an oven-dried J. Young NMR tube. The vials were washed with C_6D_6 ($2 \times 300 \mu\text{L}$) and the washes were added to the NMR tube. The total volume of solution in the tube was 2.2 mL, leaving a headspace of $< 10\%$ by volume. The tube was placed in an oil bath at 70°C until the reaction was completed (ca. 2.5 h). The tube was cooled was to rt and a ^1H NMR spectrum was acquired with the T1 relaxation time set to 25 s. The ratio of ethane to ethane- d_3 was determined by integration of the respective signals in the ^1H NMR spectrum.

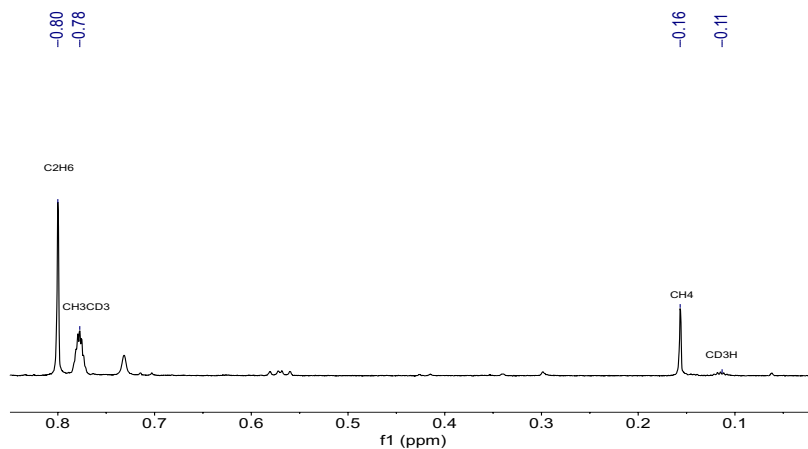


Figure S12. ^1H NMR spectrum of a solution of **1** and **1- d_6** in C_6D_6 that was heated at 70°C for 2.5 h. The NMR tube was cooled to rt prior to obtaining the spectrum. The chemical shift range of 0-1 ppm is shown, which is the range for product signals of C_2H_6 , and CH_4 (599 MHz, C_6D_6).

GC-MS Analysis

Complex **1** (11 mg, 0.125 mmol) and **1-*d*₆** (11 mg, 0.125 mmol) were each dissolved in C₆D₆ (500 μL) and added to an NMR tube. The NMR tube was sealed with a rubber septum cap and placed in an oil bath at 70 °C until the reaction was complete (ca. 2.5 h). The tube was cooled to rt and the headspace gases were injected into a GC-MS, and the chromatogram revealed an approximate 1:2:1 mixture of ethane: ethane-*d*₃: ethane-*d*₆.

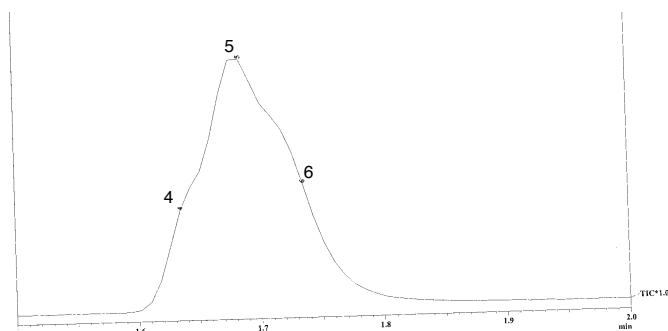
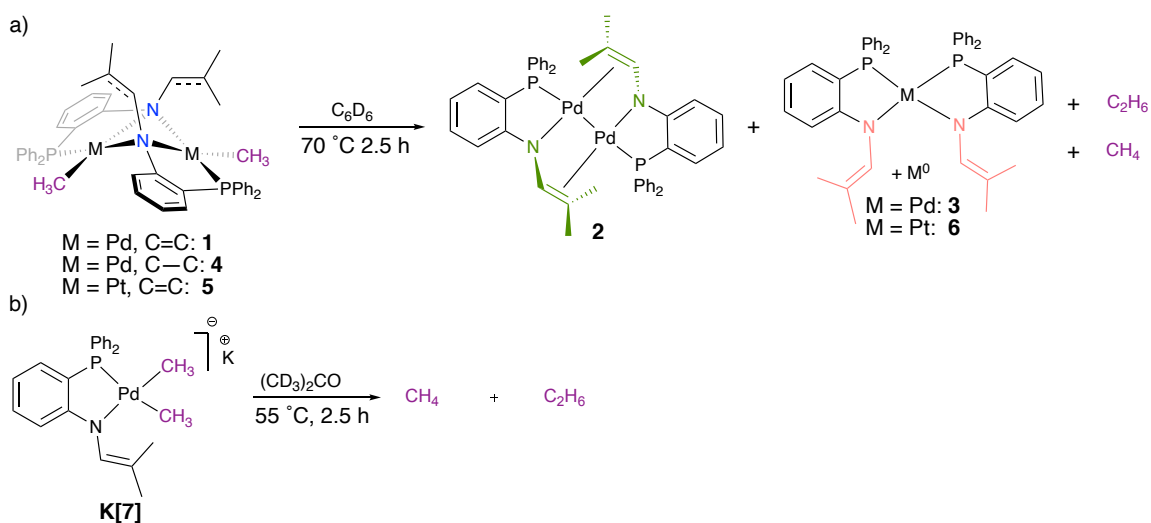


Figure S13. GC-MS spectrum of the headspace after heating **1** and **1-*d*₆** for 2.5 h at 70 °C, zoomed in to see the formation of C₂H₆ (4), C₂D₆ (5), and C₂H₃D₃ (6).

II.IV General Thermolysis Procedure

Solutions of **1**, **4**, or **6** (6 mg, 0.007, 0.007, and 0.006 mmol) in C₆D₆ (500 μL) or **K[7]** (6mg, 0.01 mmol) in acetone-*d*₆ (500 μL) was added to an NMR tube and the tube was sealed with a rubber septum. The NMR tube was heated in an oil bath at 70 °C (C₆D₆) (Scheme S1a), or 50 °C ((CD₃)₂CO) (Scheme S1b) for 2.5 h. The tube was cooled to room temperature and a ¹H and ³¹P{¹H} NMR spectrum was acquired to determine if methane or ethane were formed, and to inspect the organometallic products. Using a gas-tight syringe, 7 μL of the headspace was injected into a GC-FID. The yields of ethane and methane were determined through headspace analysis, using calibration curves generated by injection of the pure gaseous organic product into an NMR tube containing C₆H₆ (500 μL) or acetone (500 μL) as previously reported.⁴



Scheme S1. a) Solutions of **1**, **4**, and **5** in C_6D_6 were heated at $70\text{ }^\circ\text{C}$ for 2.5 h. b) A solution of **K[7]** in $(\text{CD}_3)_2\text{CO}$ was heated at $50\text{ }^\circ\text{C}$ for 2.5 h.

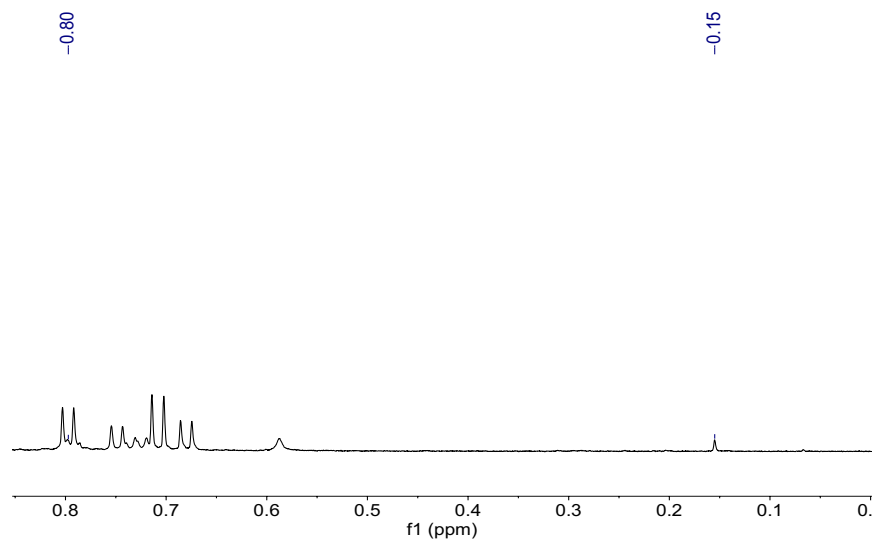


Figure S14. ^1H NMR spectrum of a solution of **4** in C_6D_6 after heating at $70\text{ }^\circ\text{C}$ for 2.5 h. The NMR tube was cooled to rt prior to data collection. $\delta: 0.80 = \text{C}_2\text{H}_6$ (s), $0.15 = \text{CH}_4$ (s) (599 MHz, C_6D_6).

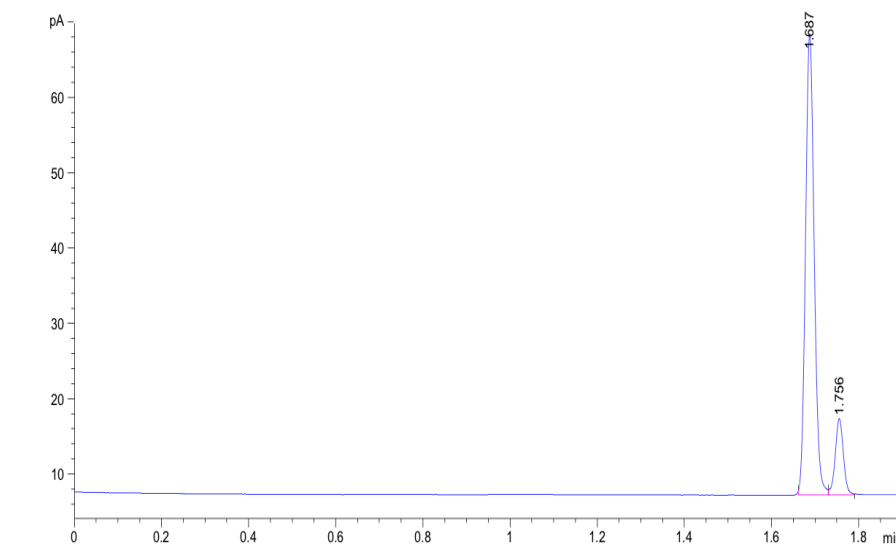


Figure S15. GC-FID chromatogram of a solution of **4** heated in C_6D_6 at $70\text{ }^\circ\text{C}$ for 2.5 h. NMR tube was cooled to rt prior to injection into the instrument. Peak assignment: 1.687 min = CH_4 , 80%; 1.756 min = C_2H_6 , 20%.

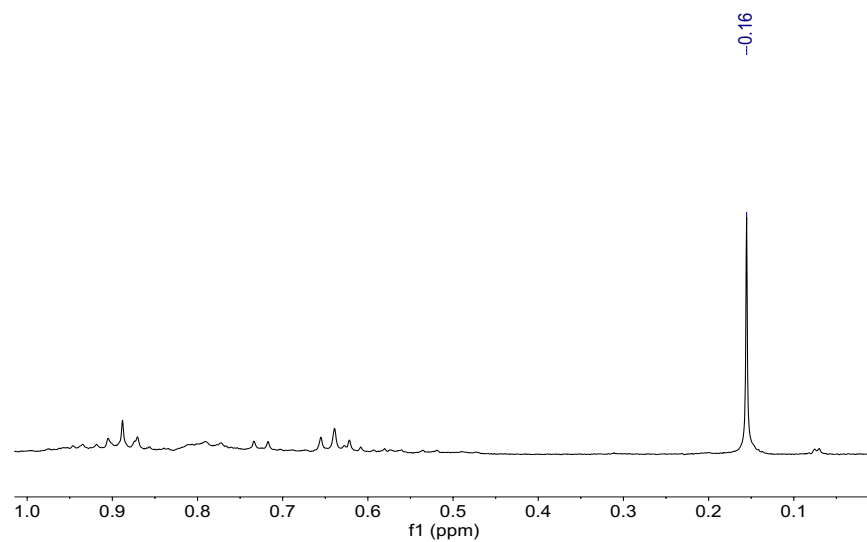


Figure S16. 1H NMR spectrum of a solution of **5** in C_6D_6 after heating at $70\text{ }^\circ\text{C}$ for 2.5 h. The NMR tube was cooled to rt prior to data collection. 0.16 = CH_4 (s) (599 MHz, C_6D_6).

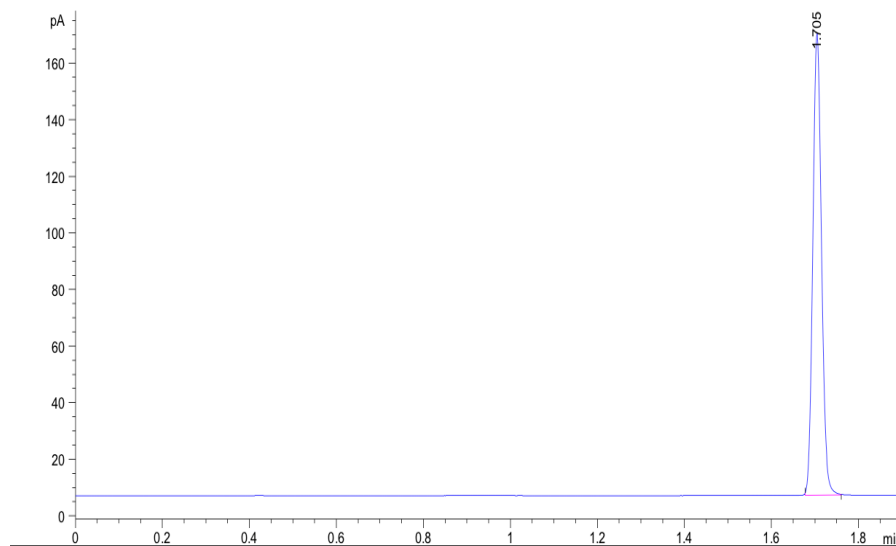


Figure S17. GC-FID chromatogram of a solution of **5** heated in C_6D_6 at $70\text{ }^\circ\text{C}$ for 2.5 h. NMR tube was cooled to rt prior to injection into the instrument. Peak assignment: 1.705 min = CH_4 , 100%.

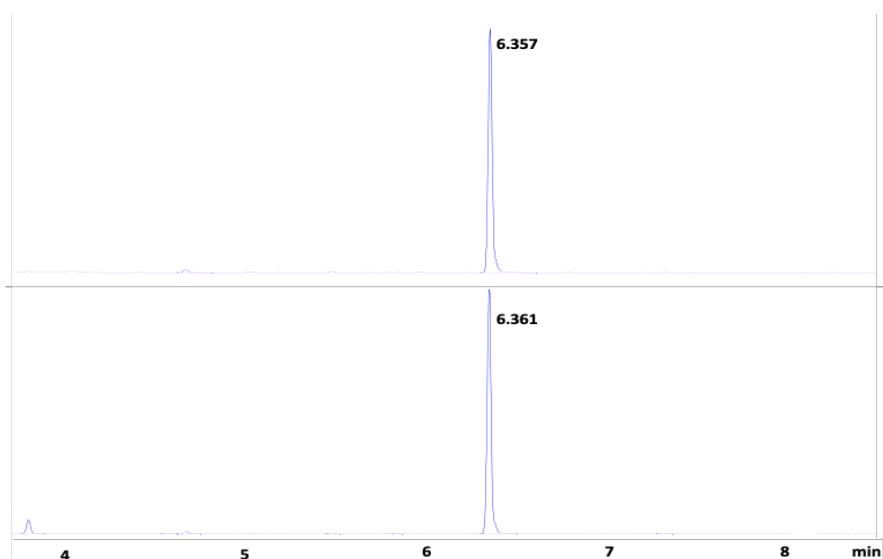


Figure S18. GC-FID chromatogram from two separate solutions of **5** heated in C_6D_6 (top) and C_6H_6 (bottom) at $70\text{ }^\circ\text{C}$ for 2.5 h. Reaction was cooled to rt prior to injection into the instrument. Peak assignment: 6.36 min = C_2H_{10} .

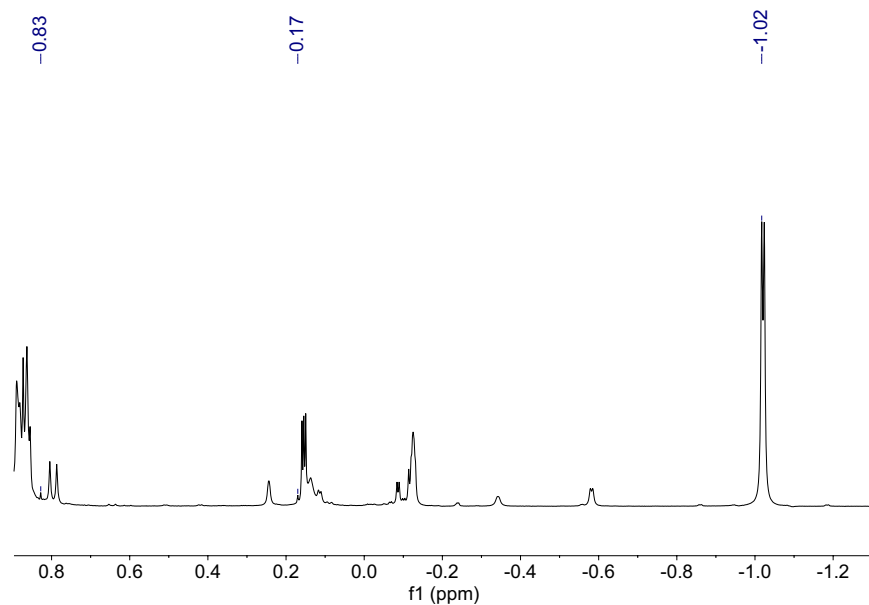


Figure S19. ^1H NMR spectrum of a solution of **K[7]** in $(\text{CD}_3)_2\text{CO}$ at $50\text{ }^\circ\text{C}$ for 2.5 h. The NMR tube was cooled to rt prior to data collection. δ : 0.83 = C_2H_6 (s), 0.17 = CH_4 (s), -1.02 (d) = Pd-CH_3 (400 MHz, $(\text{CD}_3)_2\text{CO}$).

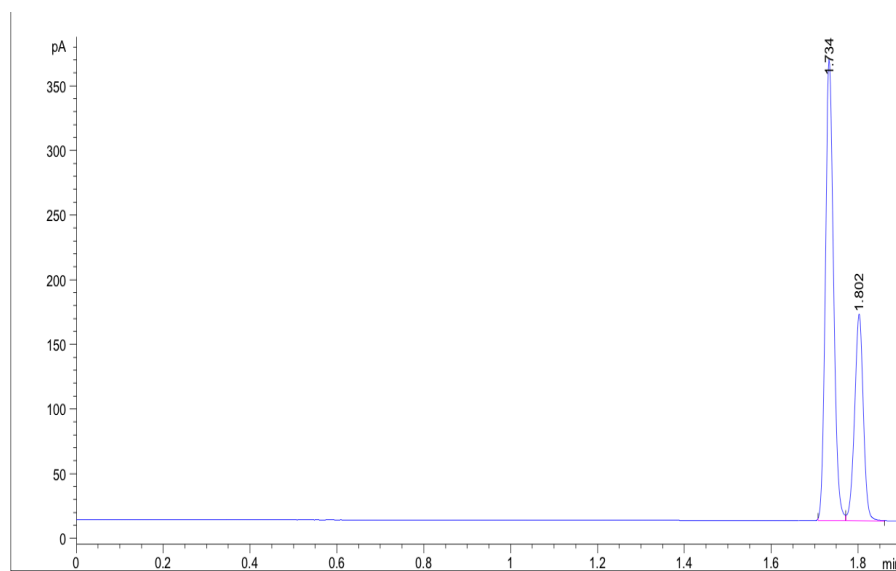


Figure S20. GC-FID chromatogram of a solution of **K[7]** heated in $(\text{CD}_3)_2\text{CO}$ at $50\text{ }^\circ\text{C}$ for 2.5 h. NMR tube was cooled to rt prior to injection into the instrument. Peak assignment: 1.734 = CH_4 ; 72%. Peak at 1.802 = C_2H_6 , 28%.

II.V Relationship Between 2 and 3

In a glovebox, complex **2** (3 mg, 0.003 mmol) or complex **3** (6 mg, 0.008 mmol) were dissolved in C_6D_6 (500 μ L) and added to an NMR tube. A sealed capillary containing DMTP (30 mM) in C_6D_6 was added to the NMR tube, and the tube was sealed with a polyethylene cap, wrapped with Parafilm, and heated at 70 °C for 2.5 h. The NMR tube was cooled to rt, and a $^{31}P\{^1H\}$ and 1H NMR spectrum were obtained. A relaxation delay (T_1) of 5 s was used for the $^{31}P\{^1H\}$ NMR experiment.

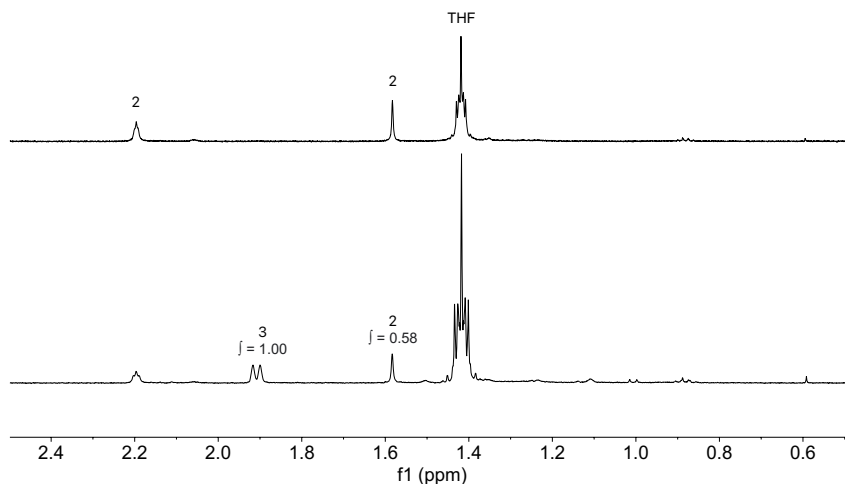


Figure S21. Stack of 1H NMR spectra of **2** a) prior to heating (T_0), and b) after heating at 70 °C for 2.5 h. The NMR tube was cooled to rt prior to obtaining the spectrum (599 MHz, C_6D_6).

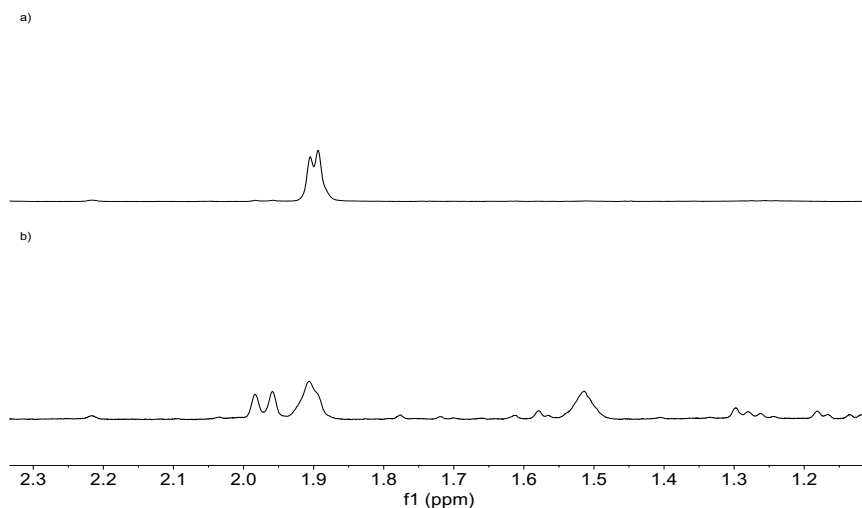


Figure S22. Stack of 1H NMR spectra of **3** a) prior to heating (T_0), and b) after heating at 70 °C for 2.5 h. The NMR tube was cooled to rt prior to obtaining the spectrum (599 MHz, C_6D_6).

III Compound NMR Spectra:

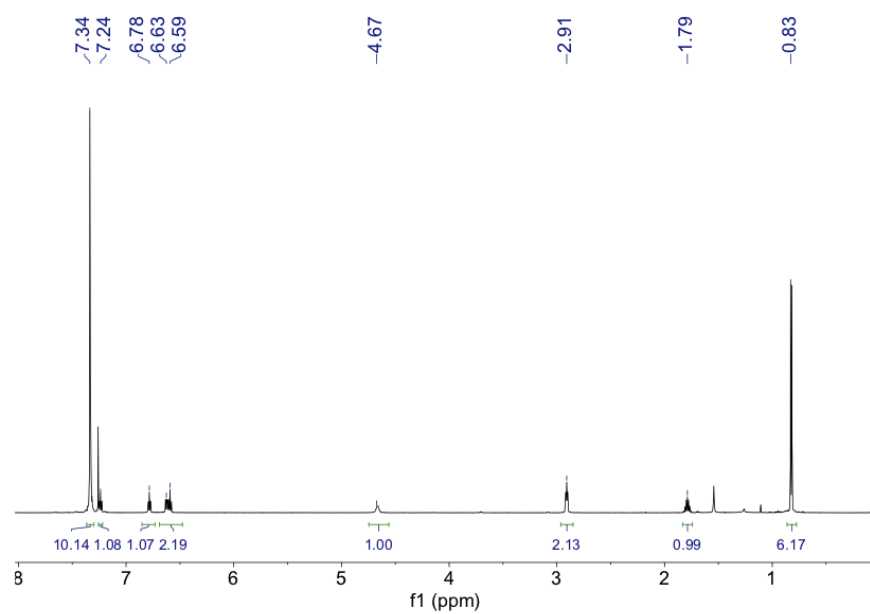


Figure S23. ^1H NMR spectrum of $\text{Ph}_2\text{P}(o\text{-C}_6\text{H}_4)\text{NH}(i\text{-Bu})$, **H[L2]** (599 MHz, CDCl_3).

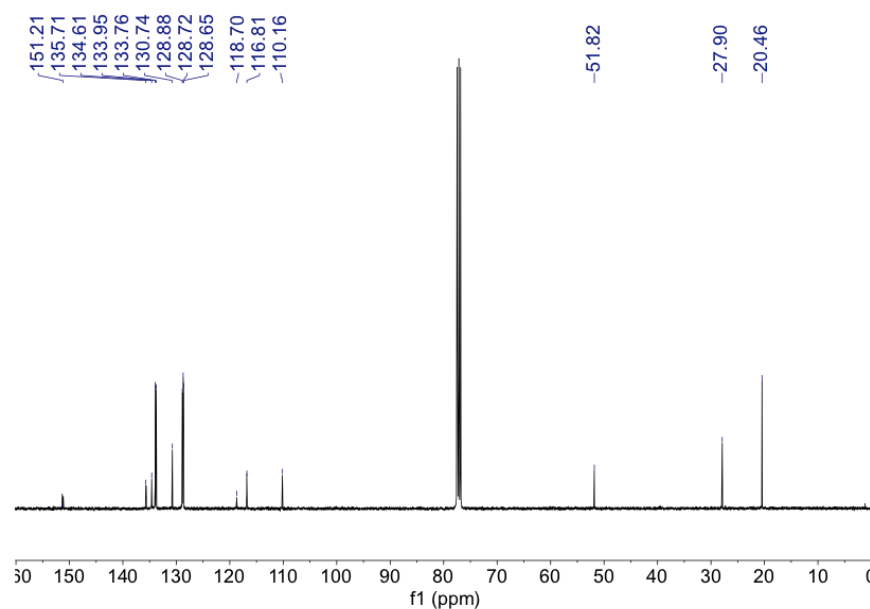


Figure S24. $^{13}\text{C}\{^1\text{H}\}$ NMR spectrum of $\text{Ph}_2\text{P}(o\text{-C}_6\text{H}_4)\text{NH}(i\text{-Bu})$, **H[L2]** (151 MHz, CDCl_3).

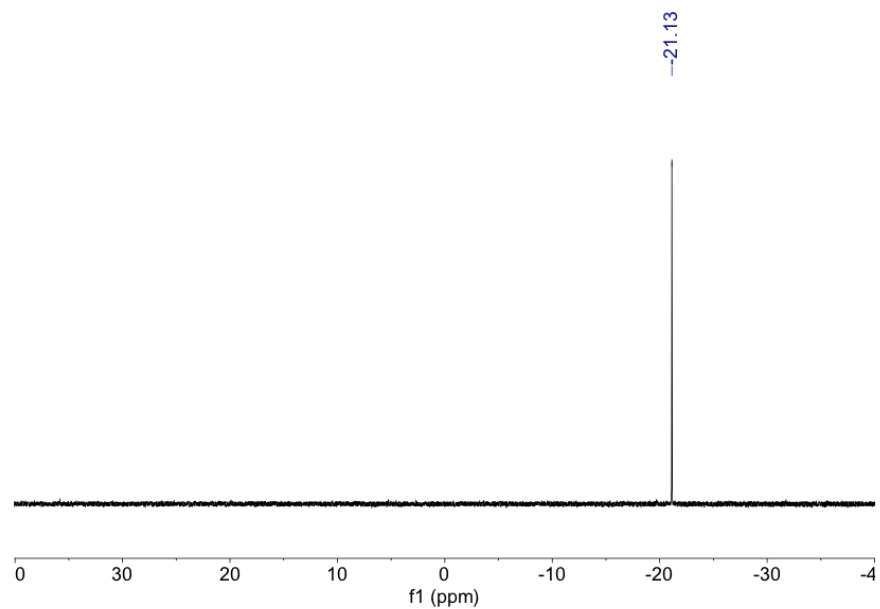


Figure S25. ³¹P{¹H} NMR spectrum of Ph₂P(*o*-C₆H₄)NH(*i*-Bu), **H[L2]** (243 MHz, CDCl₃).

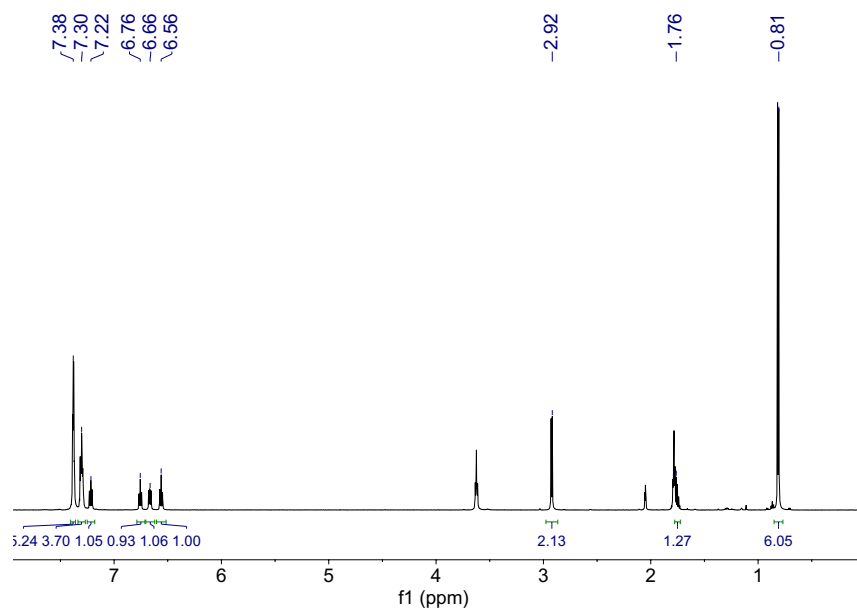


Figure S26. ¹H NMR spectrum of K[Ph₂P(*o*-C₆H₄)N(*i*-Bu)], **K[L2]** (599 MHz, (CD₃)₂CO).

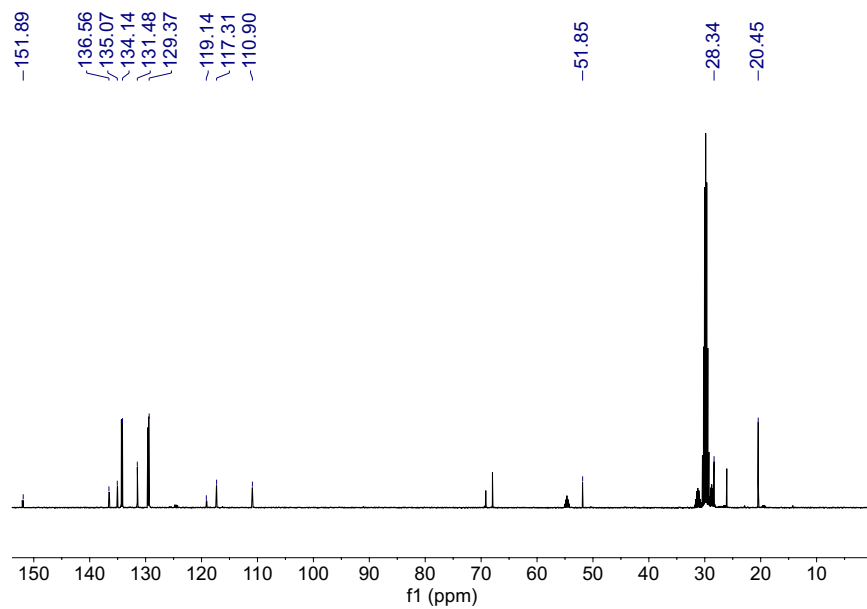


Figure S27. $^{13}\text{C}\{^1\text{H}\}$ NMR spectrum of $\text{K}[\text{Ph}_2\text{P}(o\text{-C}_6\text{H}_4)\text{N}(i\text{-Bu})]$, **K[L2]** (151 MHz, $(\text{CD}_3)_2\text{CO}$).

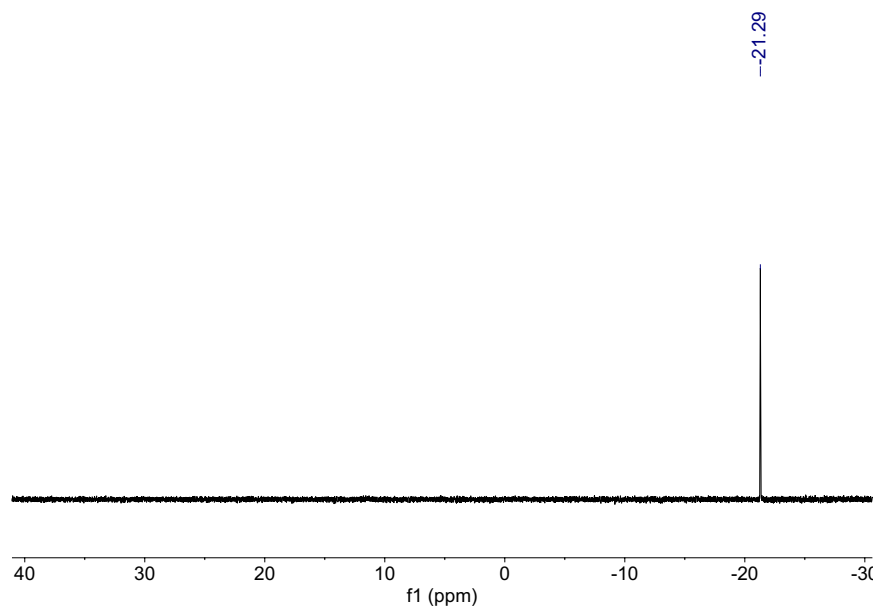


Figure S28. $^{31}\text{P}\{^1\text{H}\}$ NMR spectrum of $\text{K}[\text{Ph}_2\text{P}(o\text{-C}_6\text{H}_4)\text{N}(i\text{-Bu})]$, **K[L2]** (243 MHz, $(\text{CD}_3)_2\text{CO}$).

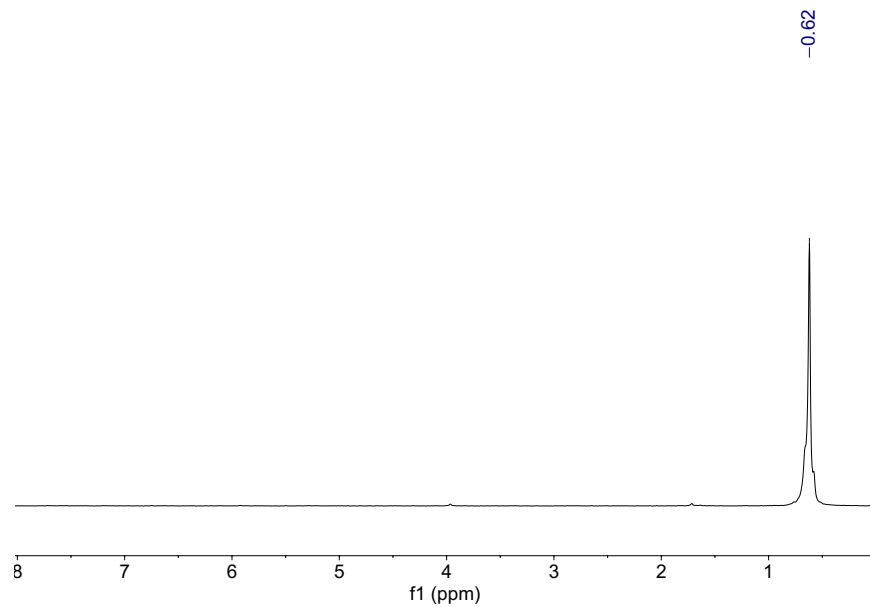


Figure S29. ^2H NMR spectrum of $\text{Sn}(\text{CD}_3)_4$ (92.1 MHz, CH_2Cl_2).

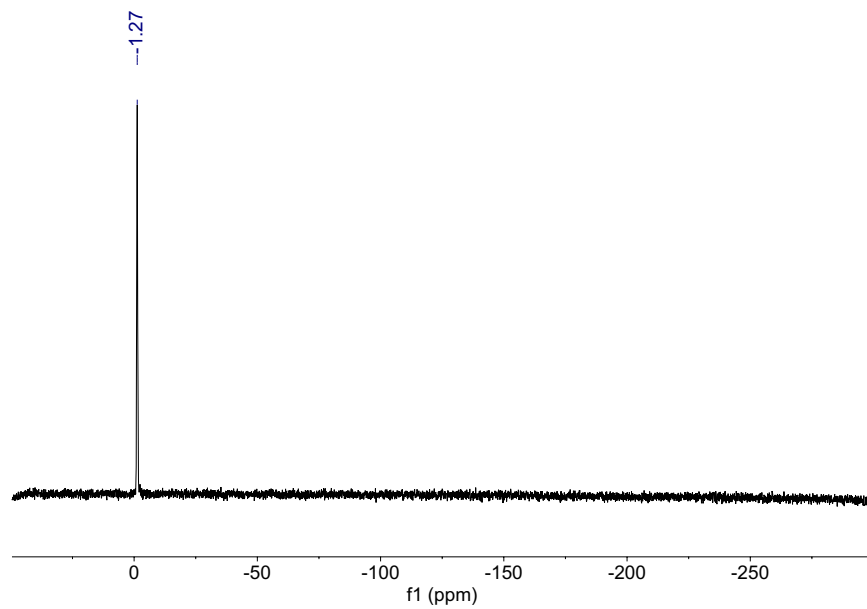


Figure S30. $^{119}\text{Sn}\{^1\text{H}\}$ NMR Spectrum of $\text{Sn}(\text{CD}_3)_4$ (223.8 MHz, CD_2Cl_2).

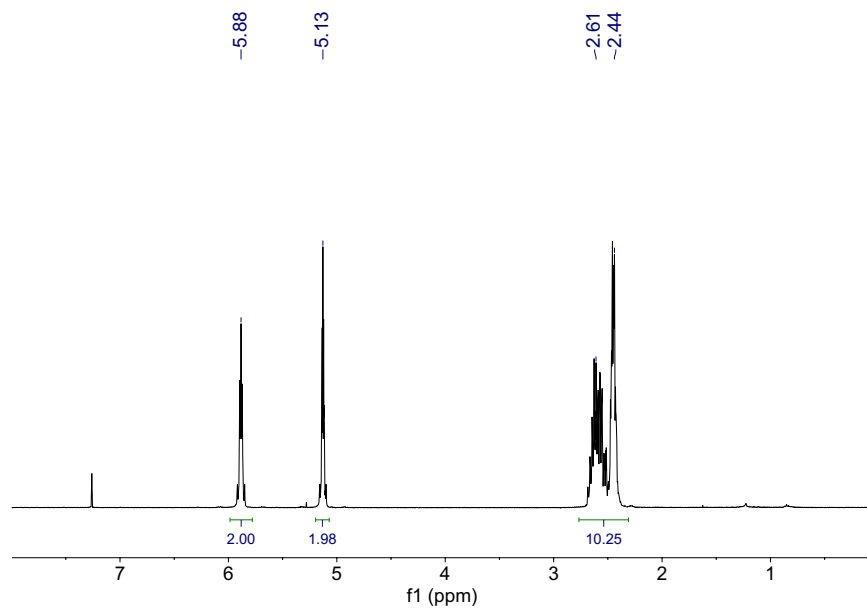


Figure S31. ¹H NMR spectrum of [PdCl(CD₃)(COD)] (599 MHz, CDCl₃).

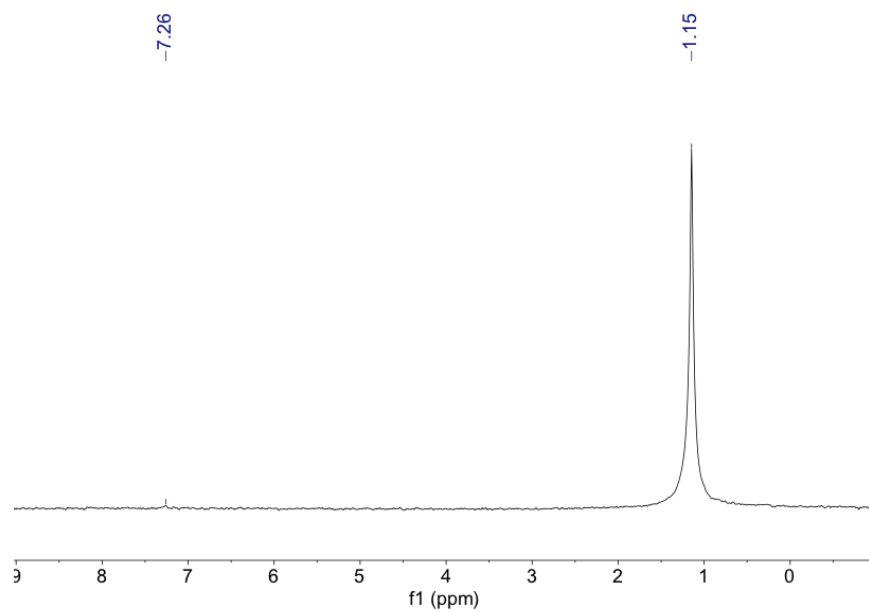


Figure S32. ²H NMR spectrum of [PdCl(CD₃)(COD)] (92 MHz, CHCl₃).

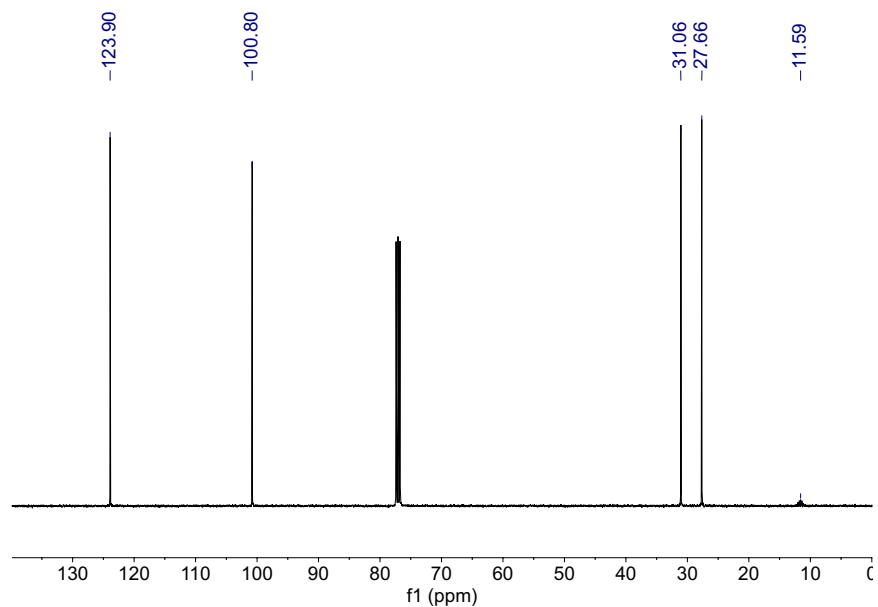


Figure S33. $^{13}\text{C}\{^1\text{H}\}$ NMR spectrum of $[\text{PdCl}(\text{CD}_3)(\text{COD})]$ (151 MHz, CDCl_3).

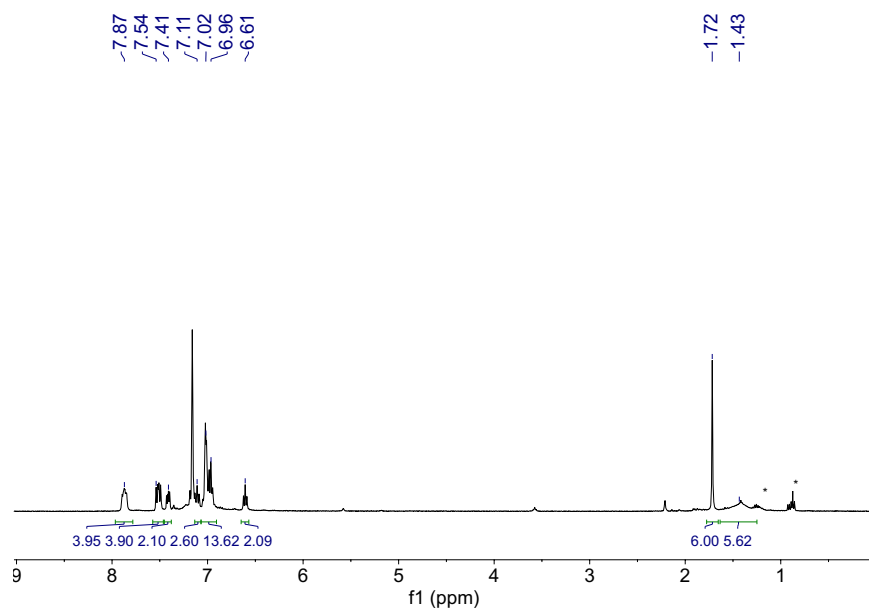


Figure S34. ^1H NMR spectrum of $[\text{Pd}(\text{CD}_3)(\text{L1})]_2$, **1- d_6** (599 MHz, C_6D_6 . * denotes pentane).

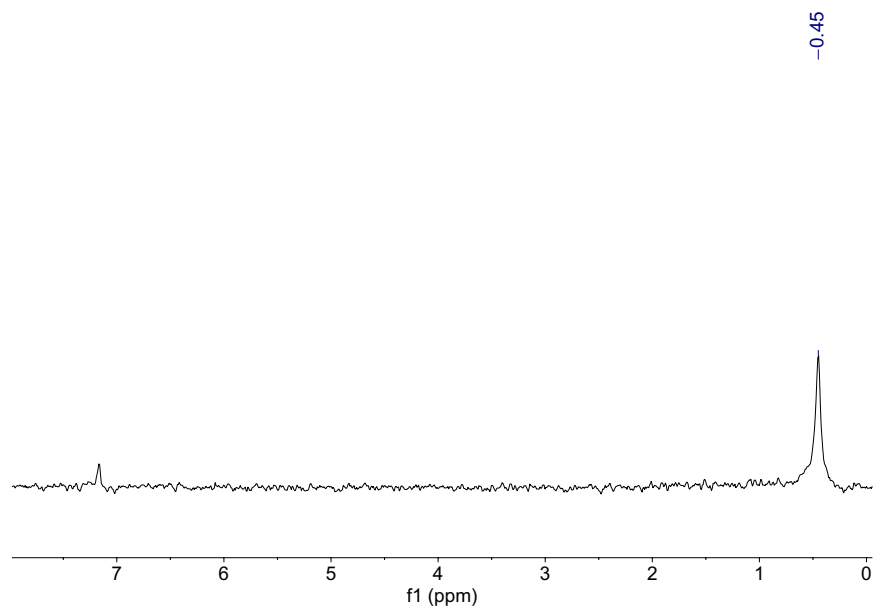


Figure S35. ^2H NMR spectrum of $[\text{Pd}(\text{CD}_3)(\text{L1})]_2$, $1\text{-}d_6$ (92 MHz, C_6D_6).

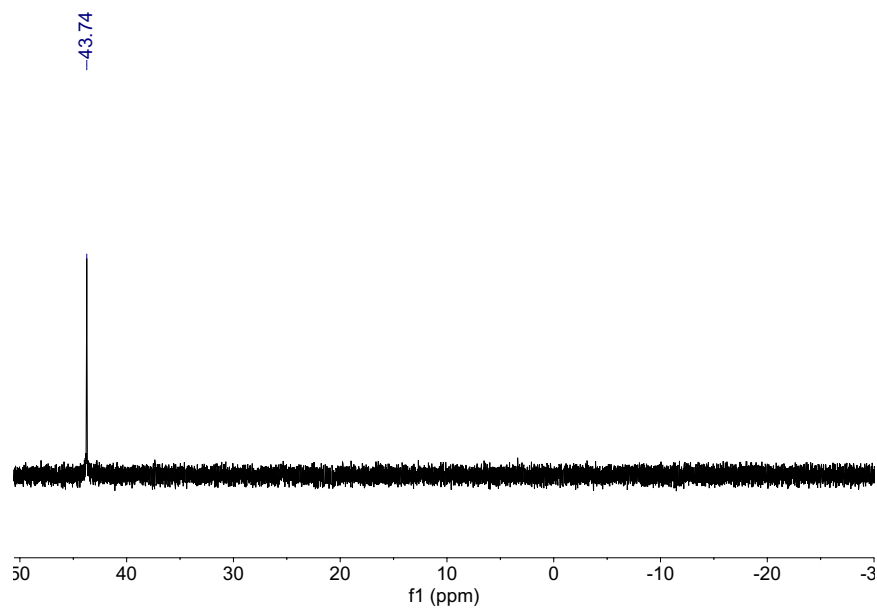


Figure S36. $^{31}\text{P}\{^1\text{H}\}$ NMR spectrum of $[\text{Pd}(\text{CD}_3)(\text{L1})]_2$, $1\text{-}d_6$ (243 MHz, C_6D_6).

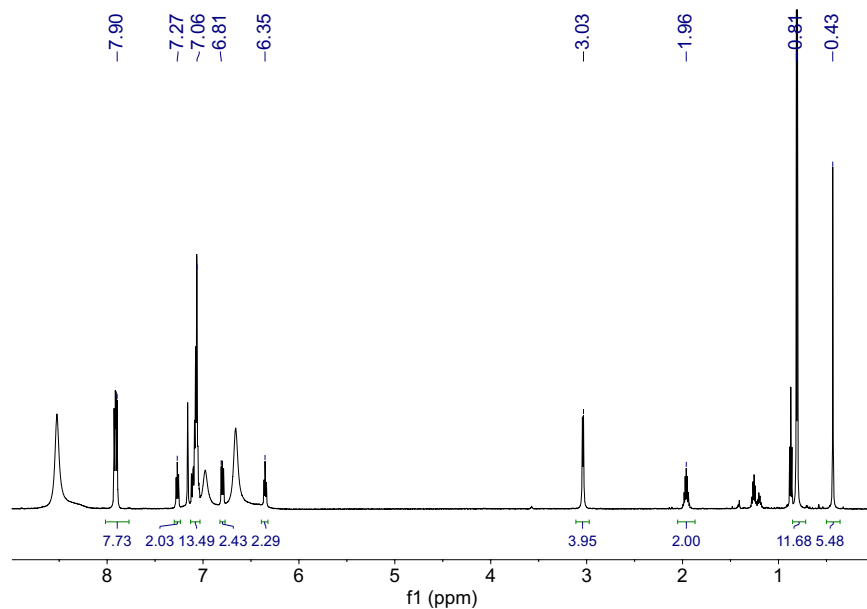


Figure S37. ^1H NMR spectrum of $[\text{Pd}(\text{CH}_3)(\text{L}2)]_2$, **4** (599 MHz, C_6D_6).

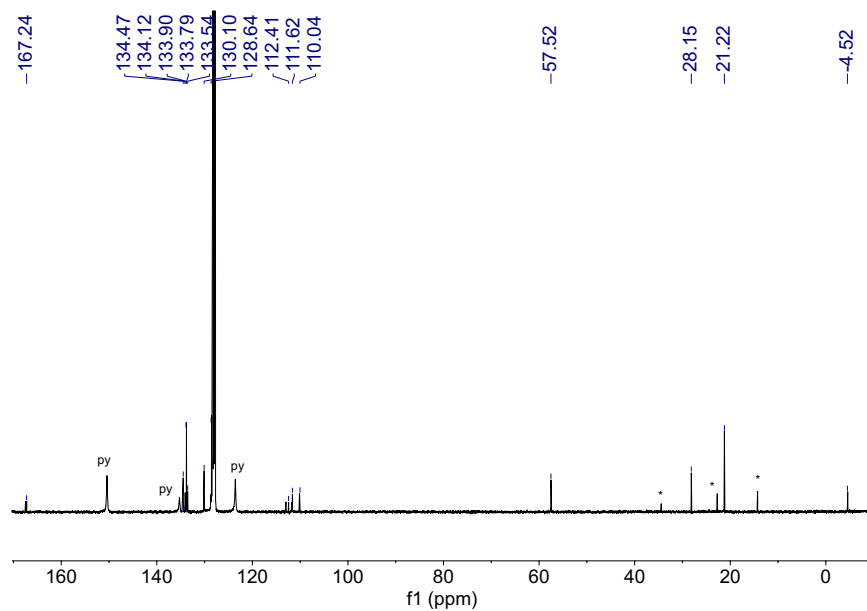


Figure S38. $^{13}\text{C}\{^1\text{H}\}$ NMR spectrum of $[\text{Pd}(\text{CH}_3)(\text{L}2)]_2$, **4** (151 MHz, C_6D_6). 'py' denotes pyridine, * denotes pentane.

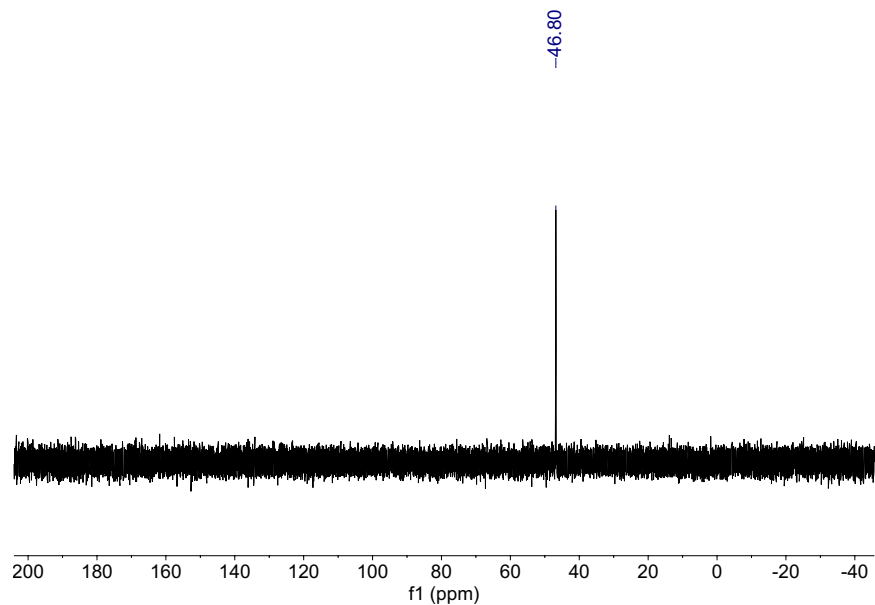


Figure S39. $^{31}\text{P}\{^1\text{H}\}$ NMR spectrum of $[\text{Pd}(\text{CH}_3)(\text{L}2)]_2$, **4** (243 MHz, C_6D_6).

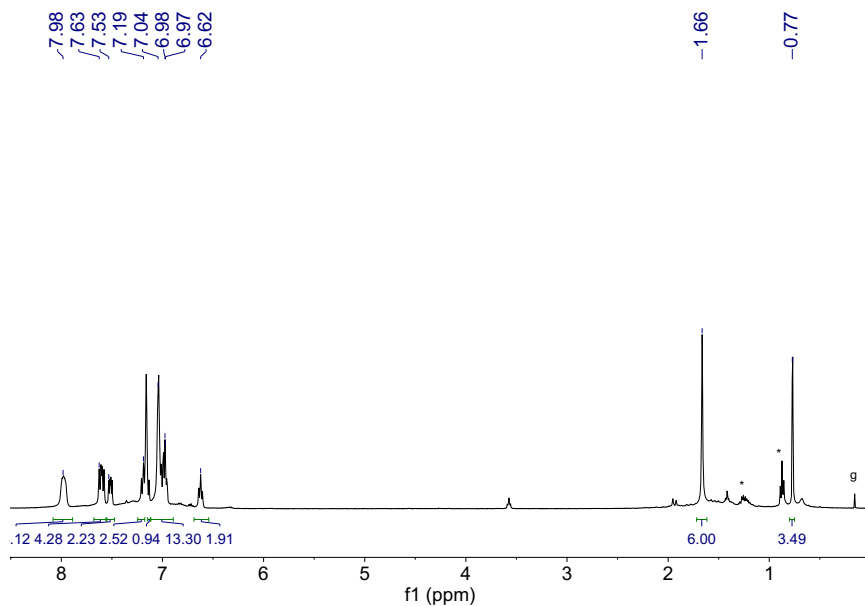


Figure S40. ^1H NMR spectrum of $[\text{Pt}(\text{CH}_3)(\text{L}1)]_2$, **5** (599 MHz, C_6D_6). * denotes pentane, 'g' denotes silicon grease.

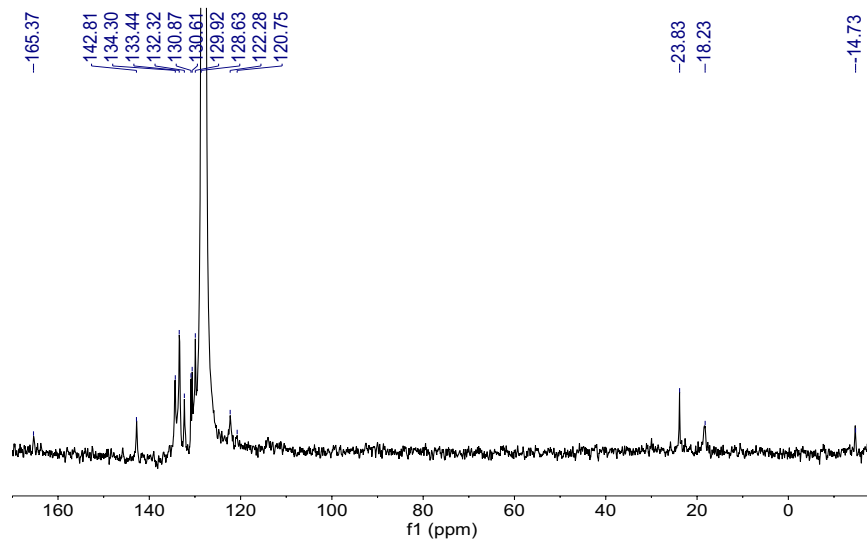


Figure S41. $^{13}\text{C}\{^1\text{H}\}$ NMR spectrum of $[\text{Pt}(\text{CH}_3)(\text{L1})_2]_2$, **5** (599 MHz, C_6D_6).

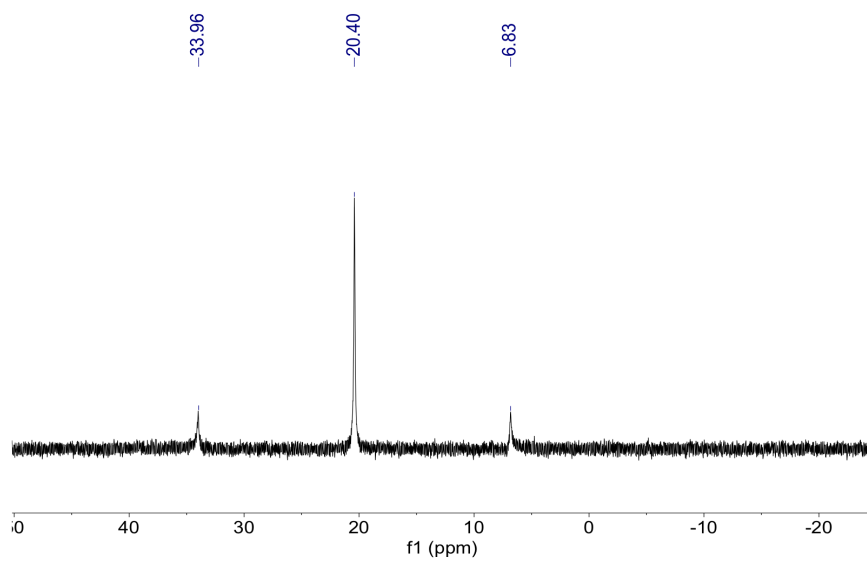


Figure S42. $^{31}\text{P}\{^1\text{H}\}$ NMR spectrum of $[\text{Pt}(\text{CH}_3)(\text{L1})_2]_2$, **5** (243 MHz, C_6D_6).

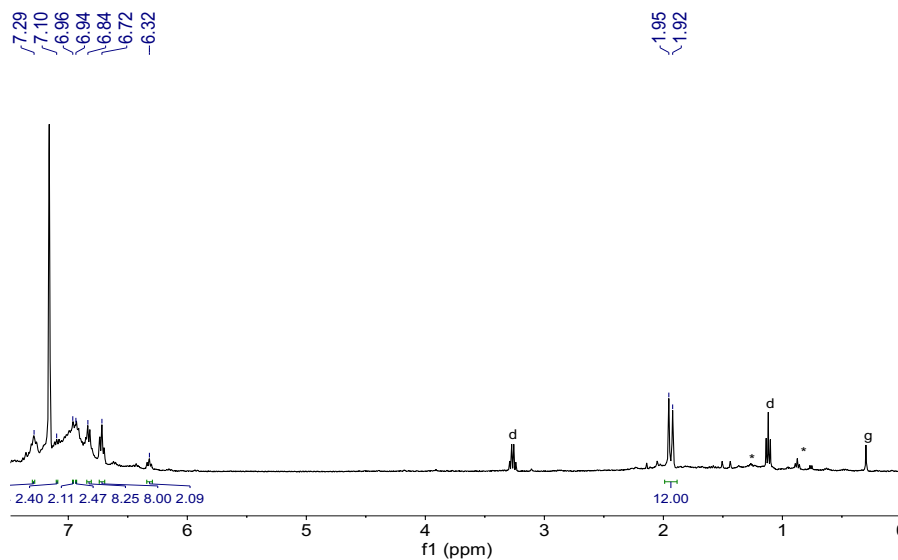


Figure S43. ^1H NMR spectrum of $\text{Pt}(\text{L1})_2$, **6** (599 MHz, C_6D_6). * denotes pentane, 'g' denotes silicon grease, 'd' denotes diethyl ether.

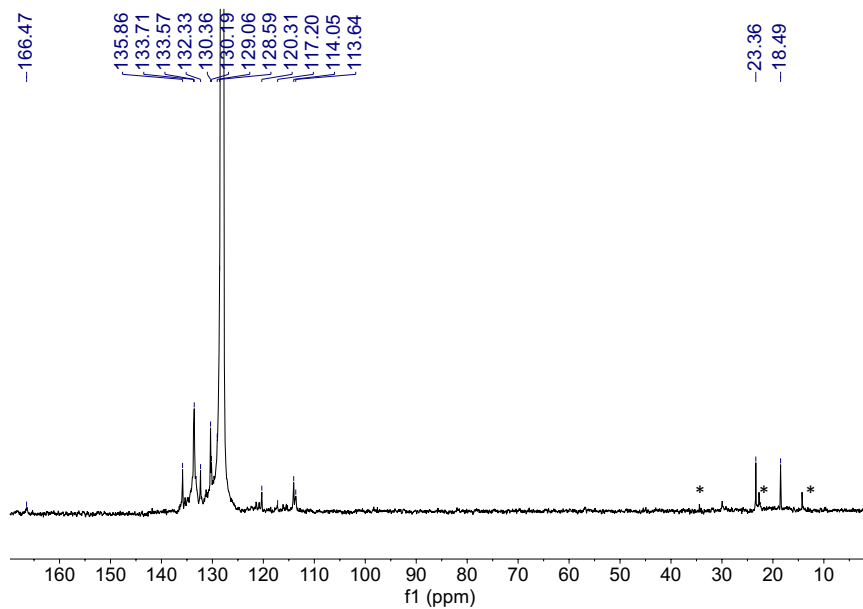


Figure S44. $^{13}\text{C}\{^1\text{H}\}$ NMR spectrum of $\text{Pt}(\text{L1})_2$, **6** (151 MHz, C_6D_6). * denotes pentane.

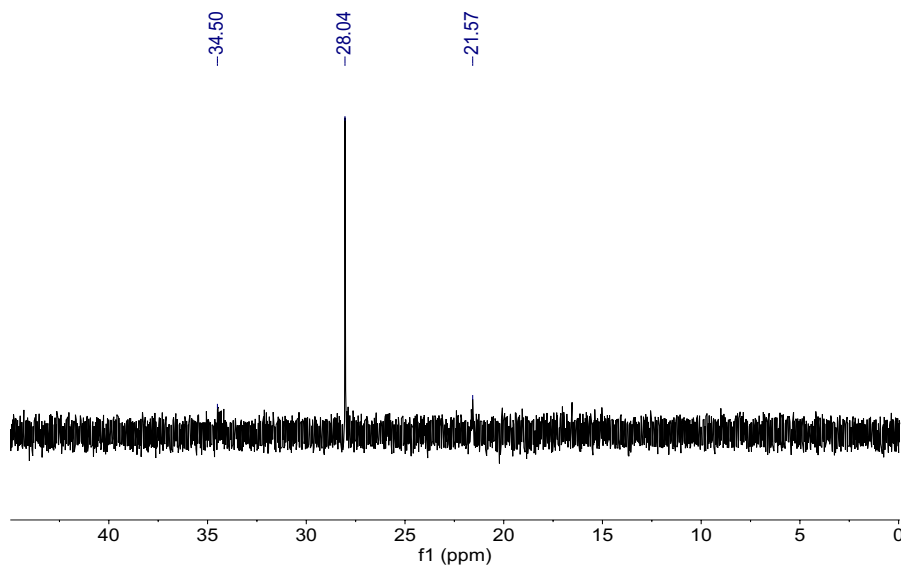


Figure S45. $^{31}\text{P}\{^1\text{H}\}$ NMR spectrum of $\text{Pt}(\text{L1})_2$, **6** (243 MHz, C_6D_6).

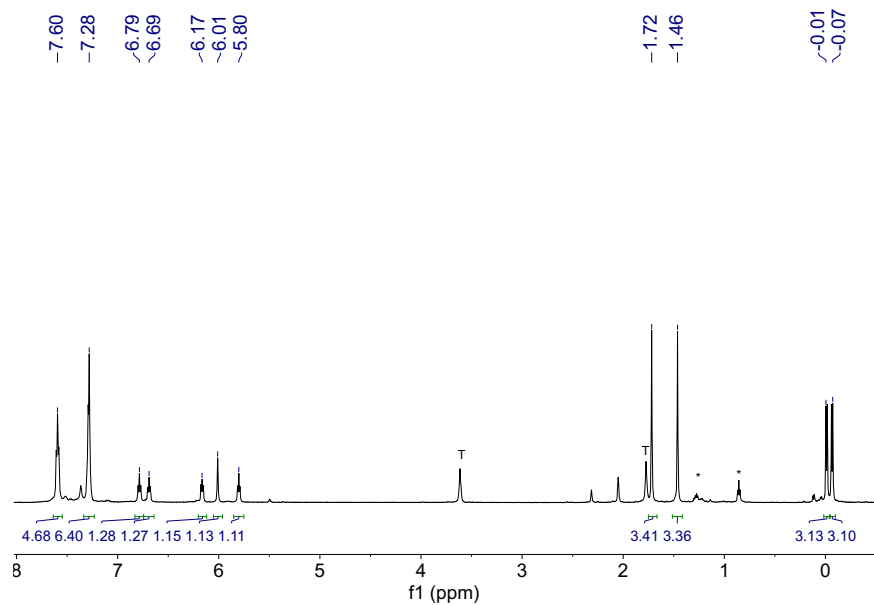


Figure S46. ^1H NMR spectrum of $\text{K}[\text{Pd}(\text{CH}_3)_2(\text{L1})]$, **K[7]** (599 MHz, $(\text{CD}_3)_2\text{CO}$). 'T' denotes THF, * denotes pentane.

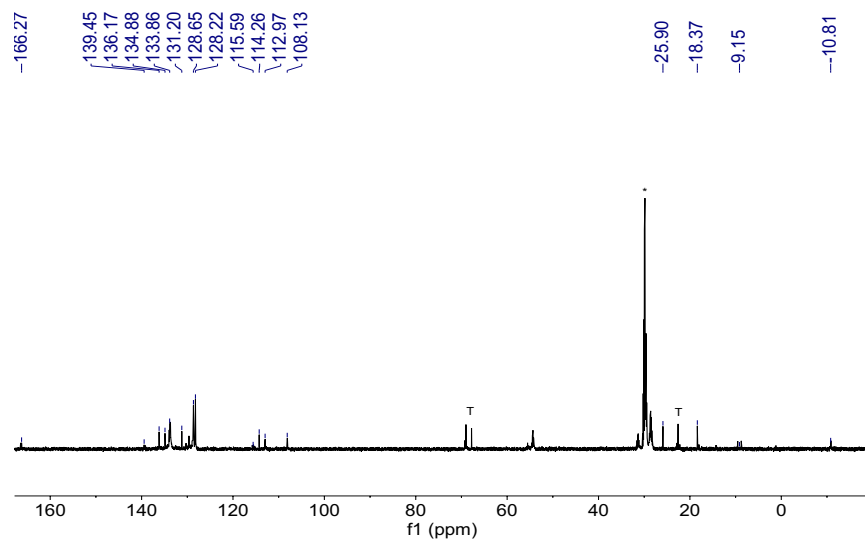


Figure S47. $^{13}\text{C}\{^1\text{H}\}$ NMR spectrum of $\text{K}[\text{Pd}(\text{CH}_3)_2(\text{L1})]$, **K[7]** (151 MHz, -20°C $(\text{CD}_3)_2\text{CO}$). 'T' denotes THF, * denotes acetone.

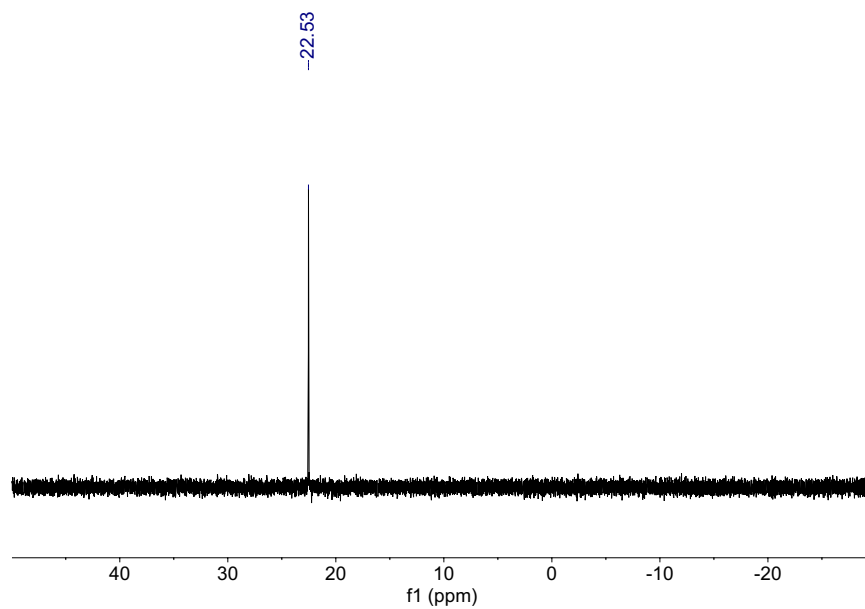


Figure S48. $^{31}\text{P}\{^1\text{H}\}$ NMR spectrum of $\text{K}[\text{Pd}(\text{CH}_3)_2(\text{L1})]$, **K[7]** (243 MHz, $(\text{CD}_3)_2\text{CO}$).

IV IR Spectra:

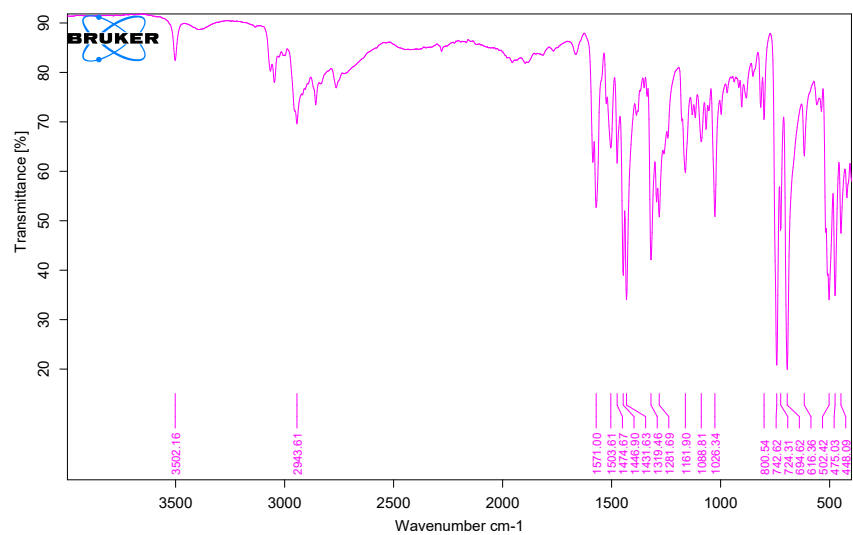


Figure S49. ATR-FTIR of solid $\text{Ph}_2\text{P}(o\text{-C}_6\text{H}_4)\text{NH}(i\text{-Bu})$, **H[L2]**.

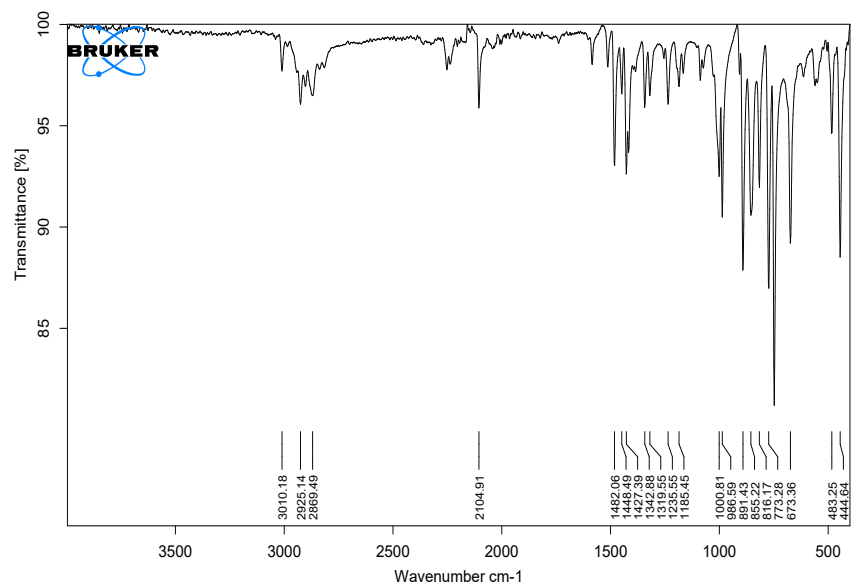


Figure S50. ATR-FTIR of solid $[\text{PdCl}(\text{CD}_3)(\text{COD})]$.

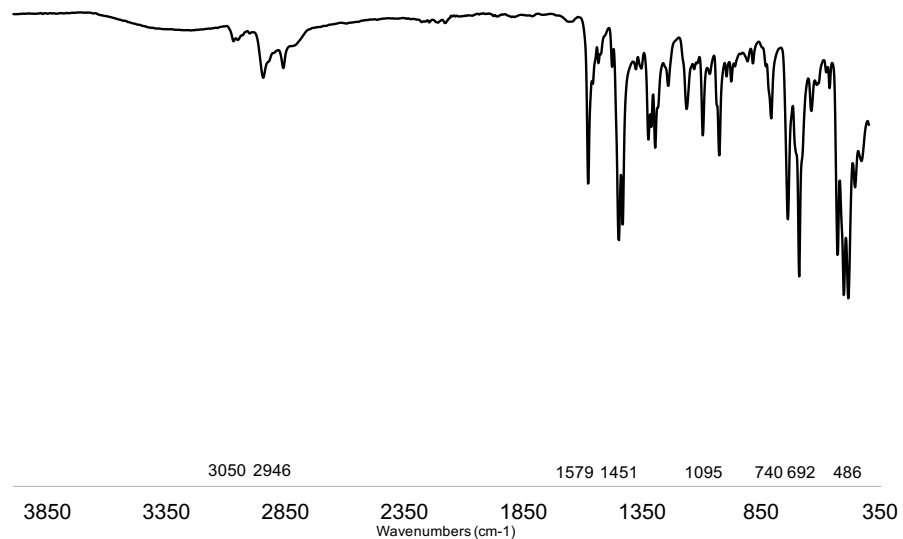


Figure S51. ATR-FTIR of solid $[\text{Pd}(\text{CH}_3)(\text{L}2)]_2$, **4**. Data acquired using Bruker Alpha II ATR-FTIR and plotted using Microsoft Excel.

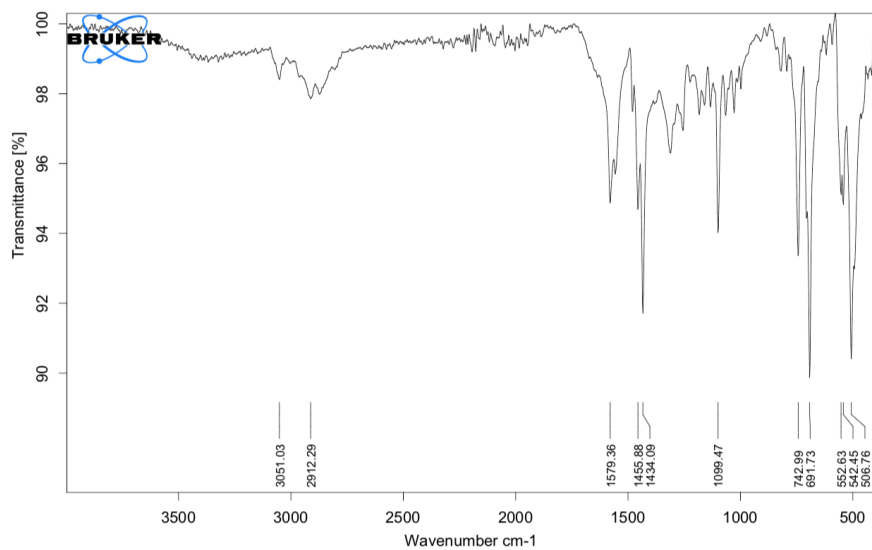


Figure S52. ATR-FTIR of solid $[\text{Pt}(\text{CH}_3)(\text{L}1)]_2$, **5**.

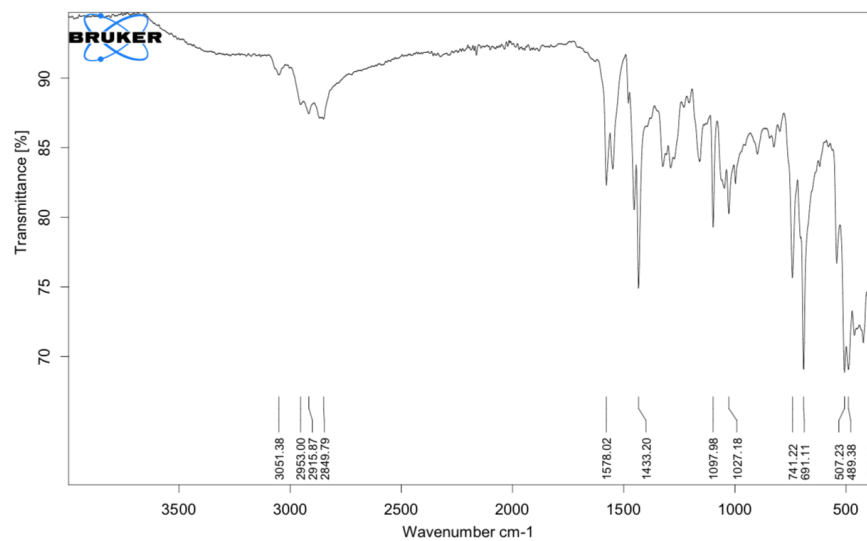


Figure S53. ATR-FTIR of solid $K[Pd(CH_3)_2(L1)]$, **K[7]**.

V Mass Spectra:

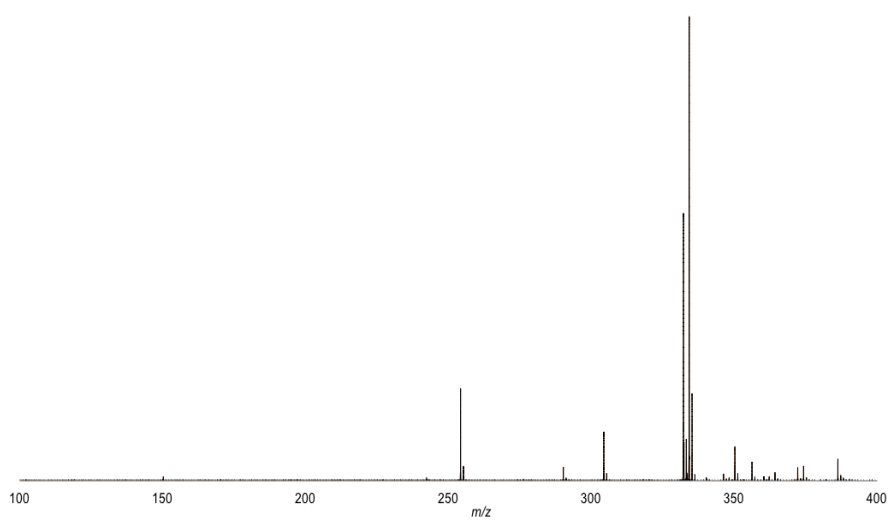


Figure S54. ESI mass spectrum of **H[L2]**.

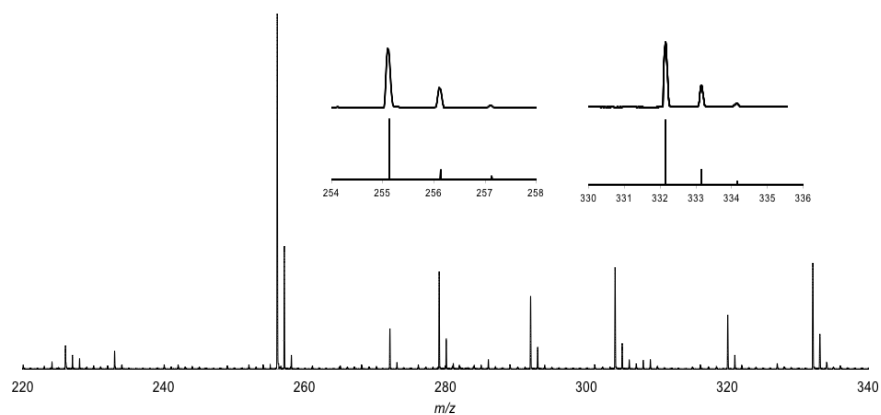


Figure S55. MALDI mass spectrum of $\text{K}[\text{Ph}_2\text{P}(o\text{-C}_6\text{H}_4)\text{N}(i\text{-Bu})]$, $\text{K}[\text{L2}]$ acquired in reflectron negative mode with pyrene as the matrix. Left inset: simulated spectrum (bottom) for $[\text{L2-C}_6\text{H}_5]^-$ and observed signal (top) at $m/z = 255.1$. Right inset: simulated (bottom) for $[\text{L2}]^-$ and observed signal (top) at $m/z = 332.2$.

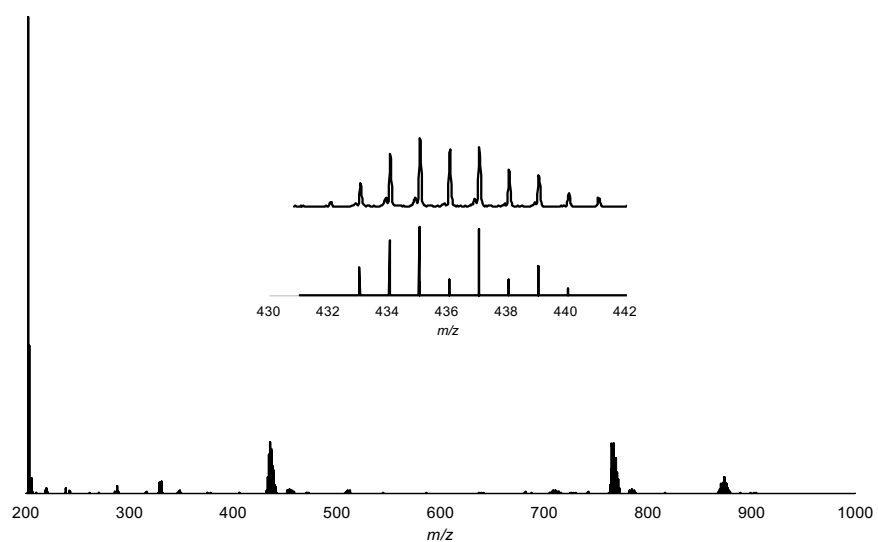


Figure S56. MALDI mass spectrum of $[\text{Pd}(\text{CD}_3)(\text{L1})_2]$, $\mathbf{1-d}_6$ with pyrene as the matrix. Inset: simulated isotope pattern (bottom) for $[\text{Pd}(\text{L1})]^{++}$ and observed signal (top) at $m/z = 435.0$. Additional major signals likely due to gas phase aggregation/fragmentation; Signal at $m/z = 766.2 = [\mathbf{3}]^{++}$; Signal at $m/z = 874.1 = [\mathbf{2}]^{++}$.

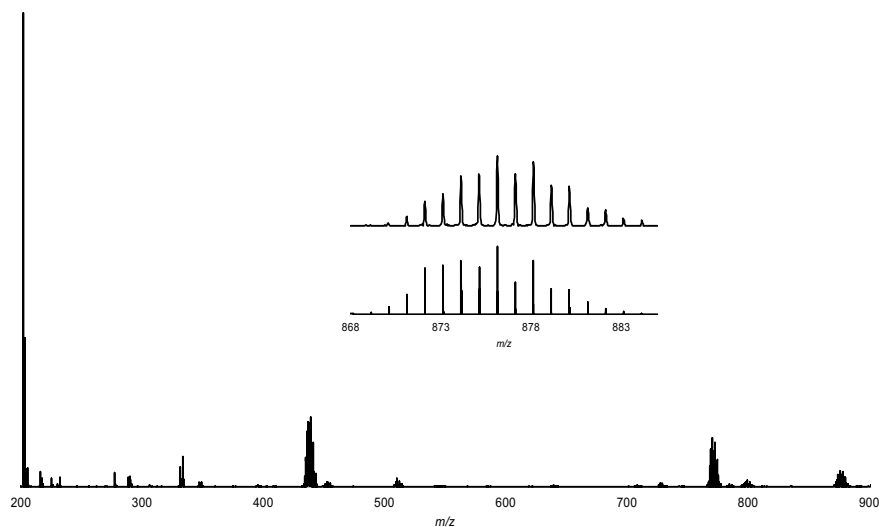


Figure S57. MALDI mass spectrum of $[\text{Pd}(\text{CH}_3)(\text{L}2)]_2$, **4** with pyrene as the matrix. Inset: simulated isotop pattern (bottom) for $[\text{4-(CH}_3)_2]^+$ and observed signal (top) at $m/z = 876.1$.

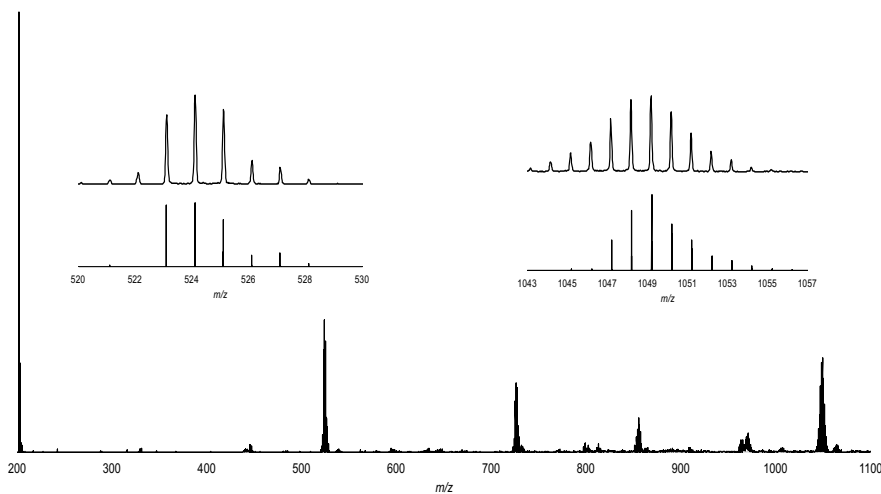


Figure S58. MALDI mass spectrum of $[\text{Pt}(\text{CH}_3)(\text{L}1)]_2$, **5** with pyrene as the matrix. Left inset: simulated isotop pattern (bottom) for $[\text{Pt}(\text{L}1)]^+$ and observed signal (top) at $m/z = 524.1$. Right inset: simulated isotop pattern (bottom) for $[\text{5-(Me)}_2]^+$ and observed signal (top) at $m/z = 1049.2$.

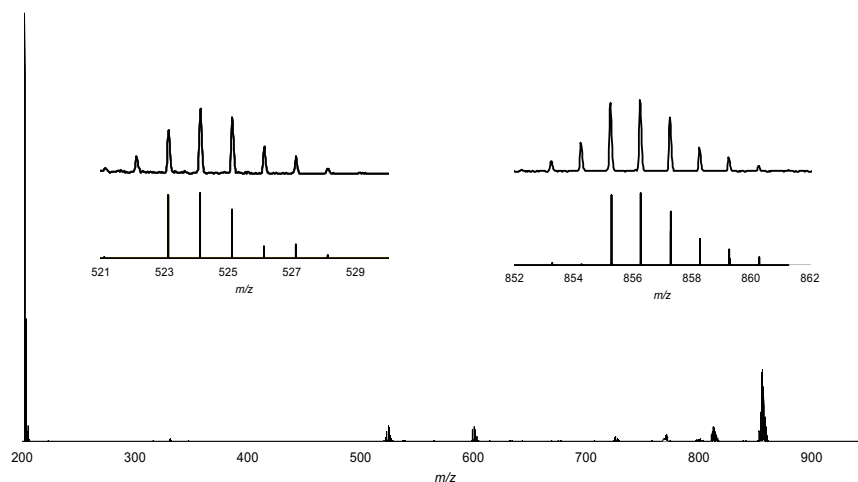


Figure S59. MALDI mass spectrum of $[\text{Pt}(\text{L1})_2]$, **6** with pyrene as the matrix. Left inset: simulated pattern (bottom) for $[\text{Pt}(\text{L1})]^+$ and observed signal (top) at $m/z = 524.1$. Right inset: simulated pattern (bottom) for $[\mathbf{6}]^+$ and observed signal (top) at $m/z = 855.3$.

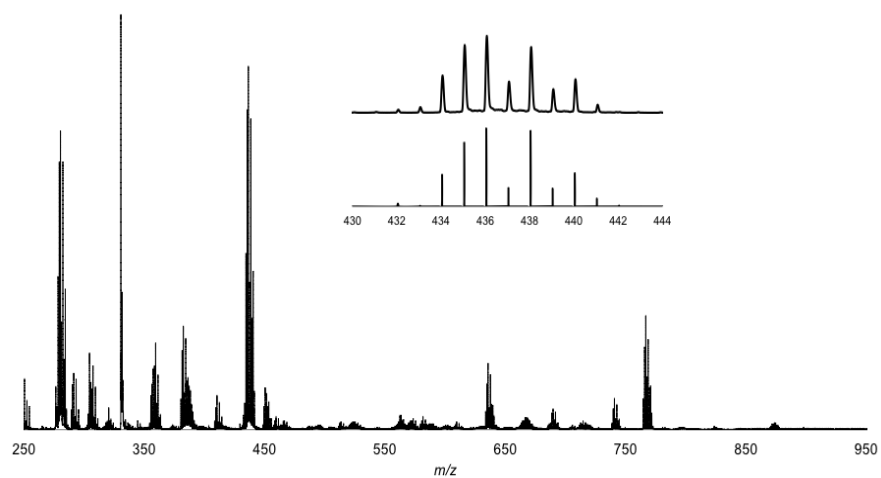


Figure S60. Negative ion MALDI mass spectrum of $\text{K}[\text{Pd}(\text{CH}_3)_2(\text{L1})]$, **7** acquired in reflectron negative mode with pyrene as the matrix. Inset: simulated pattern (bottom) for $[\mathbf{7}-(\text{CH}_3)_2]^-$ and observed signal (top) at $m/z = 436.1$. Additional major signals likely due to gas phase aggregation/fragmentation; Signal at $m/z = 766.2 = [\mathbf{3}]^-$.

VI Reaction NMR Spectra

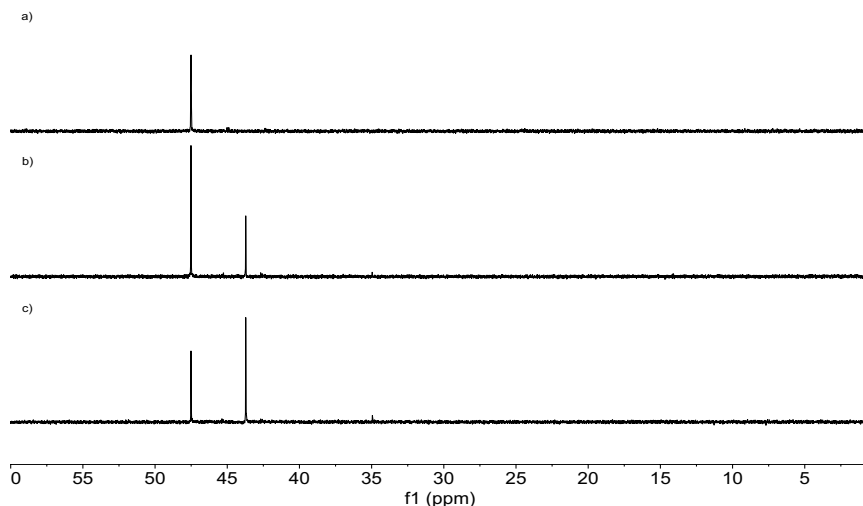


Figure S61. Stack of $^{31}\text{P}\{^1\text{H}\}$ NMR spectra of **3**: a) before the addition of $[\text{Pd}(\text{CH}_3)_2(\text{COD})]$ (T_0); b) After addition of 3.5 equiv $\text{Pd}(\text{Me})_2(\text{COD})$ at rt for 10 min (C_6D_6); and c) After addition of 3.5 equiv $\text{Pd}(\text{Me})_2(\text{COD})$ at rt for 60 min (243 MHz, C_6D_6). Complex **3** is the downfield signal at δ 47.7. Complex **1** is the upfield signal at δ 43.7.

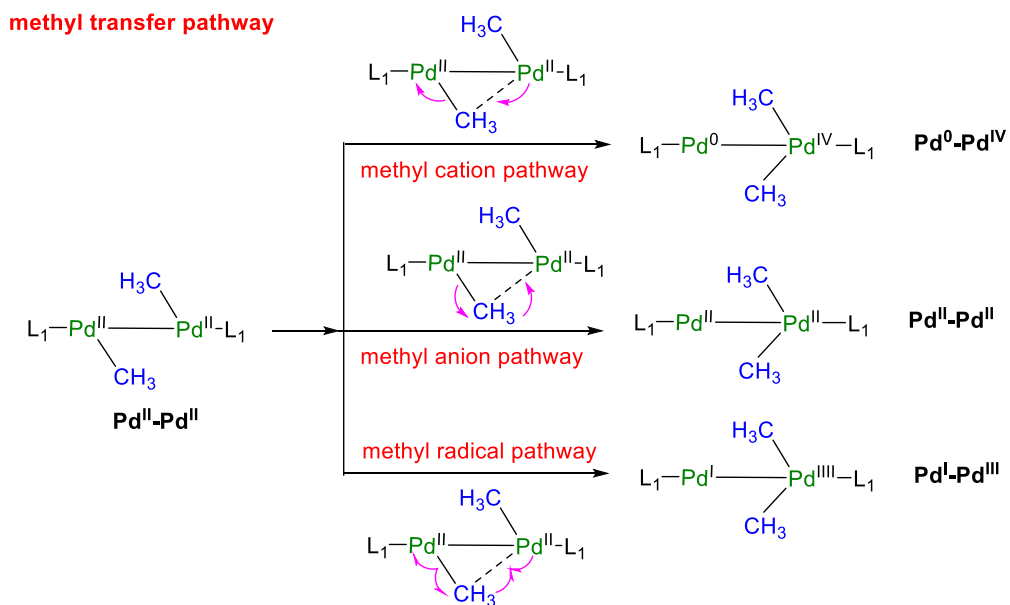
VII. Computational Details

The proposed reaction pathways were optimized using the Growing String Method (GSM)⁷⁻⁹ developed by the Zimmerman group, using the Q-Chem 5.2 software package¹⁰. The B97-D^{11, 12} density functional with basis BS1 [B97-D/BS1, BS1: 6-31G¹³ for H, C, N, LANL2DZ and fit-LANL2DZ ECP^{14, 15} for P, and Pd] were utilized in the gas phase GSM computations. Following GSM optimizations, transition states were further refined using the B97-D density functional with basis BS2 [B97-D/BS2, BS2: 6-31G(d)^{13, 16} for H, C, N, LANL2DZ and fit-LANL2DZ ECP for P, and Pd]. ECP fitting¹⁷ for the LANL2DZ basis set of P and Pd was used via keyword fit-LANL2DZ. Frequency computations (B97-D/BS2) were performed in order to verify the nature of all stationary points. A self-consistent field convergence of 10^{-6} was used for all computations. Single-point energy computations in benzene (C_6H_6) used the SMD model¹⁸ with BS3 (def-TZVP¹⁹ for H, C, N and P, def2-TZVP²⁰ and related ECP²¹ for Pd) to model the solvation effect of the chemical reactions in solution (SMD_(C₆H₆)-B97-D/BS3//B97-D/BS2). The energies

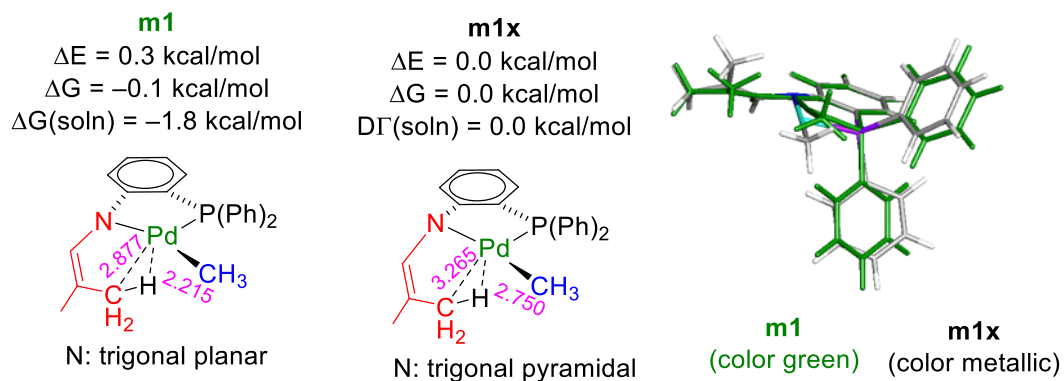
[SMD_(C₆H₆)-B97-D/BS3//B97-D/BS2] are determined at 1 atm and 298.15 K, and Gibbs free energies of activation (ΔG^\ddagger) and Gibbs free energies of reaction (ΔG°) are given in kcal mol⁻¹. Oxidation states were computed using localized orbital bonding analysis (LOBA)²² with the method of PM localization and analyzed via Löwdin population (keywords LOBA=12, and LOBA_THRESH=6015). The second order perturbation energies (E^2 , in kcal/mol) were obtained from natural bond orbital computations (NBO 5.0 package)^{23,23} incorporated in Q-Chem 5.2 package¹⁰.

Note for monomer **m1**: Two isomers of monomer **m1** and a higher energy species, **m1x**, were computed. Compared to **m1x**, a weak agostic interaction was present in isomer **m1**. The gas-phase electronic energy of **m1** is 0.3 kcal/mol higher than that of **m1x**, and the solvent-corrected Gibbs free energy of **m1** is -1.8 kcal/mol lower than that of **m1x**.

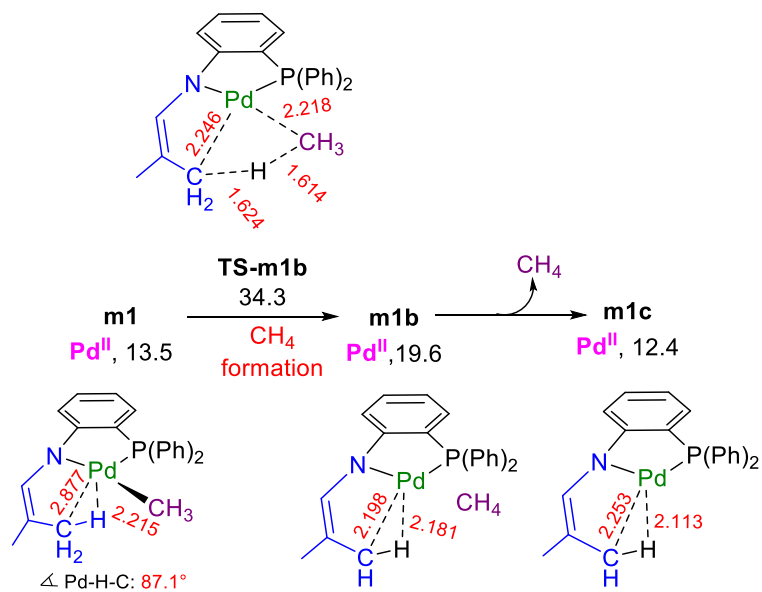
Scheme S2. The oxidation states of the Pd centers in various methyl transfer pathways.



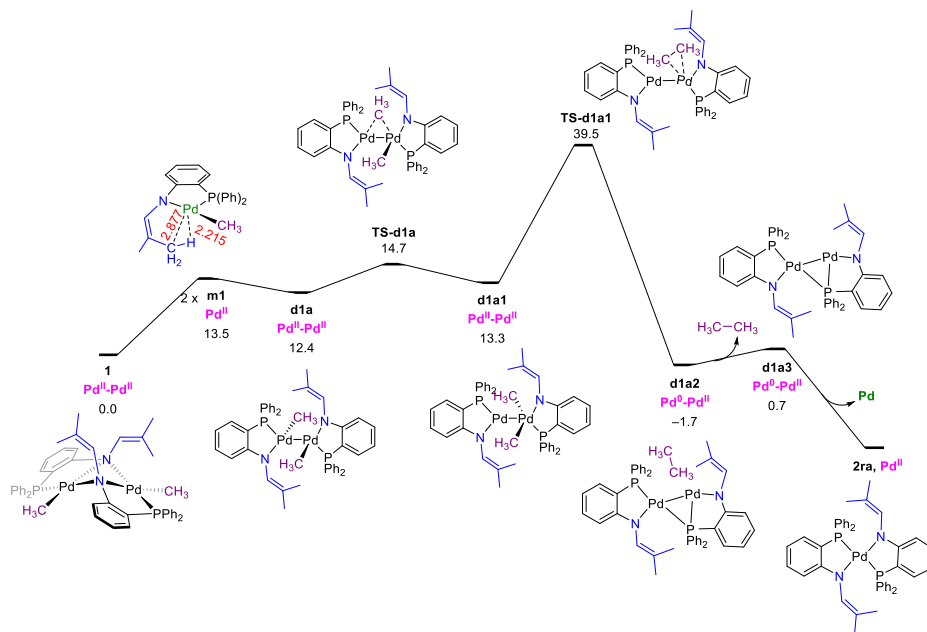
Scheme S3. Details of **m1** and **m1x**.



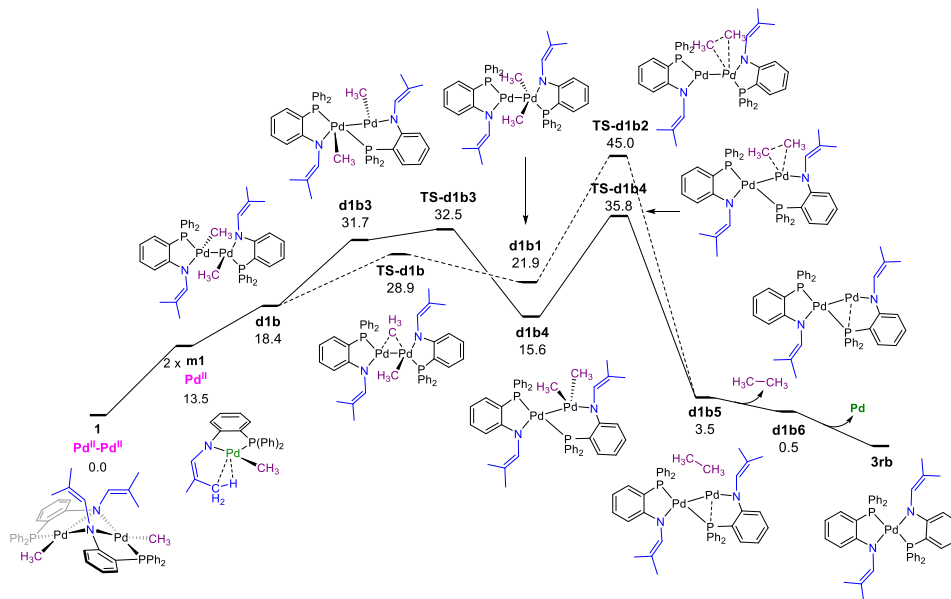
Scheme S4. Formation of methane via the CMD-type (redox neutral) C-H activation.



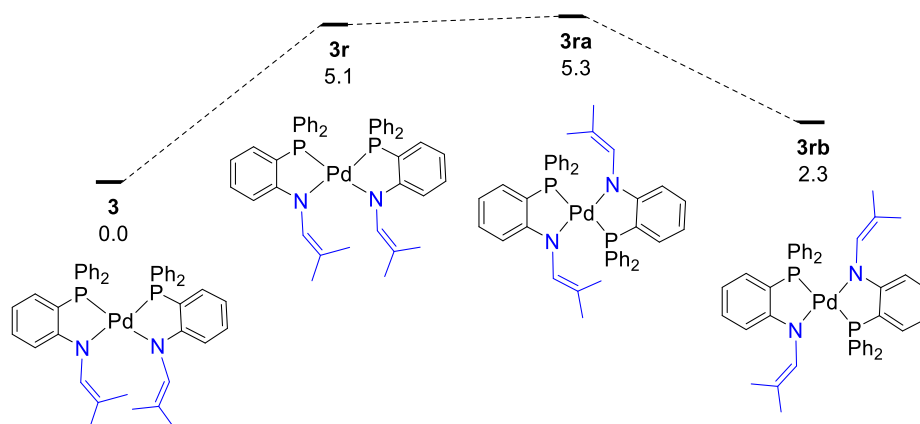
Scheme S5. Alternative pathway for generation of ethane, Pd(0), and Pd^{II}(L)₂ via dimer **d1a**. $\Delta G^\circ/\Delta G^\ddagger$ are in kcal mol⁻¹.



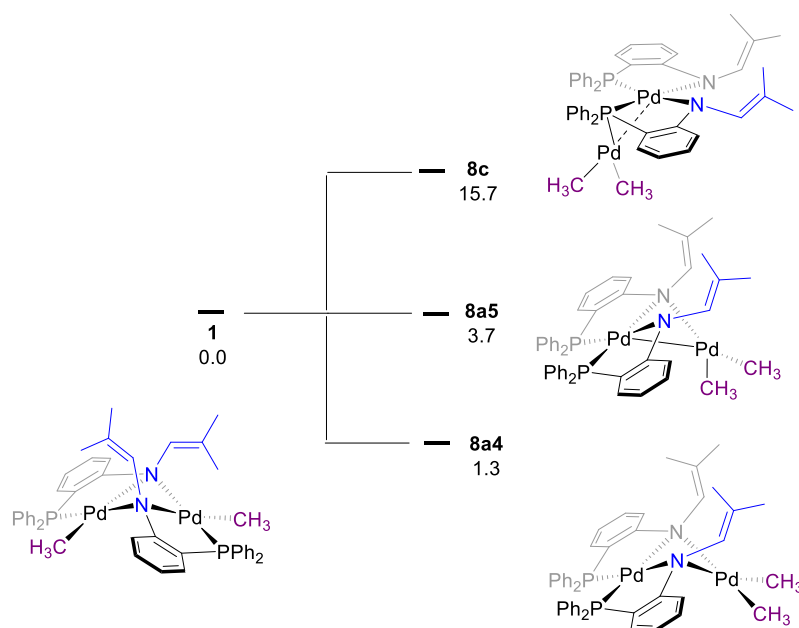
Scheme S6. The generation of ethane, Pd(0), and Pd^{II}(L)₂ via the rotamer of a pseudo methyl-bridged dimer **d1b**. $\Delta G^\circ/\Delta G^\ddagger$ are in kcal mol⁻¹.



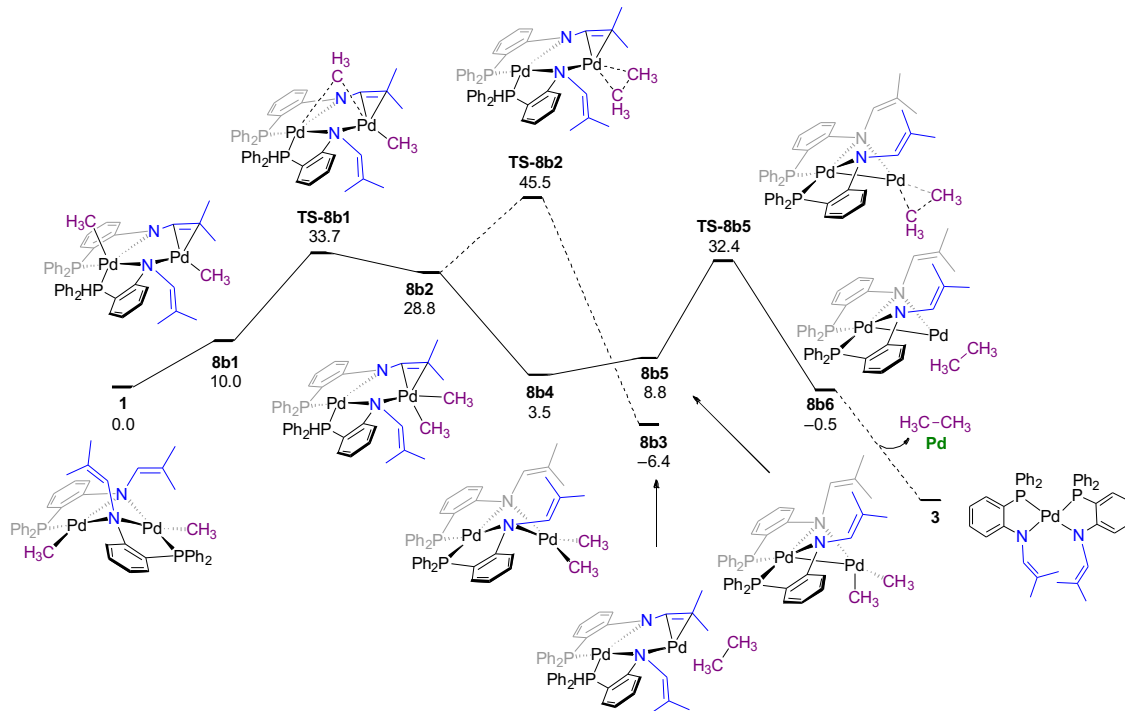
Scheme S7. The relative energies of Pd^{II}(L)₂ complex **3** and its rotamers. ΔG° are in kcal mol⁻¹.



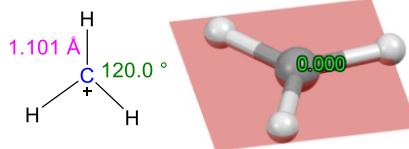
Scheme S8. Comparisons of phosphine and nitrogen coordinated Pd(Me)₂ intermediates.



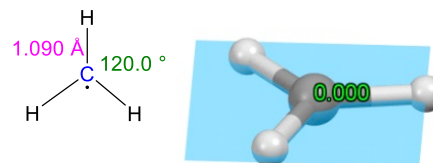
Scheme S9. Ethane formation from a dimethyl dimer **8b5**. $\Delta G^\circ/\Delta G^\ddagger$ are in kcal mol⁻¹.



Methyl Cation
trigonal planar



Methyl Radical
trigonal planar



Methyl Anion
trigonal pyramidal

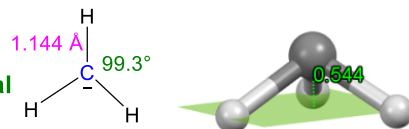


Figure S62. The geometries of various CH₃ fragments. C-HHH out-of-plane distances are in Å.

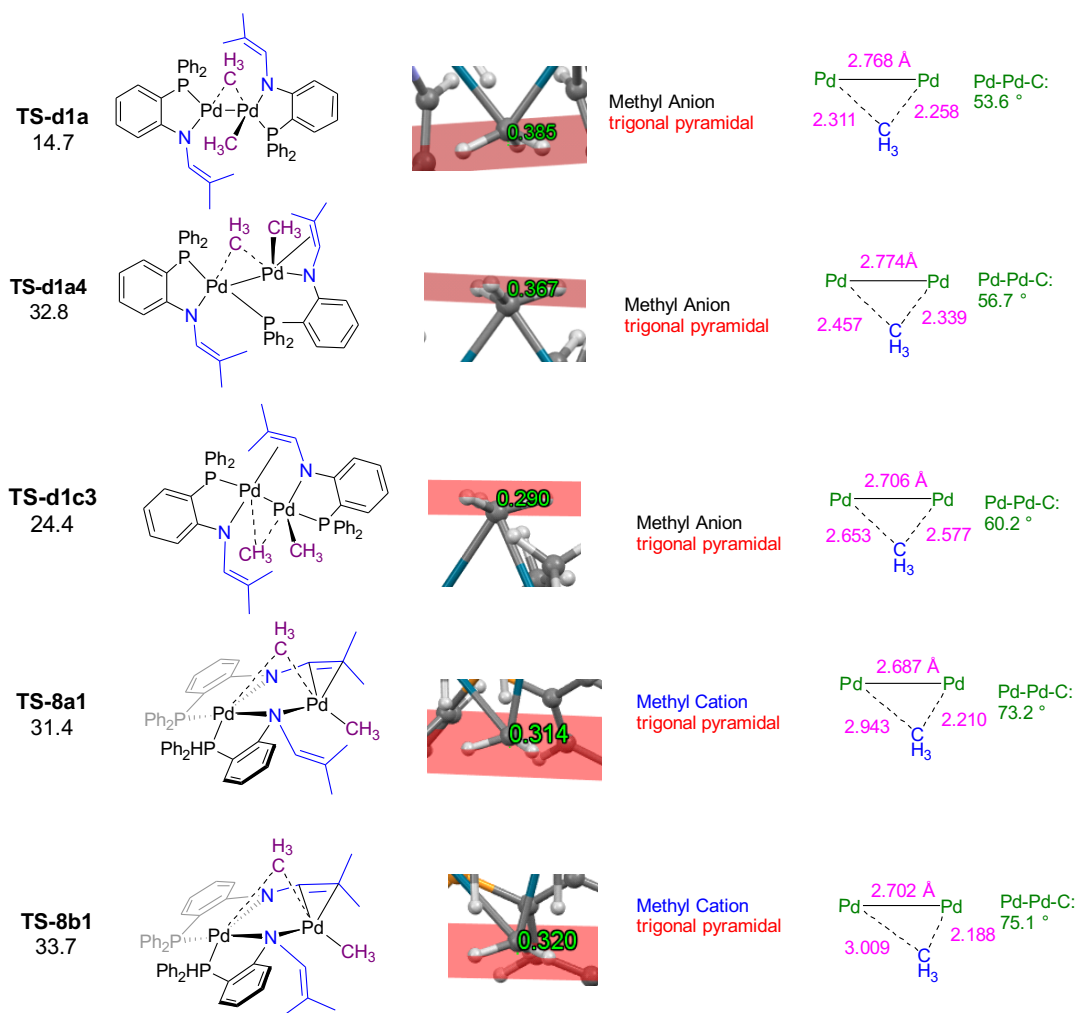
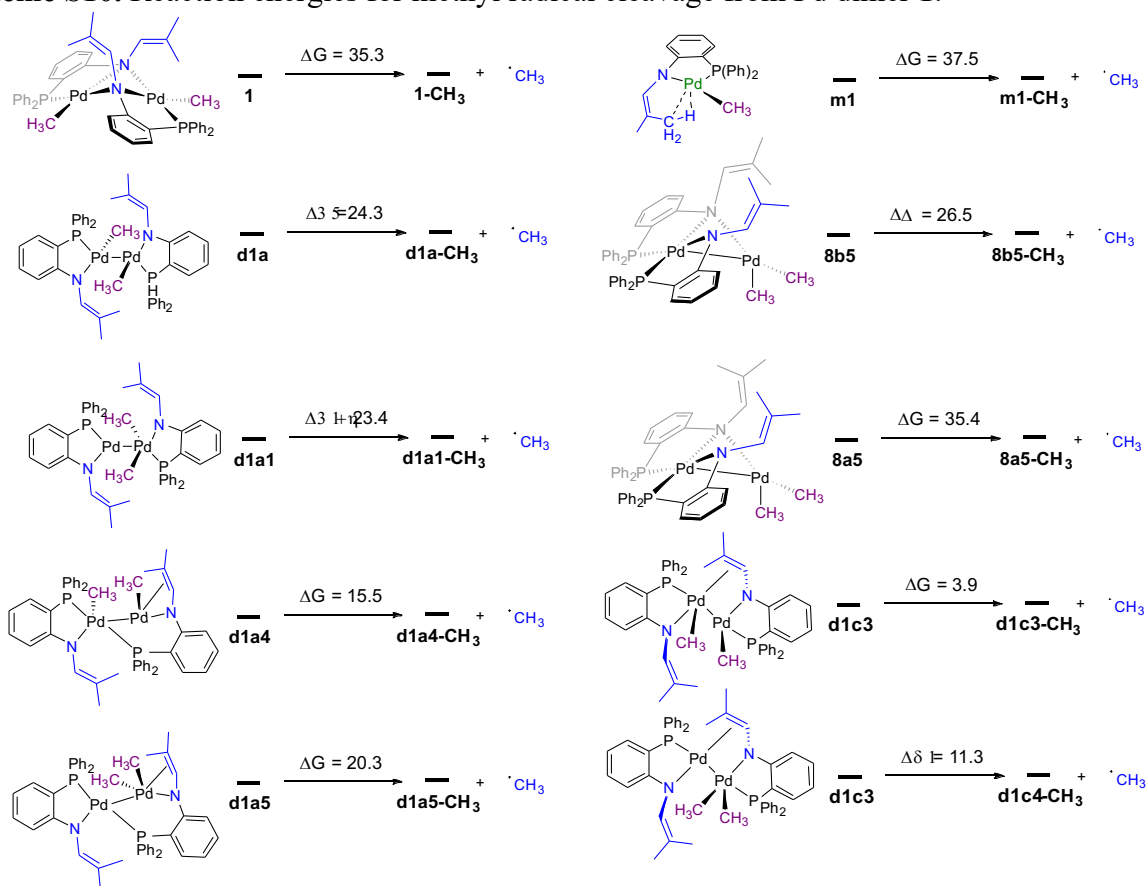
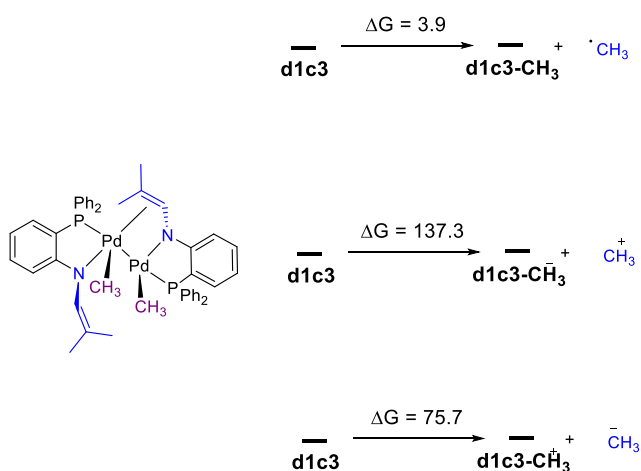


Figure S63. The geometries of CH₃ fragments in select transition states. C-HHH out-of-plane distances in Å.

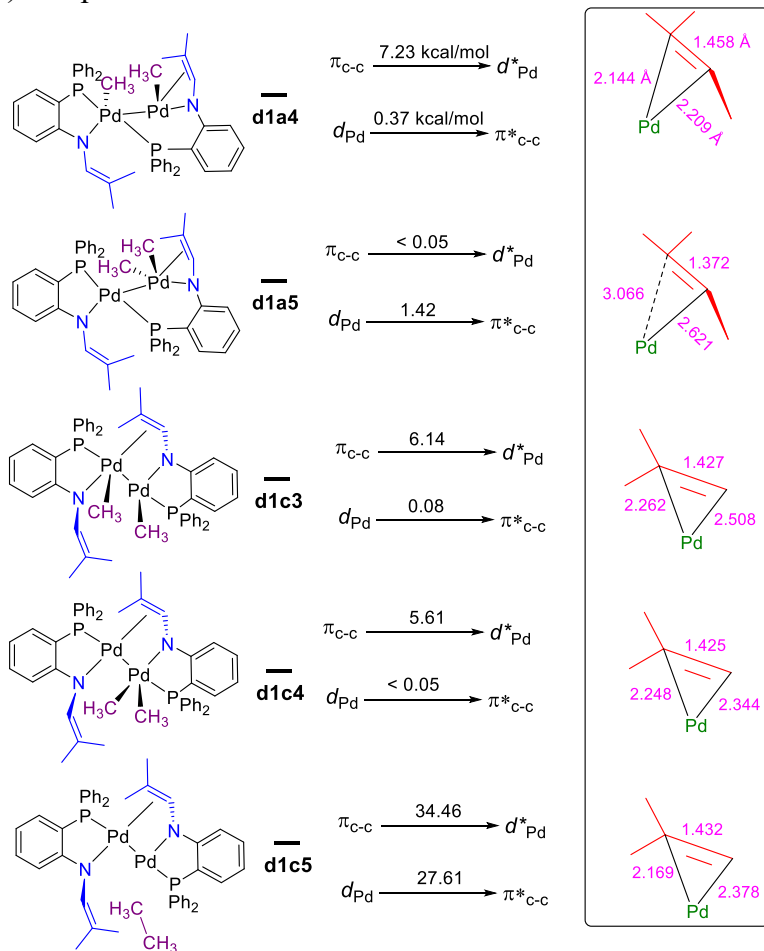
Scheme S10. Reaction energies for methyl radical cleavage from Pd dimer **1**.



Scheme S11. Reaction energies for the formation of methyl radical, methyl cation, and methyl anion from dimer **d1c3**.

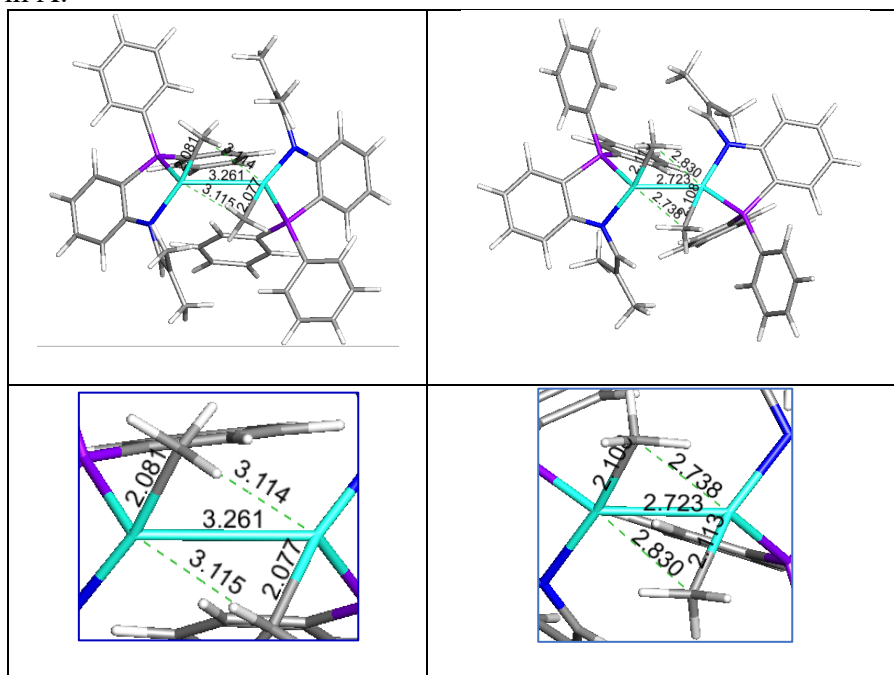


Scheme S12. The second order perturbation energies (E^2 , in kcal/mol) of Pd dimers from natural bond orbital (NBO) computations.

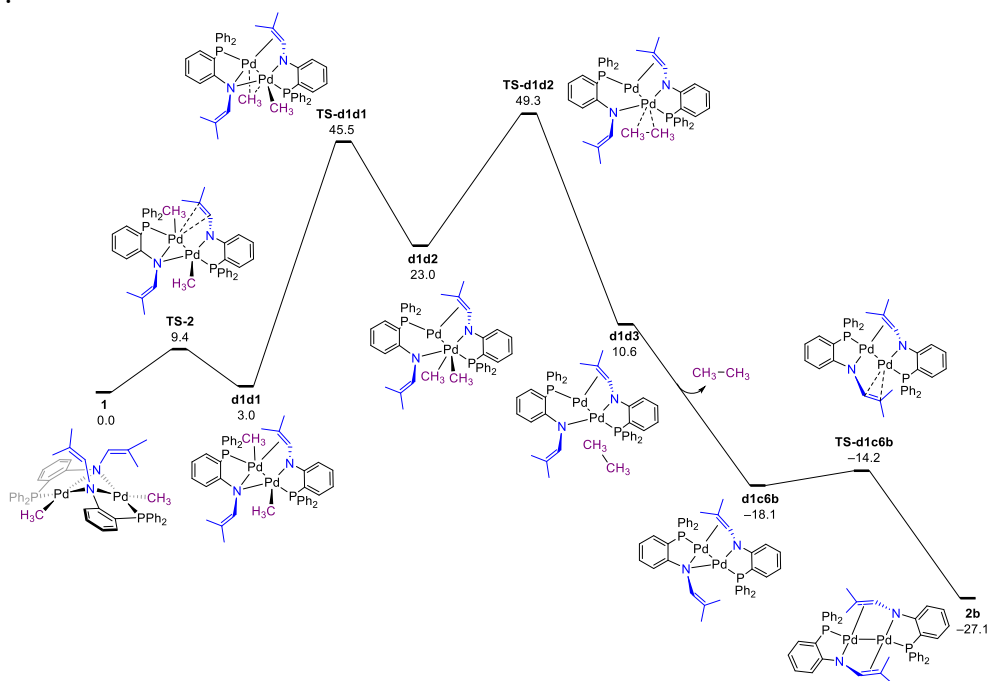


E^2 : second order perturbation energy (kcal/mol)

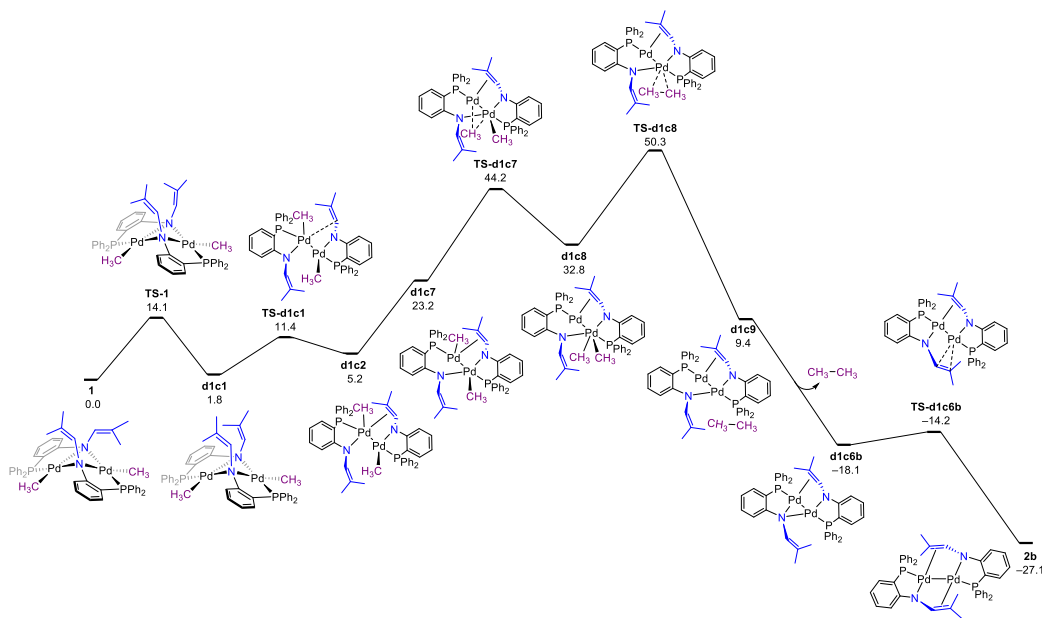
Table S2. Select interatomic distances in the pseudo methyl-bridged dimers **d1a** and **d1b**. The distances are in Å.



Scheme S13. Ethane formation from high energy ligand-bridged dimer **d1d1**. $\Delta G^\circ/\Delta G^\ddagger$ are in kcal mol⁻¹.



Scheme S14. Ethane formation from the second-high energy ligand-bridged dimer **d1c2**. $\Delta G^\circ/\Delta G^\ddagger$ are in kcal mol⁻¹.

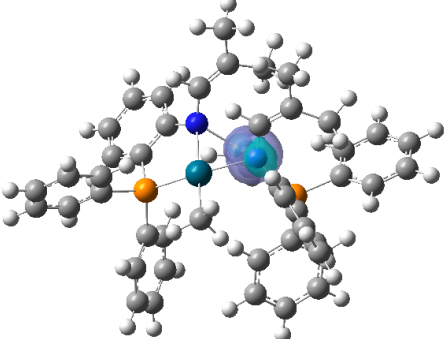
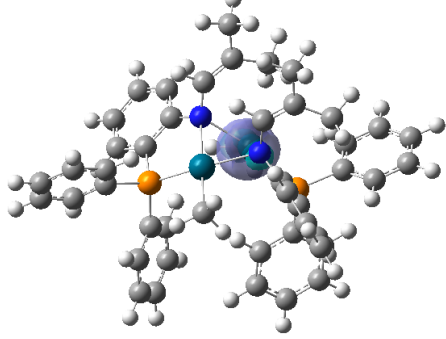
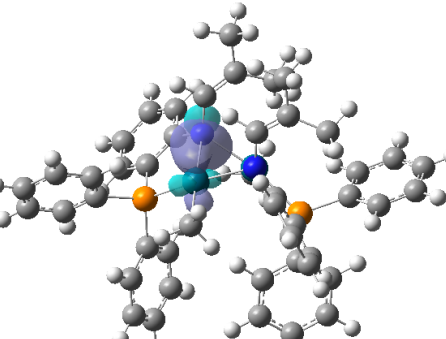
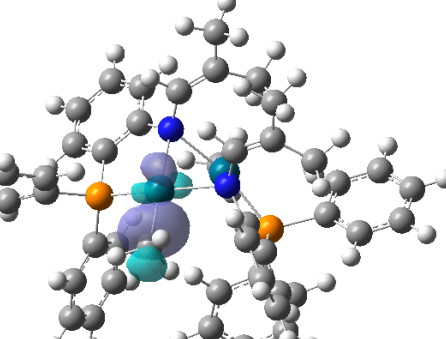


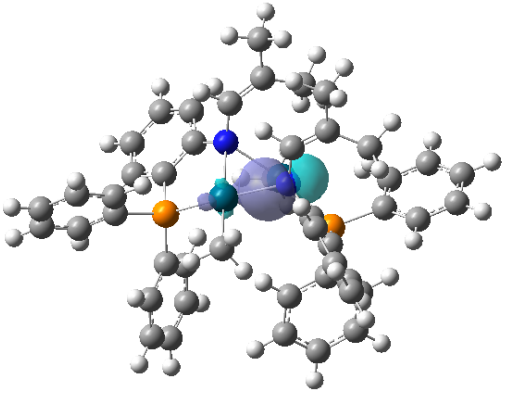
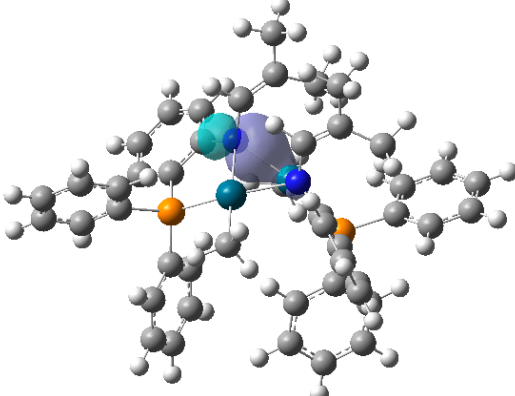
Additional Discussion of Oxidation State Analysis

The primary challenge for the localized orbital bonding analysis (LOBA)²² approach is the non-uniqueness of the localization procedure, and the fact that the orbitals in some systems do not localize cleanly, which may provide some incorrect assignments on the oxidation state of transition metal complexes.²⁴ While a new approach using oxidation state localized orbitals (OSLO) to obtain fragment-localized orbitals and to assign the oxidation state has been recently proposed,²⁵ the AdNDP approach was used herein.

The adaptive natural density partitioning (AdNDP)²⁶ was computed via the Multiwfn package (version 3.8)^{27, 28} to verify the oxidation states from LOBA. First, analysis from the compositions of the AdNDP orbitals in **1** and **2** was performed to confirm its reliability (Table S3 and S4). **1** shows (1) four heterolytic Pd-N bonds are formed via the two electrons from N, which agree with the negatively charged amide; (2) two heterolytic Pd-C_{Me} bonds are formed via the two electrons from C_{Me}, which agree with the negatively charged methyl groups. The bond compositions of the AdNDP orbitals in **1** correspond to Pd(II)-Pd(II) oxidation states.

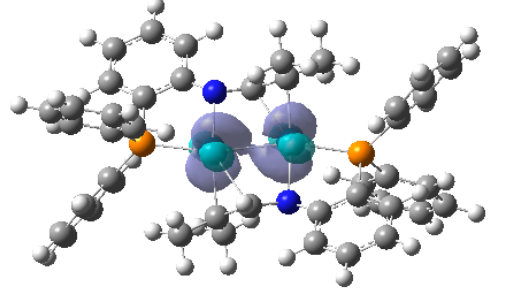
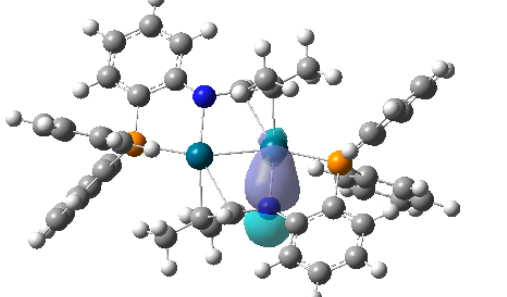
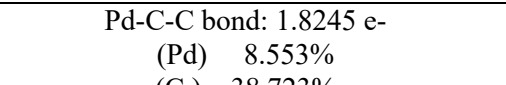
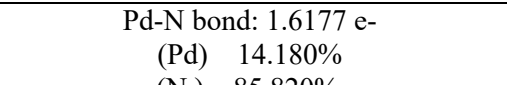
Table S3. Selected AdNDP orbitals in **1**. Isovalue of 0.05 for AdNDP orbitals presented in tables was used. Pd_A represents the Pd atom on the left and Pd_B represents the Pd atom on the right.

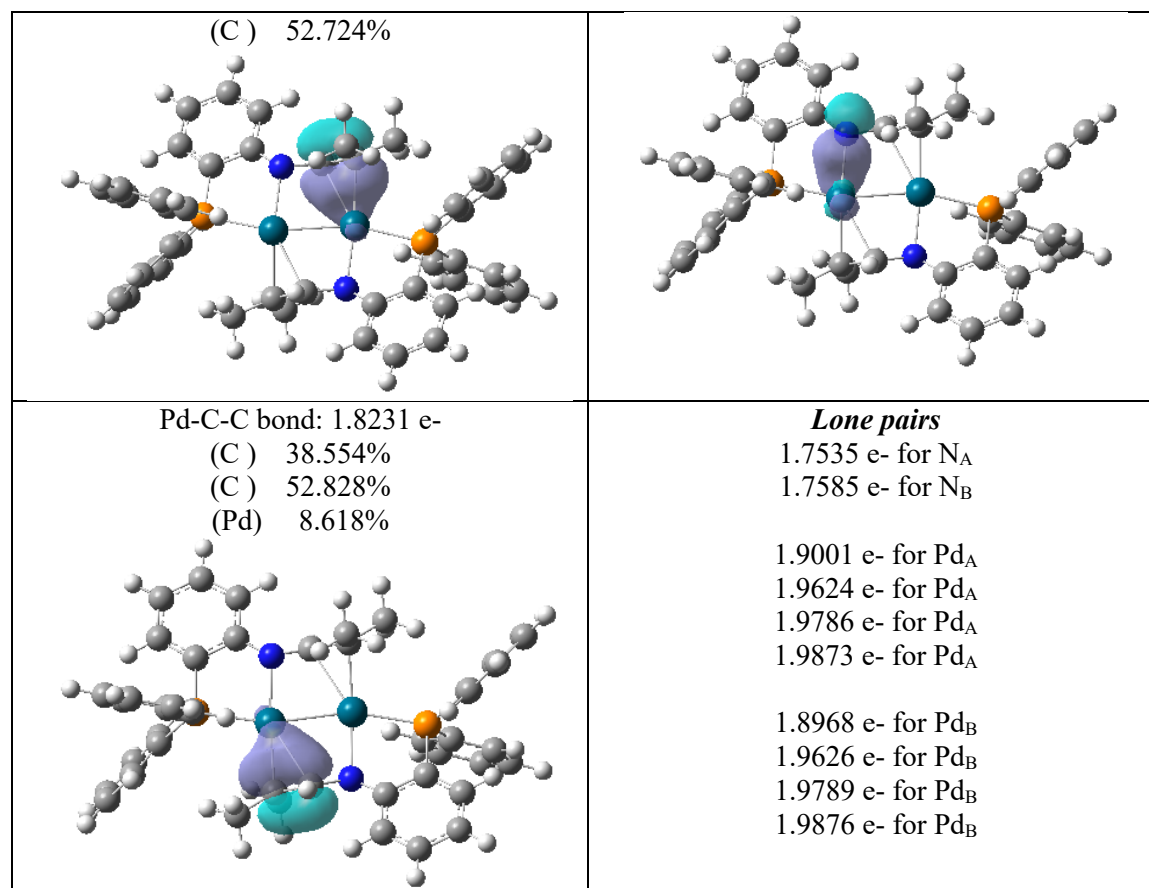
<p>Pd-N bond: 1.8868 e- (N) 75.498% (Pd) 24.502%</p> 	<p>Pd-C bond: 1.7810 e- (Pd) 36.783% (C) 63.217%</p> 
<p>Pd-N bond: 1.8849 e- (N) 74.381% (Pd) 25.619%</p> 	<p>Pd-C bond: 1.7700 e- (C) 63.221% (Pd) 36.779%</p> 
<p>N-Pd bond: 1.7202 e- (N) 88.145% (Pd) 11.855%</p>	<p>Pd-N bond: 1.7646 e- (N) 88.685% (Pd) 11.315%</p>

	
<p><i>Lone pairs</i></p> <p>1.9492 e- Pd_A 1.9627 e- Pd_A 1.9762 e- Pd_A 1.9866 e- Pd_A</p>	<p><i>Lone pairs</i></p> <p>1.9487 e- Pd_B 1.9645 e- Pd_B 1.9766 e- Pd_B 1.9867 e- Pd_B</p>

Analysis of **2** (Table S4) shows (1) two heterolytic Pd-N bonds are formed via the two electrons from N, which agree with the negatively charged amide; (2) two heterolytic η^2 -alkenyl Pd bonds are formed via the two electrons from alkenyl groups; (3) a homolytic Pd-Pd bond is presented. The bond compositions of the AdNDP orbitals in **2** are consistent with Pd(I)-Pd(I) oxidation states.

Table S4. Selected AdNDP orbitals in **2**. Isovalue of 0.05 for AdNDP orbitals presented in tables was used. Pd_A represents the Pd atom on the left and Pd_B represents the Pd atom on the right.

<p>Pd-Pd bond: 1.8804 e- (Pd) 50.286% (Pd) 49.714%</p> 	<p>Pd-N bond: 1.6059 e- (Pd) 13.721% (N) 86.279%</p> 
<p>Pd-C-C bond: 1.8245 e- (Pd) 8.553% (C) 38.723%</p> 	<p>Pd-N bond: 1.6177 e- (Pd) 14.180% (N) 85.820%</p> 



Analysis of **d1a1** (Table S5) in Scheme 18 shows (1) a heterolytic Pd-Pd bond is formed with one negatively charged Pd atom and one positively charged Pd atom; (2) two heterolytic Pd-N bonds are formed via the two electrons from N, which agree with the negatively charged amide; (3) two heterolytic Pd-C_{Me} bonds are formed via the two electrons from C_{Me}, which agree with the negatively charged methyl groups. Due to the heterolytic Pd-Pd bond, the Pd(II)-Pd(II) oxidation states in **d1a1** were assigned via AdNDP, and this assignment is consistent with LOBA. The unusual heterolytic Pd-Pd bond in **d1a5** (Table S6) is also obtained from the analysis of the bond compositions of the AdNDP orbitals, and Pd(II)-Pd(II) oxidation state in **d1a5** is assigned from the results of AdNDP and LOBA.

Table S5. Selected AdNDP orbitals in **d1a1**. Isovalue of 0.05 for AdNDP orbitals presented in tables was used. Pd_A represents the Pd atom on the left and Pd_B represents the Pd atom on the right.

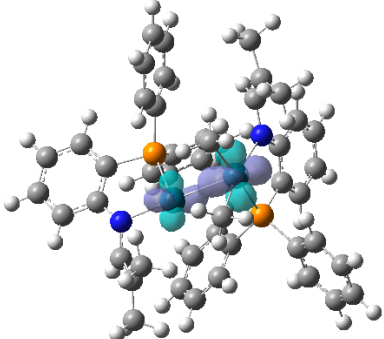
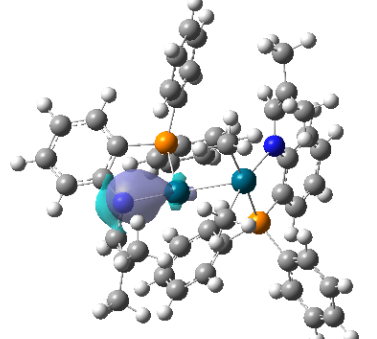
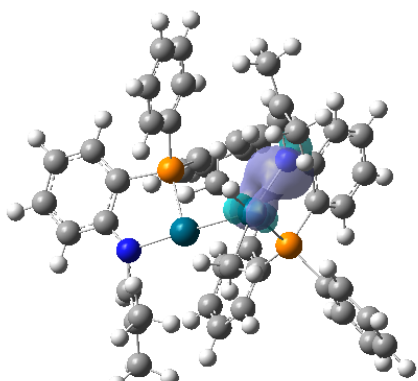
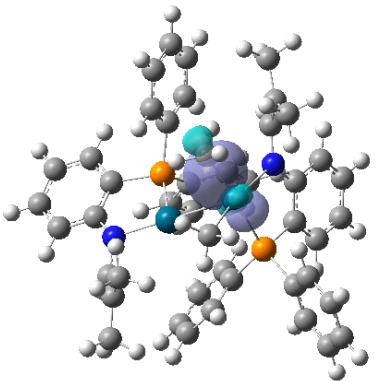
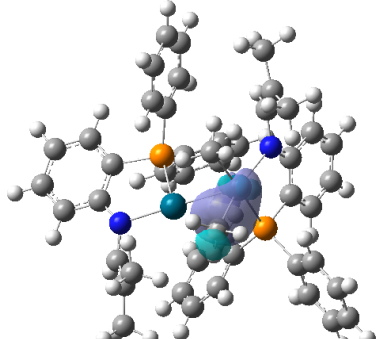
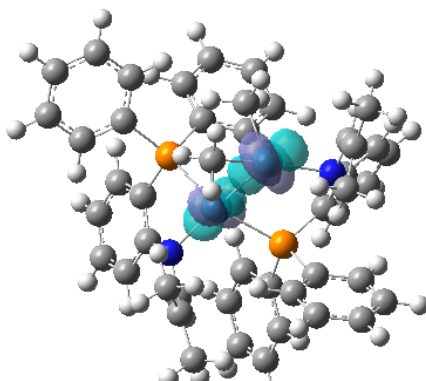
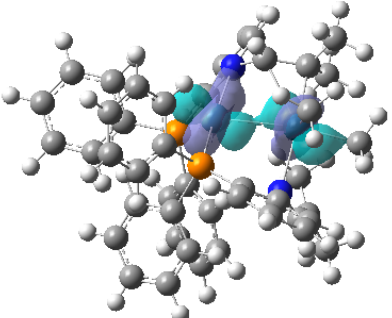
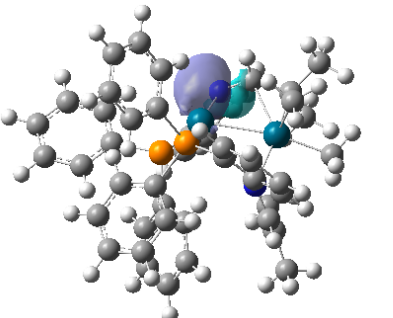
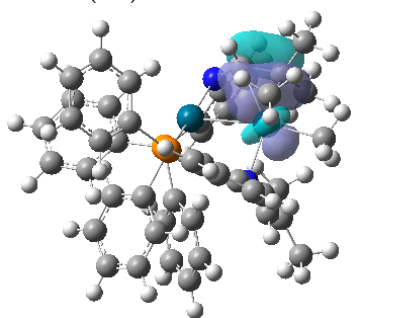
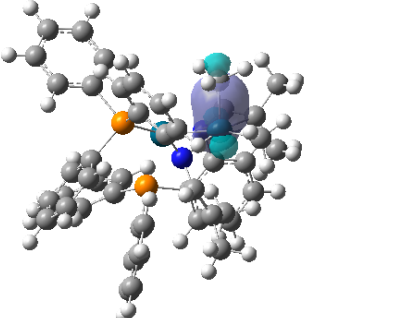
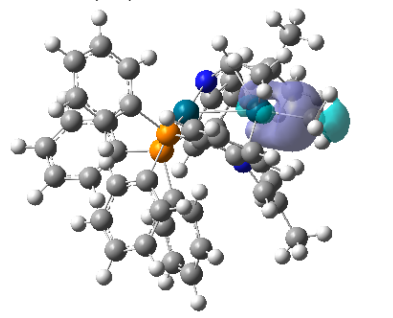
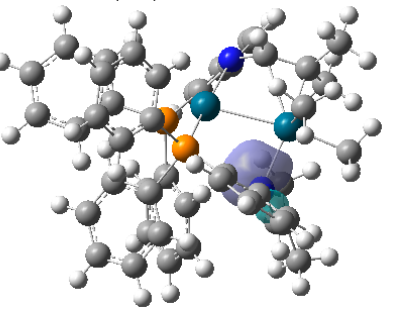
<p>Pd-Pd bond: 1.9819 e- (Pd_A) 26.095% (Pd_B) 73.905%</p> 	<p>Pd-N bond: 1.8514 e- (N) 90.291% (Pd) 9.709%</p> 
<p>Pd-N bond: 1.9317 e- (N) 76.268% (Pd) 23.732%</p> 	<p>Pd-C bond: 1.8286 e- (C) 57.290% (Pd) 42.710%</p> 
<p>Pd-C bond: 1.6793e- (Pd) 25.306% (C) 74.694%</p> 	<p><i>Lone pairs</i></p> <p>1.9507 e- Pd_A 1.9612 e- Pd_A 1.9849 e- Pd_A 1.9899 e- Pd_A</p> <p>1.9648 e- Pd_B 1.9731 e- Pd_B 1.9873 e- Pd_B</p>

Table S6. AdNDP orbitals of Pd-Pd bond in **d1a5**. Isovalue of 0.05 for AdNDP orbitals presented in tables was used. Pd_A represents the Pd atom on the left and Pd_B represents the Pd atom on the right.

<p>Pd-Pd bond: 1.9775 e- (Pd_A) 66.304% (Pd_B) 33.696%</p> 	<p><i>Lone pairs</i></p> <p>1.9406 e- Pd_A 1.9643 e- Pd_A 1.9699 e- Pd_A 1.9802 e- Pd_A</p> <p>1.9774 e- Pd_B 1.9840 e- Pd_B 1.9890 e- Pd_B</p>
--	--

Analysis of **8a2** (Table S7) shows (1) a heterolytic Pd-Pd bond with one negatively charged Pd atom and one positively charged Pd atom; (2) two heterolytic Pd-N bond is formed via the two electrons from N, which agrees with the negatively charged amide; (3) the heterolytic η^2 -alkenyl Pd bond is formed via the two electrons from alkenyl group; (4) two heterolytic Pd-C bond presented in the Pd(Me)₂ fragment with negatively charged methyl groups. The unusual heterolytic Pd-Pd bond in **8a2** is obtained from the analyses of the bond compositions of the AdNDP orbital, and Pd(0)-Pd(IV) oxidation state is assigned from the results of AdNDP and LOBA.

Table S7. Selected AdNDP orbitals in **8a2**. Isovalue of 0.05 for AdNDP orbitals presented in tables was used. Pd_A represents the Pd atom on the left and Pd_B represents the Pd atom on the right.

<p>Pd-Pd bond: 1.8635 e- (Pd_A) 44.284% (Pd_B) 55.716%</p> 	<p>Pd-N bond: 1.8282 e- (N) 94.949% (Pd) 5.051%</p> 
<p>Pd-C-C bond: 1.8734 e- (C) 18.882% (C) 42.748% (Pd) 38.370%</p> 	<p>Pd-C bond: 1.7491 e- (Pd) 38.451% (C) 61.549%</p> 
<p>Pd-C bond: 1.5816 e- (Pd) 26.178% (C) 73.822%</p> 	<p>Pd-N bond: 1.8583 e- 3(N) 95.967% 92(Pd) 4.033%</p> 
<p><i>Lone pairs</i> 1.9326 e- Pd_A 1.9498 e- Pd_A 1.9654 e- Pd_A 1.9774 e- Pd_A</p>	<p><i>Lone pairs</i> 1.9680 e- Pd_B 1.9835 e- Pd_B 1.9883 e- Pd_B</p>

VIII Crystallographic Details

VIII.I Experimental for $C_{50}H_{60}N_2OP_2Pd_2$ (**4**)

Data Collection and Processing. The sample was mounted on a Mitegen polyimide micromount with a small amount of Paratone N oil. All X-ray measurements were made on a Bruker Kappa Axis Apex2 diffractometer at a temperature of 110 K. The unit cell dimensions were determined from a symmetry constrained fit of 9838 reflections with $4.44^\circ < 2\theta < 61.28^\circ$. The data collection strategy was a number of ω and ϕ scans which collected data up to 75.604° (2θ). The frame integration was performed using SAINT.²⁹ The resulting raw data was scaled and absorption corrected using a multi-scan averaging of symmetry equivalent data using SADABS.³⁰

Structure Solution and Refinement. The structure was solved by using a dual space methodology using the SHELXT program.³¹ All non-hydrogen atoms were obtained from the initial solution. In addition to compound **4**, the asymmetric unit contained one THF molecule of solvation. The hydrogen atoms were introduced at idealized positions and were allowed to ride on the parent atom. The structure of the compound **4** exhibited a number of disorders. Both Pd atoms, Pd1 and Pd2, were disordered over 2 sites. The occupancy of the major component refined to a value of 0.864(7). Two phenyl groups bound to atom P2 also were disordered over two positions. The occupancies for the major components refined to values of 0.67(2) and 0.813(7) for the rings containing atoms C35-C40 and C41-C46 respectively. The isopropyl group of the isopropyl amine group comprised of atoms N2, C7, C8, C9, and C10 was disordered over two orientations. The occupancy for the major component refined to a value of 0.843(3). The structural model was fit to the data using full matrix least-squares based on F^2 . The calculated structure factors included corrections for anomalous dispersion from the usual tabulation. The structure was refined using the SHELXL program from the SHELX suite of crystallographic software.³² Graphic plots were produced using the Mercury program.³³

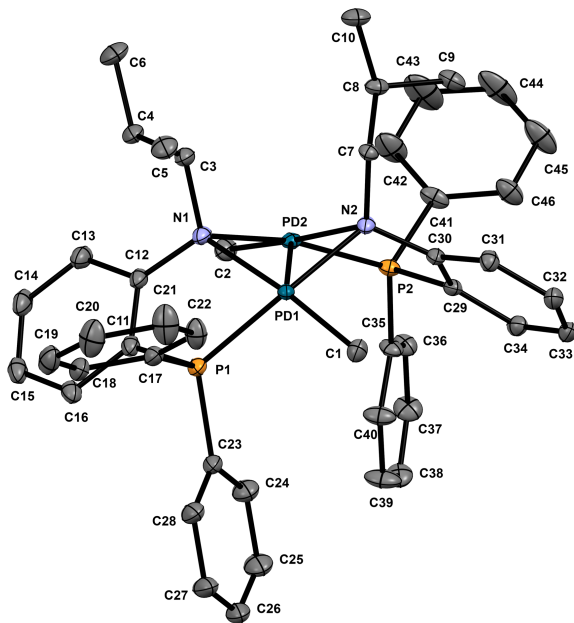


Figure S65. ORTEP Drawing of **4** showing naming and numbering scheme. Ellipsoids are at the 30% probability level. Only the major components of the various disorders are shown for clarity.

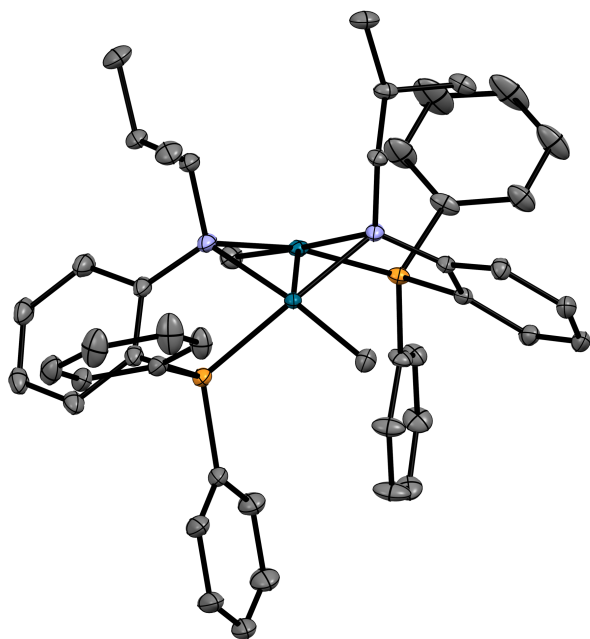


Figure S66. ORTEP Drawing of **4**. Ellipsoids are at the 30% probability level and hydrogen atoms were omitted for clarity. Only the major components of the various disorders are shown for clarity.

VIII.II Experimental for C₄₄H₄₂N₂P₂Pt (6)

Data Collection and Processing. The sample was mounted on a Mitegen polyimide micromount with a small amount of Paratone N oil. All X-ray measurements were made on a Bruker Kappa Axis Apex2 diffractometer at a temperature of 110 K. The unit cell dimensions were determined from a symmetry constrained fit of 9678 reflections with $5.38^\circ < 2\theta < 74.78^\circ$. The data collection strategy was a number of ω and ϕ scans which collected data up to 77.548° (2θ). The frame integration was performed using SAINT.²⁹ The resulting raw data was scaled and absorption corrected using a multi-scan averaging of symmetry equivalent data using SADABS.³⁰

Structure Solution and Refinement. The structure was solved by using a dual space methodology using the SHELXT program.³¹ All non-hydrogen atoms were obtained from the initial solution. The hydrogen atoms were introduced at idealized positions and were allowed to ride on the parent atom. The structural model was fit to the data using full matrix least-squares based on F^2 . The calculated structure factors included corrections for anomalous dispersion from the usual tabulation. The structure was refined using the SHELXL program from the SHELX suite of crystallographic software.³² Graphic plots were produced using the Mercury program.³³

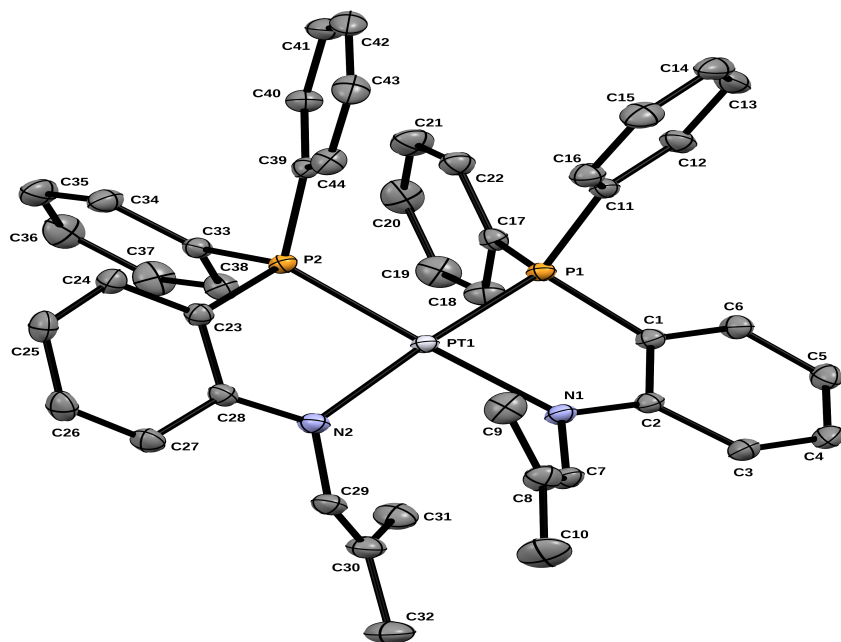


Figure S67. ORTEP Drawing of **6** showing naming and numbering scheme. Ellipsoids are at the 50% probability level.

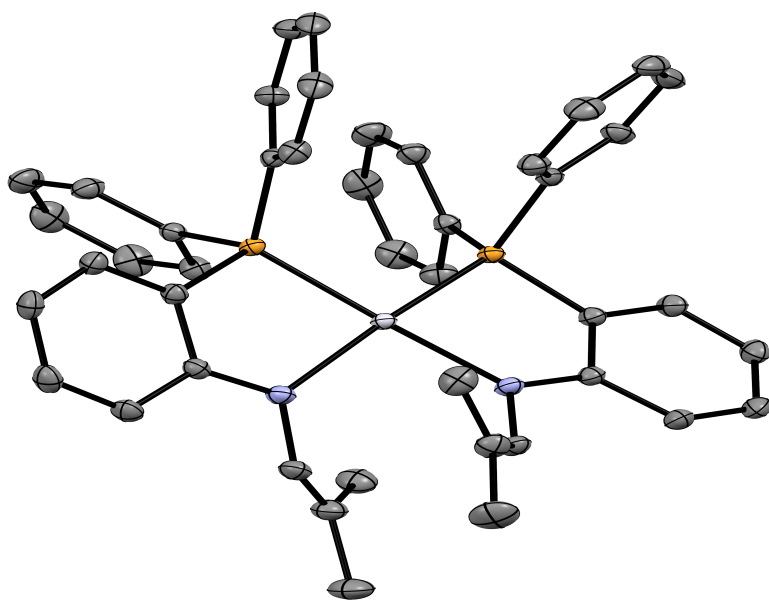


Figure S68. ORTEP Drawing of **6** without naming and numbering scheme. Ellipsoids are at the 50% probability level

Table S8. Summary of Crystal Data for **4** and **6**

Compound # (CCDC)	4 (2092272)	6 (2092271)
Formula	C ₅₀ H ₆₀ N ₂ OP ₂ Pd ₂	C ₄₄ H ₄₂ N ₂ P ₂ Pt
Formula Weight (g/mol)	979.74	855.82
Crystal Dimensions (mm)	0.288 × 0.193 × 0.087	0.347 × 0.279 × 0.087
Crystal Color and Habit	yellow prism	red prism
Crystal System	triclinic	monoclinic
Space Group	P -1	P 2 ₁ /c
Temperature, K	110	110
<i>a</i> , Å	10.568(4)	15.551(4)
<i>b</i> , Å	11.581(3)	13.574(4)
<i>c</i> , Å	18.826(5)	17.328(4)
α, °	95.004(9)	90
β, °	101.514(13)	90.105(17)
γ, °	91.357(9)	90
V, Å ³	2247.3(12)	3657.8(17)
Number of reflections to determine final unit cell	9838	9678
Min and Max 2θ for cell determination, °	4.44, 61.28	5.38, 74.78
Z	2	4
F(000)	1008	1712
ρ (g/cm ³)	1.448	1.554
λ, Å, (MoKα)	0.71073	0.71073
μ, (cm ⁻¹)	0.910	3.958
Diffraction Type	Bruker Kappa Axis Apex2	Bruker Kappa Axis Apex2
Scan Type(s)	φ and ω scans	φ and ω scans

Max 2 θ for data collection, °	75.604	77.548
Measured fraction of data	0.999	0.999
Number of reflections measured	171381	260731
Unique reflections measured	23901	20861
R _{merge}	0.0531	0.0611
Number of reflections included in refinement	23901	20861
Cut off Threshold Expression	I > 2 σ (I)	I > 2 σ (I)
Structure refined using	full matrix least-squares using F ²	full matrix least-squares using F ²
Weighting Scheme	w=1/[$\sigma^2(F_o^2)+(0.0311P)^2+1.4293P$] where P=(F _o ² +2F _c ²)/3	w=1/[$\sigma^2(F_o^2)+(0.0199P)^2+2.6085P$] where P=(F _o ² +2F _c ²)/3
Number of parameters in least-squares	684	446
R ₁	0.0363	0.0277
wR ₂	0.0741	0.0499
R ₁ (all data)	0.0660	0.0553
wR ₂ (all data)	0.0863	0.0571
GOF	1.029	1.006
Maximum shift/error	0.011	0.008
Min & Max peak heights on final ΔF Map (e ⁻ /Å)	-1.072, 0.947	-2.282, 2.168

Where:

$$R_1 = \sum (|F_o| - |F_c|) / \sum F_o$$

$$wR_2 = [\sum (w(F_o^2 - F_c^2)^2) / \sum (w F_o^4)]^{1/2}$$

$$GOF = [\sum (w(F_o^2 - F_c^2)^2) / (\text{No. of reflns.} - \text{No. of params.})]^{1/2}$$

References

1. Salo, E. V.; Guan, Z., Late-Transition-Metal Complexes with Bisazaferrocene Ligands for Ethylene Oligomerization. *Organometallics* **2003**, *22* (24), 5033-5046.
2. Dekker, G. P. C. M.; Buijs, A.; Elsevier, C. J.; Vrieze, K.; Van Leeuwen, P. W. N. M.; Smeets, W. J. J.; Spek, A. L.; Wang, Y. F.; Stam, C. H., New neutral and ionic methyl and chloro palladium and platinum complexes containing hemilabile phosphorus-nitrogen ligands. Study of the insertion of carbon monoxide into the metal-methyl bond. *Organometallics* **1992**, *11* (5), 1937-1948.
3. Stubbs, J. M.; Firth, K. F.; Bridge, B. J.; Berger, K. J.; Hazlehurst, R. J.; Boyle, P. D.; Blacquiere, J. M., Phosphine-imine and -enamido ligands for acceptorless dehydrogenation catalysis. *Dalton Trans.* **2017**, *46* (3), 647-650.
4. Jackman, K. M. K.; Bridge, B. J.; Sauv e, E. R.; Rowley, C. N.; Zheng, C. H. M.; Stubbs, J. M.; Boyle, P. D.; Blacquiere, J. M., C(sp³)–C(sp³) Coupling with a Pd(II) Complex Bearing a Structurally Responsive Ligand. *Organometallics* **2019**, *38* (8), 1677-1681.
5. Khusnutdinova, J. R.; Qu, F.; Zhang, Y.; Rath, N. P.; Mirica, L. M., Formation of the Palladium(IV) Complex [(Me₃tacn)PdIVMe₃]⁺ through Aerobic Oxidation of (Me₃tacn)PdIIMe₂ (Me₃tacn = N,N',N''-Trimethyl-1,4,7-triazacyclononane). *Organometallics* **2012**, *31* (13), 4627-4630.
6. Patiny, L.; Borel, A., ChemCalc: A Building Block for Tomorrow's Chemical Infrastructure. *J. Chem. Inf. Model.* **2013**, *53* (5), 1223-1228.
7. Zimmerman, P. M., Growing string method with interpolation and optimization in internal coordinates: Method and examples. *J. Chem. Phys.* **2013**, *138* (18), 184102.
8. Zimmerman, P., Reliable Transition State Searches Integrated with the Growing String Method. *J. Chem. Theory Comput.* **2013**, *9* (7), 3043-3050.
9. Zimmerman, P. M., Single-Ended Transition State Finding with the Growing String Method. *J. Comput. Chem.* **2015**, *36* (9), 601-611.
10. Shao, Y.; Gan, Z.; Epifanovsky, E.; Gilbert, A. T. B.; Wormit, M.; Kussmann, J.; Lange, A. W.; Behn, A.; Deng, J.; Feng, X.; Ghosh, D.; Goldey, M.; Horn, P. R.; Jacobson, L. D.; Kaliman, I.; Khaliullin, R. Z.; Ku s, T.; Landau, A.; Liu, J.; Proynov, E. I.; Rhee, Y. M.; Richard, R. M.; Rohrdanz, M. A.; Steele, R. P.; Sundstrom, E. J.; Woodcock, H. L.; Zimmerman, P. M.; Zuev, D.; Albrecht, B.; Alguire, E.; Austin, B.; Beran, G. J. O.; Bernard, Y. A.; Berquist, E.; Brandhorst, K.; Bravaya, K. B.; Brown, S. T.; Casanova, D.; Chang, C.-M.; Chen, Y.; Chien, S. H.; Closser, K. D.; Crittenden, D. L.; Diedenhofen, M.; DiStasio, R. A.; Do, H.; Dutoi, A. D.; Edgar, R. G.; Fatehi, S.; Fusti-Molnar, L.; Ghysels, A.; Golubeva-Zadorozhnaya, A.; Gomes, J.; Hanson-Heine, M. W. D.; Harbach, P. H. P.; Hauser, A. W.; Hohenstein, E. G.; Holden, Z. C.; Jagau, T.-C.; Ji, H.; Kaduk, B.; Khistyayev, K.; Kim, J.; Kim, J.; King, R. A.; Klunzinger, P.; Kosenkov, D.; Kowalczyk, T.; Krauter, C. M.; Lao, K. U.; Laurent, A. D.; Lawler, K. V.; Levchenko, S. V.; Lin, C. Y.; Liu, F.; Livshits, E.; Lochan, R. C.; Luenser, A.; Manohar, P.; Manzer, S. F.; Mao, S.-P.; Mardirossian, N.; Marenich, A. V.; Maurer, S. A.; Mayhall, N. J.; Neuscammann, E.; Oana, C. M.; Olivares-Amaya, R.; O'Neill, D. P.; Parkhill, J. A.; Perrine, T. M.; Peverati, R.; Prociuk, A.; Rehn, D. R.; Rosta, E.; Russ, N. J.; Sharada, S. M.; Sharma, S.; Small, D. W.; Sodt, A.; Stein, T.; St uck, D.; Su, Y.-C.; Thom, A. J. W.;

Tsuchimochi, T.; Vanovschi, V.; Vogt, L.; Vydrov, O.; Wang, T.; Watson, M. A.; Wenzel, J.; White, A.; Williams, C. F.; Yang, J.; Yeganeh, S.; Yost, S. R.; You, Z.-Q.; Zhang, I. Y.; Zhang, X.; Zhao, Y.; Brooks, B. R.; Chan, G. K. L.; Chipman, D. M.; Cramer, C. J.; Goddard, W. A.; Gordon, M. S.; Hehre, W. J.; Klamt, A.; Schaefer, H. F.; Schmidt, M. W.; Sherrill, C. D.; Truhlar, D. G.; Warshel, A.; Xu, X.; Aspuru-Guzik, A.; Baer, R.; Bell, A. T.; Besley, N. A.; Chai, J.-D.; Dreuw, A.; Dunietz, B. D.; Furlani, T. R.; Gwaltney, S. R.; Hsu, C.-P.; Jung, Y.; Kong, J.; Lambrecht, D. S.; Liang, W.; Ochsenfeld, C.; Rassolov, V. A.; Slipchenko, L. V.; Subotnik, J. E.; Van Voorhis, T.; Herbert, J. M.; Krylov, A. I.; Gill, P. M. W.; Head-Gordon, M., Advances in molecular quantum chemistry contained in the Q-Chem 4 program package. *Mol. Phys.* **2015**, *113* (2), 184-215.

11. Grimme, S., Semiempirical GGA-type density functional constructed with a long-range dispersion correction. *J. Comput. Chem.* **2006**, *27* (15), 1787-1799.
12. Becke, A. D., Density-functional thermochemistry. V. Systematic optimization of exchange-correlation functionals. *J. Chem. Phys.* **1997**, *107* (20), 8554-8560.
13. Hehre, W. J.; Ditchfield, R.; Pople, J. A., Self-Consistent Molecular Orbital Methods. XII. Further Extensions of Gaussian-Type Basis Sets for Use in Molecular Orbital Studies of Organic Molecules. *J. Chem. Phys.* **1972**, *56* (5), 2257-2261.
14. Wadt, W. R.; Hay, P. J., Ab initio effective core potentials for molecular calculations. Potentials for main group elements Na to Bi. *J. Chem. Phys.* **1985**, *82* (1), 284-298.
15. Hay, P. J.; Wadt, W. R., Ab initio effective core potentials for molecular calculations. Potentials for K to Au including the outermost core orbitals. *J. Chem. Phys.* **1985**, *82* (1), 299-310.
16. Hariharan, P. C.; Pople, J. A., The influence of polarization functions on molecular orbital hydrogenation energies. *Theoret. Chim. Acta* **1973**, *28* (3), 213-222.
17. McKenzie, S. C.; Epifanovsky, E.; Barca, G. M. J.; Gilbert, A. T. B.; Gill, P. M. W., Efficient Method for Calculating Effective Core Potential Integrals. *J. Phys. Chem. A* **2018**, *122* (11), 3066-3075.
18. Marenich, A. V.; Cramer, C. J.; Truhlar, D. G., Universal Solvation Model Based on Solute Electron Density and on a Continuum Model of the Solvent Defined by the Bulk Dielectric Constant and Atomic Surface Tensions. *J. Phys. Chem. B* **2009**, *113* (18), 6378-6396.
19. Schäfer, A.; Huber, C.; Ahlrichs, R., Fully optimized contracted Gaussian basis sets of triple zeta valence quality for atoms Li to Kr. *J. Chem. Phys.* **1994**, *100* (8), 5829-5835.
20. Weigend, F.; Ahlrichs, R., Balanced basis sets of split valence, triple zeta valence and quadruple zeta valence quality for H to Rn: Design and assessment of accuracy. *Phys. Chem. Chem. Phys.* **2005**, *7* (18), 3297-3305.
21. Andrae, D.; Häußermann, U.; Dolg, M.; Stoll, H.; Preuß, H., Energy-adjusted ab initio pseudopotentials for the second and third row transition elements. *Theoret. Chim. Acta* **1990**, *77* (2), 123-141.
22. Thom, A. J. W.; Sundstrom, E. J.; Head-Gordon, M., LOBA: a localized orbital bonding analysis to calculate oxidation states, with application to a model water oxidation catalyst. *Phys. Chem. Chem. Phys.* **2009**, *11* (47), 11297-11304.

23. Glendening, E. D.; Badenhop, J. K.; Reed, A. E.; Carpenter, J. E.; Bohmann, J. A.; Morales, C. M.; Weinhold, F., NBO 5.0. *Theoretical Chemistry Institute, University of Wisconsin, Madison, WI* **2001**.
24. Gimferrer, M.; Van der Mynsbrugge, J.; Bell, A. T.; Salvador, P.; Head-Gordon, M., Facing the Challenges of Borderline Oxidation State Assignments Using State-of-the-Art Computational Methods. *Inorg. Chem.* **2020**, *59* (20), 15410-15420.
25. Gimferrer, M.; Aldossary, A.; Salvador, P.; Head-Gordon, M., Oxidation State Localized Orbitals: A Method for Assigning Oxidation States Using Optimally Fragment-Localized Orbitals and a Fragment Orbital Localization Index. *J. Chem. Theory Comput.* **2022**, *18* (1), 309-322.
26. Zubarev, D. Y.; Boldyrev, A. I., "Developing paradigms of chemical bonding: adaptive natural density partitioning. *Phys. Chem. Chem. Phys.* **2008**, *10* (34), 5207-5217.
27. Multiwfn, version 3.8. <http://sobereva.com/multiwfn/> (accessed 2021).
28. Lu, T.; Chen, F., Multiwfn: A multifunctional wavefunction analyzer. *J. Comput. Chem.* **2011**, *33* (5), 580-592.
29. Bruker-Nonius; SAINT; version; 2013.8, **2013**, Bruker-Nonius, Madison, WI 53711, USA
30. Bruker-Nonius; SADABS; version; 2012.1, **2012**, Bruker-Nonius, Madison, WI 53711, USA.
31. Sheldrick, G., SHELXT - Integrated space-group and crystal-structure determination. *Acta Crystallogr. Sect. A* **2015**, *A71* (1), 3-8.
32. Sheldrick, G., Crystal structure refinement with SHELXL. *Acta Crystallogr. Sect. C* **2015**, *C71* (1), 3-8.
33. Macrae, C. F.; Bruno, I. J.; Chisholm, J. A.; Edgington, P. R.; McCabe, P.; Pidcock, E.; Rodriguez-Monge, L.; Taylor, R.; van de Streek, J.; Wood, P. A., Mercury CSD 2.0 - new features for the visualization and investigation of crystal structures. *J. Appl. Cryst.* **2008**, *41* (2), 466-470.